UNIVERSITAT POLITÈCNICA DE VALÈNCIA

Escuela Técnica Superior de Ingeniería del Diseño

CFD STUDY OF THE TRANSONIC FLOW OVER TURBOMACHINE BLADES

FINAL PROJECT OF

Aerospace Engineering Degree

AUTHOR

Noelia Ortiz Álvarez

TUTOR

Xandra Marcelle Margot

ACADEMIC COURSE: 2019/2020

Abstract

The aim of this project is the accomplishment of a CFD study about the development of the transonic flow on the first IGV(stator)-rotor stage of an axial turbine. In the first part of the study a selected stage blade geometry is analysed with different pressure drops. The next study involves the comparison between the first case and a new and flatter rotor airfoil. From this part it is obtained that the curved rotor blade performs better than the flat one in terms of isentropic efficiency and shock wave development.

Once these studies are carried out, an intermediate pressure case of the curved rotor geometry is selected since it is the one providing the highest isentropic efficiency. With this airfoil geometry the number of stator and rotor blades are varied. The number of vanes and blades selection is fundamental for the performance of a turbine since flow slip and boundary layer separation can occur if too many stator vanes or too few rotor blades are included.

Resumen

El objetivo de este proyecto es la realización de un estudio CFD sobre el desarrollo del flujo transónico en la primera etapa de IGV(estátor)-rotor de una turbina axial.

En la primera parte del estudio, se analiza una determinada geometría de pala de etapa con diferentes caídas de presión. El siguiente estudio implica la comparación entre el primer caso y un perfil de rotor nuevo y más plano. De esta parte se obtiene que la pala curva del rotor funciona mejor que la plana en términos de eficiencia isentrópica y desarrollo de ondas de choque.

Una vez que se realizan estos estudios, se selecciona un caso de presión intermedia de la geometría del rotor curvado, ya que es el que proporciona la mayor eficiencia isentrópica. Con esta geometría aerodinámica, el número de palas del estátor y del rotor es variado. La selección del número de paletas y álabes es fundamental para el rendimiento de una turbina, ya que puede producirse el deslizamiento del flujo y la separación de la capa límite si se incluyen demasiados estátors o muy pocos rotores.

Resum

L'objectiu d'aquest projecte és la realització d'un estudi CFD sobre el desenvolupament del flux transsònic en la primera etapa d'IGV(estàtor)-rotor d'una turbina axial.

En la primera part de l'estudi, s'analitza una determinada geometria de pala d'etapa amb diferents caigudes de pressió. El següent estudi implica la comparació entre el primer cas i un perfil de rotor nou i més pla. D'aquesta part s'obté que la pala corba del rotor funciona millor que la plana en termes d'eficiència isentròpica i desenvolupament d'ones de xoc.

Una vegada que es realitzen aquests estudis, es selecciona un cas de pressió intermitja de la geometria del rotor corbat, ja que és el que proporciona la major eficiència isentròpica. Amb aquesta geometria aerodinàmica, el nombre de pales de l'estàtor i del rotor és variat. La selecció del nombre de paletes i àleps és fonamental per al rendiment d'una turbina, ja que pot produir-se el lliscament del flux i la separació de la capa límit si massa estàtors o pocs rotors son inclosos.

Acknowledgements

In first place, I would like to acknowledge the professor Xandra Marcelle Margot who has been my tutor all along this project. She has helped me solving all the doubts I had, specially on CFD setting and has directed me so I could carry out the study I selected. So I want to thank you, for your patience and for having been available whenever I have needed it.

I would like to thank my family for the unconditional support they have given to me over these four years of degree. They know how great the effort has been and they have been the ones that, despite the difficulties that may have arisen, have been by my side to help me achieve my dream.

Finally I want to thank all the friends that I have made throughout the process, who have helped making these years of study more fun and in good company. For all those moments lived I would like to mention especially my close group of friends who, in addition to all the help provided throughout the courses, have been there at this last moments for conferring their opinion when has been necessary and contributing to the project with its support.

Contents

List of Figures

List of Tables

Notation

Symbol	Meaning
a	Speed of sound
α_1	Flow exit angle form the IGV
α_1'	Exit angle of the IGV
β_1	Flow inlet angle to the rotor blade
β_1'	Inlet angle of the rotor blade
β_2	Flow exit angle from the rotor blade
BOE	Boletín Oficial del Estado
c	Absolute velocity
CFD	Computational Fluid Dynamics
CMT	Centro de Motores Térmicos
c_p	Pressure coefficient
EGV	Exit Guide Vane
IGV	Inlet Guide Vane
M	Mach number
OE	Own Elaboration
p	Pressure
R	Constant of ideal gases
T	Temperature
U	Velocity of the rotor blades due to ratational speed
u	Speed
η	Efficiency
UPV	Universitad Politècnica de València
W	Work
w	Velocity vector

1. Introduction

1.1 General Introduction and Motivation

One of the most important parts in a jet engine design is the constitution of an efficient turbine that can be capable of generating the needed energy. In a gas turbine the compressor that directs the flow into the combustion chamber is moved by the turbine. The high temperature gases exiting the combustion chamber are expanded through the different stages of stator and rotor blades that form the turbine. From the expansion of the burnt gases the turbine extracts the power needed to drive the compressor.

In the last decades, most of the turbomachine design investigations have had as target the improvement of the efficiency of this process. Some of this researches have resulted in the reduction of the gap between the stator and the rotor. Nevertheless, this reduction has also had a damaging impact on the turbine, causing an increase in the rotor-stator interaction.[1] The expansion is carried out at high temperatures and pressures, producing that the gas being expanded achieves utterly high velocities that can even be supersonic.This effect, connected with the proximity of the rows of rotor and stator blades, generates shock waves in the flow that can lead to large scale flow oscillation over the surface, known as transonic buffeting.[2]

The shock motion and associated flow field oscillations can change the aerodynamics and moments over the turbine blades. These unsteady flow phenomena can provoke vibrations that result in mechanical fatigue which is an utterly important factor when talking about the life time of a turbomachine part.[3] Moreover, the break of a turbine blade can cause catastrophic consequences if the failure is produced during its operation, specially when occurring in aircraft engines. In jet engines, around 50% of the failures are due to fatigue. In addition, almost half of the failures are caused by deterioration of turbine blades or discs.[4]

This is why the design of a high efficiency turbine is not an easy task and involves structural, thermal and aerodynamic analysis. With the development of software experienced in the last decades, it has been possible to use CFD (Computational Fluid Dynamics) and structural programs in order to help in the conception of the most efficient turbomachine blades. Therefore, in this document the rotor-stator interaction will be studied in order to analyse how different rotor blades affect to the shock-buffet phenomena development and to the efficiency of a turbine stage.

1.2 Objectives

The objectives of this study are:

- The obtention of the airfoils of the stator and rotor blades that are going to compound a stage of an axial turbine.
- The constitution of a mesh departing from the turbine geometry first established. This mesh will be structured using the software STAR CCM+ 11.0.
- A CFD study of the rotor-stator interaction and all phenomena occurring in the transonic flow of a turbomachine stage. In this study, two different geometries of rotor blades will be studied in order to see the importance of its design. Some geometric parameters are varied, too.
- The obtainment of some conclusions regarding turbine stage design and performance.

1.3 Overall Project Perspective

This project is structured in eight chapters. The first one, in which the reader is at this moment, is the introduction chapter. It is follower by Chapter 2, which involves the theoretical framework in which this project is located, in it a brief introduction to important turbine concepts is bgiven. Chapter 3 talks about the election of the geometries and how the domain to study has been set. It follows Chapter 4 with the explanation of the mesh generation process. Once the mesh is obtained the CFD simulations can be run with the setting described in Chapter 5. The obtained results are showed and analysed in Chapter 6. Chapter 7 constitutes a summary of the conclusions arised. Finally, Chapter 8 contains the estimated budget for the carry out of this process.

2. Theoretical Framework

2.1 Gas Turbine History

The desire of flying through the skies is inherent to the human being. Since the 150 BC the propulsion applications have been investigated through the Action-Reaction Newton's law. This knowledge has been developed across the time with the contributions of thousands of cientifics all over the world. Some of the pioneers include Hero of Alexandria in the Roman Egypt in 150 AD with a bladeless radial steam turbine, the chinese with the Gunpowder, a low explosive, around the 1100-1200 AD, Leonardo da Vinci in 1490 who wrote around 35000 pages and 500 sketches and drawings concerning flight and G. Branca who developed, in 1629, the first steam turbine. The development of the gas turbine saw the light with the patent of a stationary turbine by John Barber, in England, in 1791. However, it was not until the 1903 with Ægidius Elling that the first gas turbine that was able to produce excess power was built.[5] This turbine was improved and in 1912 a new version arised. It had a compressor and a turbine separated in series, which was the precursor of the today's turbines.[6]

In the XX century, the development of turbines was accelerated due to the first aircraft flight and the World War I, which created the necessity of developing faster aircraft. Due to this urgency, the French engineer Maxime Guillaume, in 1921, got the patent for using a gas turbine to power an aircraft. His design consisted on a series of stages that compress the air, which, after being mixed with fuel and ignited could produce thrust by its expansion, it can be seen in Figure 2.1.[7] Nevertheless, his design was never built due to the fact that the available technology for compressors at that moment was not enough for its project. Some improvements would be needed before it was constructed. Despite this fact, his axial-flow turbojet became the base of nowadays engines.[8] After years of developments in different laboratories, the first jet plane was born on in 1939 by the German physicist Hans von Ohain.[9]

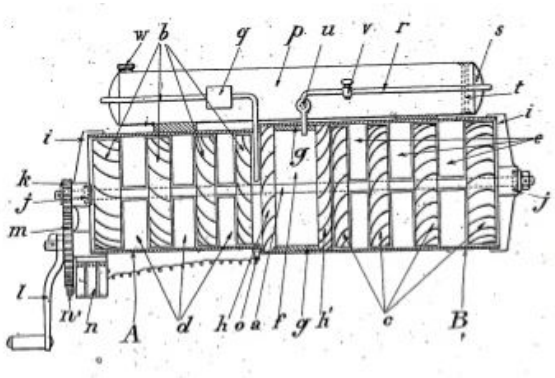

Figure 2.1: Maxime Guillaume's gas turbine design.[10]

2.2 Axial Turbine

In a gas turbine engine, the turbine itself is in charge of moving the compressor, and the propeller, if exists, apart from other accessories. Therefore, the compressor is coupled to the turbine shaft. For managing completing this task the turbine extracts the energy from the burned gasses (air-fuel mixture) going out from the combustion chamber. This gaseous energy is transformed into mechanical one by the expansion of the gases from high pressure and hot temperature to lower pressure and temperature.

In order to accomplish the expansion, the turbine is constituted by one or several stages consisting of a row of fixed vanes and a row of rotating blades. It must be highlighted that, despite the similarities in the geometrical description with a compressor, the order of the blades in a turbine (stator-rotor) is the opposite of the one in a compressor. Thus, this geometry enables that the stator vanes increase the flow velocity so that the rotor blades can extract the energy required for driving the above mentioned engine's parts.

According to the way the gasses enter into the turbine, a clear differentiation can be done. If the inlet airflow is radial to the shaft, the turbine is called radial. If the airflow enters parallel to the shaft inside the turbine, it is called axial. Figure 2.2 reflects differences in geometry related with how the airflow is introduced inside the turbine. The radial turbines are commonly used in those sectors where low power ranges are required, while the axial ones are used in mayor power plants. In the middle ranges, where both can be used, the principal differences in performance appear when talking about expansion ratios. While the radial turbine are capable of achieving an expansion ratio of 9 to 1 in a single stage, the axial turbines require more than one stages for achieving it.[11] This study will focus on axial turbines, widely used in the aeronautical sector due to the necessity of great amount of power in order to make an aircraft fly.

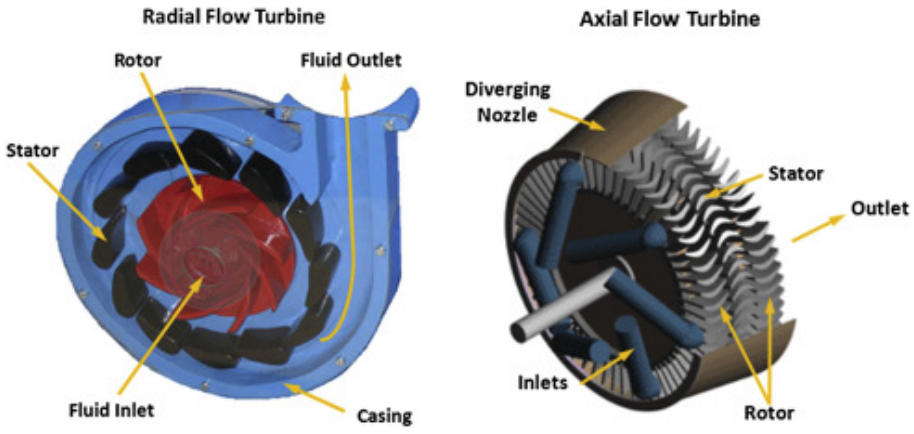

Figure 2.2: Radial and axial turbine.[12]

Axial turbines are composed usually by more that one stage, as said before, of rotor blades, attached to the disks and shaft, and stator vanes, attached to the engine case. Sometimes, inlet guide vanes (IGV) are used before the first stage to prepare the flow for the first set of rotor blades. They can be also used at the end to prepare it for the afterburner or nozzle, where they are called exit give vanes (EGV).

Therefore, the fluid enters the turbine through the inlet guide vane and is directed to

the rotating stage. The rotor blades, as shown in Figure 2.3, have a linear velocity if represented in 2D that corresponds to the radius R of the passage multiplied by its angular velocity ω. After having passed through the rotor blades, the airflow goes into the stator vanes where the fluid is redirected to a new set of rotor blades. As can be observed the static pressure is being reduced all along the stages, is reduced along the stator and also along the rotor. However, the total pressure remains almost constant along the stator vanes while decreases along the rotor blades.

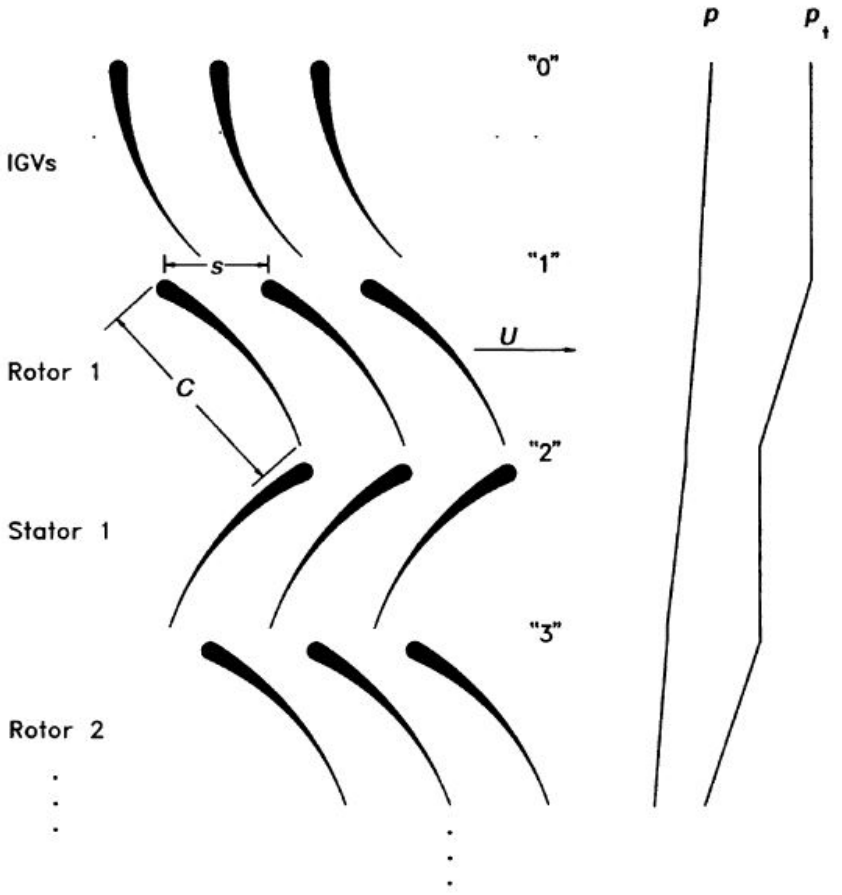

Figure 2.3: 2D turbine blade cascade.[13]

One of the principal parameters when designing a turbine is the velocity triangle, because the pressure drop is directly dependent on the velocity magnitudes and directions in a turbine. Figures 2.4, 2.5 and 2.6 show a clear representation. It is assumed that the air coming from the combustion chambers enters aligned with the engine's axis. Then the velocity of the flow relative to the IGV or to the stator if there is no IGV is c_0. When the air passes through the IGV it exits with a velocity c1 and a flow angle α_1 relative to the axis of the engine which is similar to the IGV exit angle α_1'. This process can be observed in Figure 2.4.

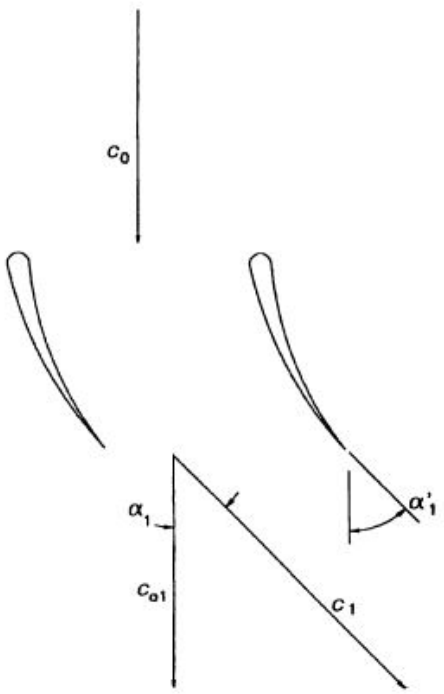

Figure 2.4: Velocity triangle in a turbine: IGV flow direction.[13]

This angle will not be the one experienced at the rotor inlet. This is due to the fact that the rotor blades are rotating and thus, the blades have a velocity of U_1 in the tangential direction that must be taken into account, as shown in Figure 2.5. This blade velocity vector must be subtracted from the absolute flow velocity one to obtain the velocity of the fluid relative to the rotor blades. The resulting vector is w_1 with a flow angle relative to the axis called β_1. The exit relative angle of the flow when having passed through the rotor is β_2, which usually does not match with the exit blade angle, β'_2. The exit relative velocity is w_2.

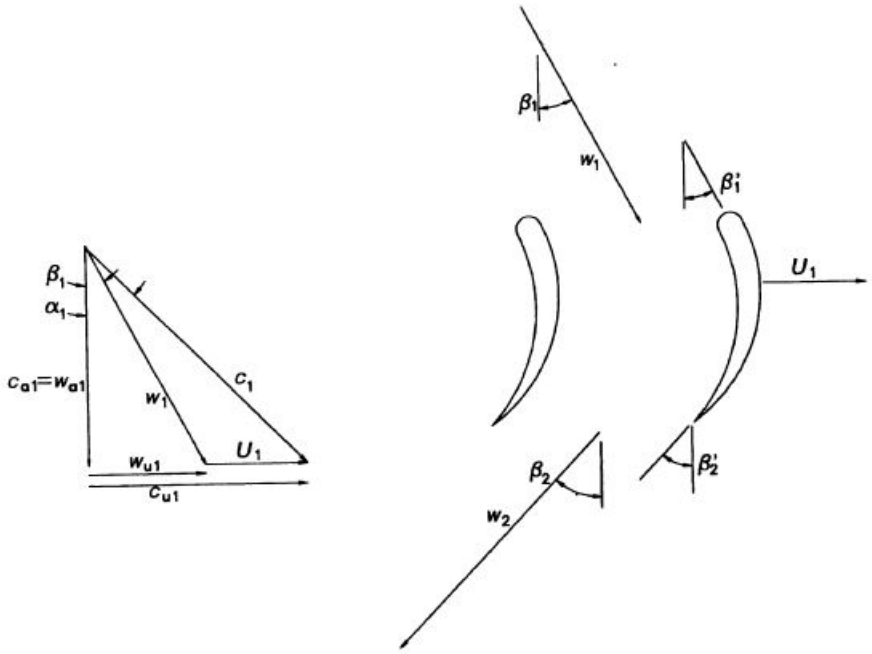

Figure 2.5: Velocity triangle in a turbine: rotor flow direction.[13]

If now the blade velocity at the blade exit U_2 is vectorially added to w_2, then, the absolute exit velocity c_2 at an angle α_2 could be obtained, Figure 2.6. This conditions will be the ones at the stator inlet, with an inlet vane angle α_2'. The exit absolute velocity will be c_3 at an angle relative to the exit of the engine α_3. This entire process is repeated all along the stages.

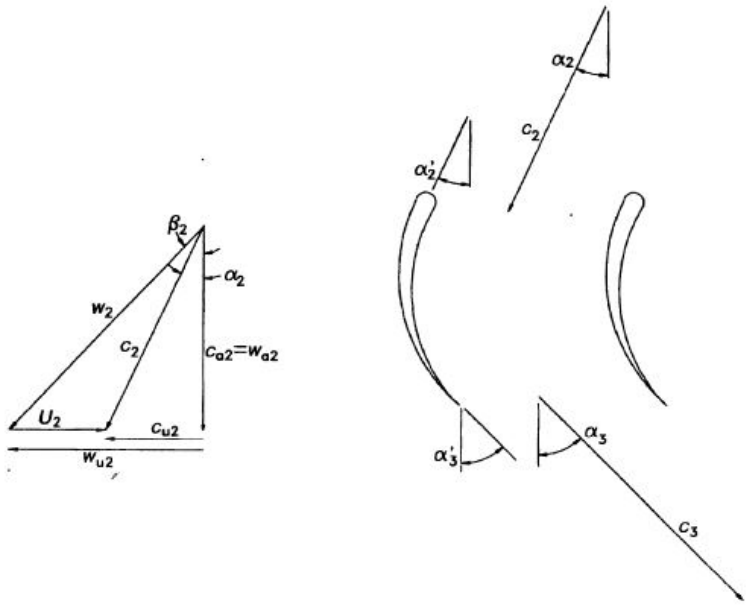

Figure 2.6: Velocity triangle in a turbine: stator flow direction.[13]

Some other relevant parameters when talking about turbine design are the solidity, the relation between rotor and stator number, the pressure ratio of an stage, etc. All this will

be developed in Chapter 3.

If the velocity triangle is considered some equations can be stated in order to calculate the behaviour of the turbine. Equations 2.1 and 2.2 show the calculation of the pressure drop of the rotor and the shaft power delivered .

$$\frac{p_{t2}}{p_{t1}} = \left[\frac{U_2 \cdot c_{u2} - U_1 \cdot c_{u1}}{\eta_{12} \cdot c_p \cdot T_{t1}} + 1\right]^{\frac{\gamma}{\gamma-1}} \tag{2.1}$$

$$\dot{W}_{sh} = \dot{m} \cdot [U_2 \cdot c_{u2} - U_1 \cdot c_{u1}] \tag{2.2}$$

These are just a few of the equations necessary to solve the complete stage of the turbine. If you want to know more about the resolution of these problems it is recommended to consult some books related to the subject, such as chapter 8 of the reference [13].

2.3 Transonic Phenomena

The flow inside the turbine is highly unsteady due to the periodic flow distortions caused by the upstream and downstream blade rows. This unsteadiness has important consequences for the turbine stage efficiency, blade loading and mechanical fatigue. The turbine process involves a expansion from high temperature and pressure to lower values of these variables. This procedure involves an increment of the velocity that can reach the supersonic regime in some stages of the turbine.

- **Shock Wave Generation**

The flow passes through the stator and accelerates itself, it arrives to the transonic regime and a shock wave starts to be created at the end of the stator vane, Figure 2.9. This wave propagates downstream and impacts into the leading edge of the rotor blades. The static pressure on the rotor variates creating strong fluctuations of the pressure forces on the rotor.

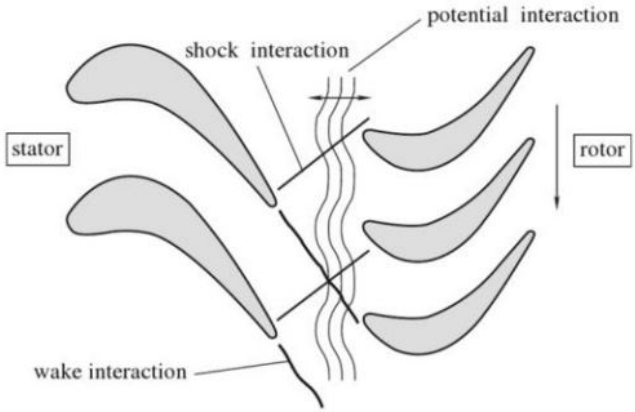

Figure 2.7: Rotor-Stator interaction scheme.[1]

- **Rotor-Stator Interaction**

The movable surfaces inside a turbine, rotor blades, are constantly changing their relative position with respect to the fixed ones, stator vanes. Thus, each time that the rotor blade passes in front of the stator vane variations in the pressure field appear. This process is repeated periodically making that diverse boundary layers associated with the different surfaces generate wakes that travel along the stages. The pressure wakes generated can produce non-stationary phenomena.[1]

The obtention of more efficient turbomachines has made that the gap between rotor and stator rows was reduced. This approximation has caused higher interactions between the rotor and stator rows. Since then, the pressure waves have played an utterly important roll on shock waves development and affects adversely the fluid dynamics and the structure of the system. Thus, the stage design of turbomachinery is not a trivial task.[14]

- **Buffeting**

One of the non-stationary phenomena occurring in blades is buffeting. It appears due to an increase of the angle of attack or to an increase in the Mach number when a boundary layer separation occurs after a shock wave. Then, oscillations in pressure in the boundary layer separation can occur causing the variation of its thickness and then fluctuations appear. As a result, the shock wave starts varying its intensity and oscillates all along the chord of the blade as seen in Figure 2.8. This fluctuations in the shock wave strength and location and the fluctuations in the boundary layer of the airfoil generate changes in the aerodynamics and moments over the blades that can lead to aeroelastic instabilities.[2]

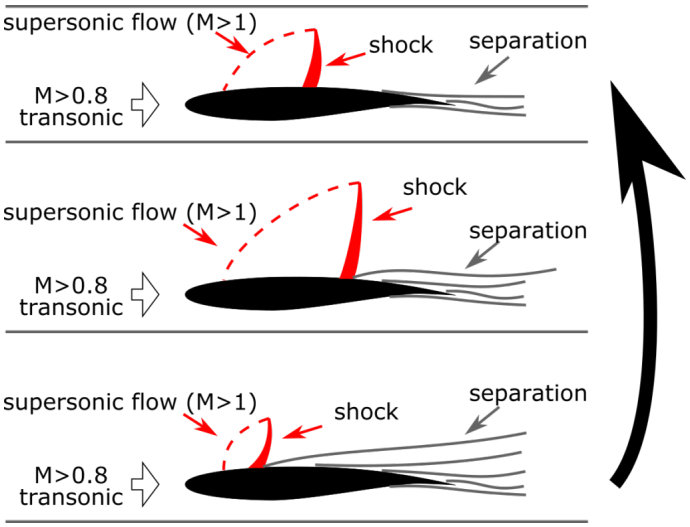

Figure 2.8: Buffet cycle.[15]

- **Flutter**

Flutter is an aeroelastic instability that causes self-excited structural oscillations generated by the blade mechanical response to the unsteady disturbances. These oscillations can cause mechanical fatigue affecting significantly in the life-time of turbomachinery parts. That is why the unsteady flow phenomena have been deeply investigated when designing turbine blades.

2.4 Previous Studies

This section will focus on introducing some researches that have already been performed over the flow development in axial turbines and the improvement of their performance. The main attention will be given to those driving CFD studies.

Each study focuses on different geometrical, aerodynamic or structufal factors that affect the performance of a turbine with the aim of achieving and improvement. Between these factors it can be found: the tip clearance, the number of rotor blades and stator vanes, the blade stagger angle, the velocity triangles, the Mach numbers achieved over the blades and the rotor-stator interactions.

The first thing to note is that until CFD appeared, all the researches that involved turbine design calculations where performed through velocity triangle theory and some important effects of the flow development could not be predicted efficiently such as rotor-stator interaction, recirculations or tip clearance interaction. Experimental studies in test turbines were then needed in order to compare results. Some of this studies include NASA investigations [16] on the increment of tip clearance that can lead to reduction in specific work and static and total efficiencies. Also the study of L.Stewart for the NASA that related the blade-loss characteristics to the turbine mean-section velocity diagrams. [17]

The introduction of CFD in turbomachinery has increased the number of investigations carried out over turbines and the variety of these studies. Along the last decades the CFD studies have focused on the enhancement of the performance of the turbine by the prediction of the behaviour of the flow along the rotor and stator blades. Some of them carry out more simple 2D studies like the one performed by the Technical Institute of Karbala that steadily analysed a turbine stage in order to see the influence of the number of rotor and stator[18] or the thermal efficiency study for military applications by Nader A. Elqussas.[19] Others perform more complex 3D studies like the study of a one stage turbine by Cleverson Bringhenti, Figure 2.9 (illustration of tip clearance flow), in order to define the gas turbine design point[20].

The intention of this study is to follow these steps and perform a 2D steady study of one stage of a turbine. The shock wave creation, development and strength will be studied in this document, paying attention to the effect that the geometry of the turbomachine blades has on the transonic flow behaviour.

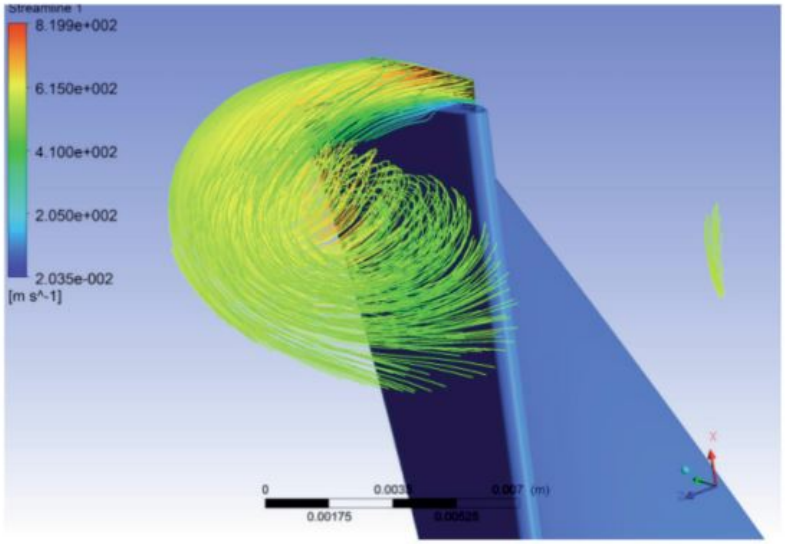

Figure 2.9: 3D test.[20]

3. Geometric Design

3.1 Blade Selection

Axial gas turbine plants have played a major role in the supply of power for diverse applications, all along the world. Since its creation the technology has been focused on the enhancement of the efficiency. The principal ways of improving this parameter are the following ones. [21]

- Increase of the pressure and temperature at the turbine inlet.
- Increase of the turbine development and capability of the longer last-stage blades.
- Increase the aerodynamic efficiency of the turbine.

Since the aim of this study is to analyse how the transonic flow develops on turbomachines, the third aspect will be of our concern.

To increase a turbine efficiency, aerodynamic losses must be minimized. The flow around a turbine stage can be unsteady, with oscillation in some parameters and therefore non-linearities appear. This unsteadiness leads to increasing losses due to phenomena like boundary layer separation, rotor-stator wake interaction and shock waves, among others. A more schematic view of the phenomena affecting the aerodynamic efficiency of a turbine can be seen on Table 3.1.

Blade loss	Friction losses due to rotor and stator surfaces Separation and vortex losses due to blade surfaces Separation and vortex losses due to trailing edges Shock wave losses Boundary layer interaction losses Inter-blade row and inter-stage losses
Leakage loss	Rotor blade tip leakage and stator vane inner seal leakage

Table 3.1: Losses that affect the efficiency.[21]

When a new turbine blade needs to be designed, all these phenomena are taken into account in order to generate the most efficient geometry. Until 1990's all blade design and research was based on loss models, such as Ainley and Mathieson model or Craig and Cox one, and on tunnel test where cascade flow tests were performed. In the following decades, the CFD calculations have been introduced becoming one of the principal sources of data involved in turbomachinery design process, specially involved in the aerodynamic design, as seen in Figure 3.1.

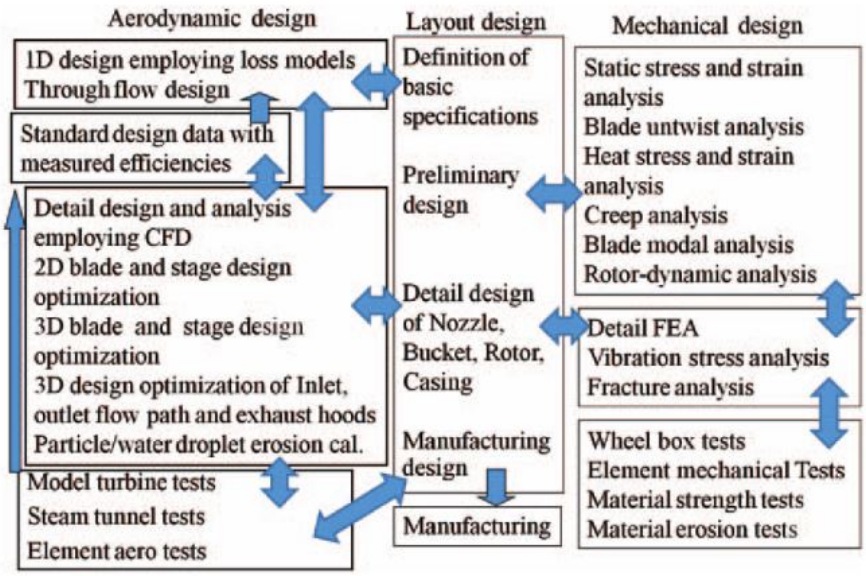

Figure 3.1: Blade design process.[21]

In this study the selected blade has been provided by the CMT (*Centro de Motores Térmicos*) of the UPV (*Universitad Politècnica de València*). The blade seen at Figure 3.2 has been extracted from the engine of the *Mirage F1* fighter aircraft that the UPV owns inside its buildings. This engine is the SNECMA Atar 09K-50. As observed in Figure 3.3 the blade constitutes a part of an entire blade ring. This blade is used in this project as the rotor.

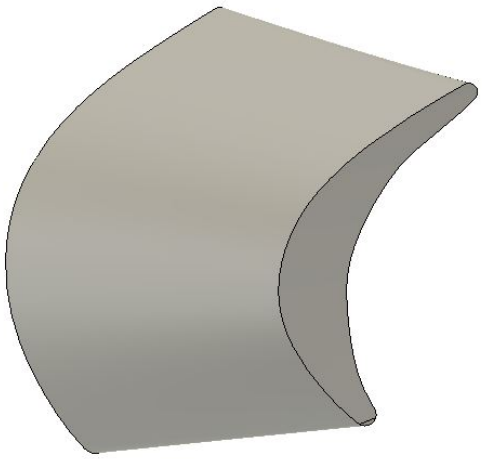

Figure 3.2: *Mirage F1* blade.[OE]

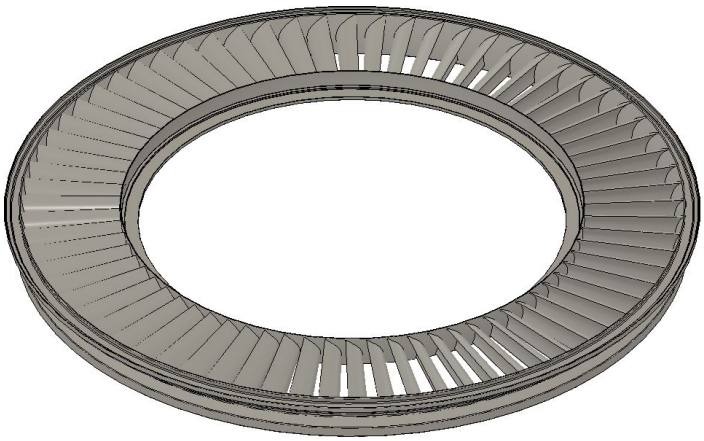

Figure 3.3: *Mirage F1* blade ring.[OE]

This project proposes an study of the importance of the geometry of a rotor when talking about flow development, focusing on shock wave generation and rotor-stator interaction. For this reason a second rotor blade geometry has been looked for. In this case the second rotor presents a more plane geometry with a lower exit angle (trailing edge) and with a less accused inlet angle (leading edge). The geometry in Figure 3.4 has been extracted form a similar project that will appear in the following chapters as the source of the input data chosen, Reference [20].

Figure 3.4: Second rotor blade geometry.[OE]

Since the study pretends to analyse the first stage of a turbine, an IGV as stator is needed, for such function the geometry in Figure 3.5 has been selected, again form Reference [20].

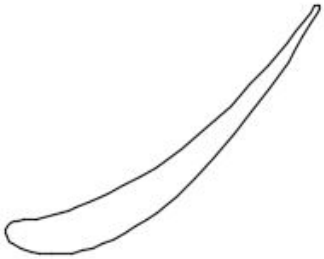

Figure 3.5: Stator blade geometry.[OE]

3.2 Geometric Parameters

The last step in the geometric design is the obtainment of the domain that is going to be introduced in the CDF software STAR CCM+. For accomplishing this task several geometric parameters have been taken into account.

- **Number of Blades per Stage**

The number of blades for turbine ring is a very important factor when designing a turbine cascade. The number of blades must ensure that the flow is correctly directed and that it does not separate creating adverse pressure gradients that affect the functioning of the engine. Nevertheless, so many blades may increase the frictional losses and reduce the efficiency of the turbine. A trade-off between these two aspects above must be satisfied.

Moreover, it must be highlighted the fact that if the same number of rotor blades as stator vanes is used, resonance can be generated. Resonance interactions are willing to be avoided because they produce vibrations and noise that reduces the life of the blades and affects engine's safety.

The numbers of blades and vanes that are usually selected are prime numbers. There is not any rule or equation to be followed in order to set these numbers. Measurements in a real engine could not be done, so bibliography has been inspected in order to obtain adequate values. Table 3.2 show the data collected.

	Nº Rotor Blades	**Nº Stator Vanes**	**Ratio**
Case 1	40	17	2.35
Case 2	64	36	1.7
Case 3	54	27	2

Table 3.2: Rotor-Stator blade number per ring.[20],[22]

Based on this data the ratio selected has been 1.67 that enables to create a domain region with 5 rotor blades and 3 stator vanes as seen in Tabele 3.3.

	Nº Rotor blades	Nº Stator Vanes	Ratio
Selection	5	3	1.67

Table 3.3: Rotor-Stator blade number selection for the domain region.[OE]

- **Inlet and Exit Areas**

The function of a turbine is opposite to the compressor, thus, the inlet and exit areas between two rotor blades have also a contrary relation. While in a compressor the inlet pressure is lower that the exit one, in a turbine the pressure at the inlet is greater than the exit one. Therefore in a turbine, the inlet blade area must be greater than the exit blade one so the velocity suffers an increment producing a reduction in the pressure, Figure 3.6.

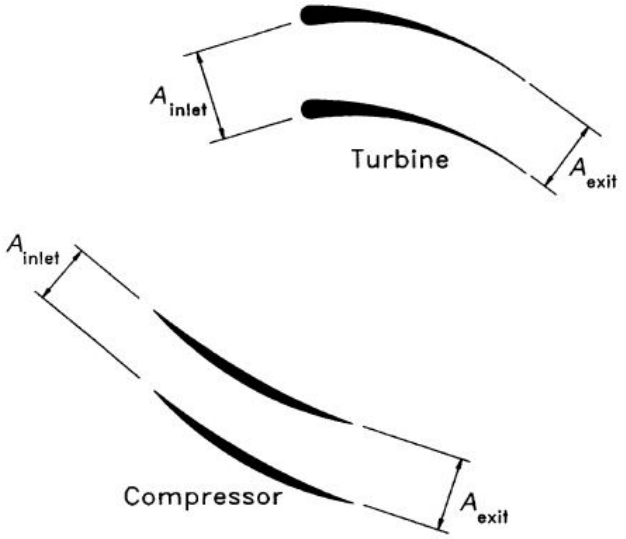

Figure 3.6: Blade inlet and exit areas.[13]

- **Solidity**

The solidity is a geometric parameter that relates the chord with blade spacing or pitch, (C/s), Figure 3.7. It is the inverse of the pitch-to-chord ratio, (s/C). Its correct selection is utterly relevant since affects directly the performance of a turbine stage. If the solidity takes small values, then it means that the spacing between blades is too large and the flow will slip and will not follow the blades. Instead, if the solidity is too large, the space between blades will be small compared with the chord and frictional losses will be considerable. An agreement between these effects should be obtained. Usually in turbines, as in compressors, solidity takes values of unity.[13] The chosen solidity is 1.55 and has been obtained form the 3D CAD model supplied by the CMT.

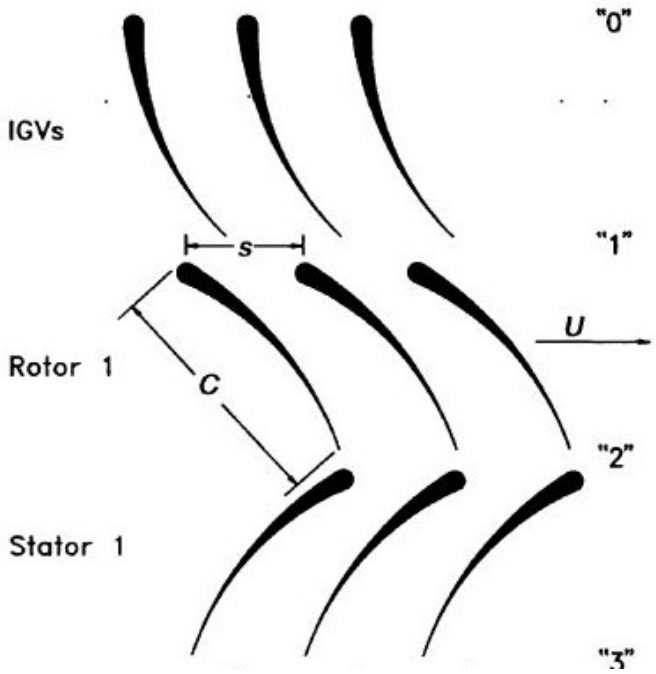

Figure 3.7: Solidity.[13]

- **Rotor-Stator in between Gap**

As said in Chapter 2, the gap between the rotor and stator rows has become more narrow in the last years as the turbine stage efficiency has been enhanced. Therefore, this value has been selected to be 1/3 of the chord in a way that the flow has time to adapt form the stator vanes to the rotor blades but ensuring that the flow follows the appropriated path.

- **Number of Stages**

This study is performed over the first stage of a turbine, so only one stage of stator and rotor blades has been be needed.

- **Blade Length**

The rotor blades length has been extracted form the CAD model. Its chord is 3.1 cm in length so it is applied in both rotors. The stator has been set in concordance with the rotor so it has 3.3 cm in chord length.

- **Domain Length**

Finally, since the project is based on CFD study a box domain through which the flow passes is set. The distance from the inlet to the first IGV or stator vane is two rotor chords, that lets the flow establishes but keeping the real dimensions of a turbine. Nevertheless, the outlet distance has been set seven chords downstream the rotor. This is not the real distance to the next stage but is needed in order not to obtain errors in calculations due to the wake produced by the rotor impacting in the boundary outlet.

3.3 Final Domain

In Table 3.4 a summary of all the parameters is presented and in Figures 3.8 and 3.9 the final dispositions are shown. Figures 3.10, 3.11 and 3.12 show a close up of the geometry

of the blades with the value of the inlet, outlet and chord angles.

Geometric Parameter		**Amount**	**Unit**
Rotor	Nº Blades	5	-
	Chord Length	3.1	cm
	Chord Angle	162	º
	Inlet Angle 1	136	º
	Outlet Angle 1	60	º
	Inlet Angle 2	151	
	Outlet Angle 2	48	
Stator	Nº Vanes	3	-
	Chord Length	3.3	cm
	Chord Angle	144	º
	Inlet Angle	152	º
	Outlet Angle	58	º
Rotor-Stator Gap		1	cm
Rotor Solidity		1.55	-
Nº Stages		1	-
Chords Upstream		2	-
Chords Downstream		7	-

Table 3.4: Summary of geometric parameters.[OE]

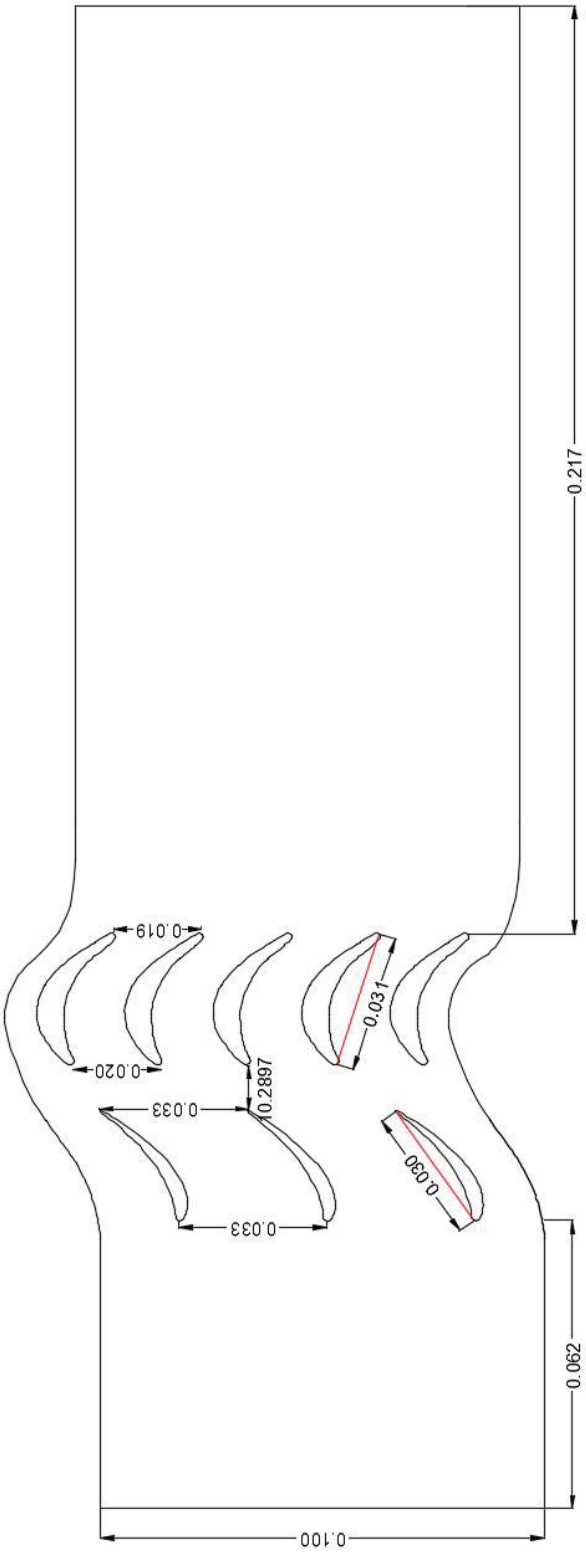

Figure 3.8: Domain geometry with rotor 1. (Units in meters)[OE]

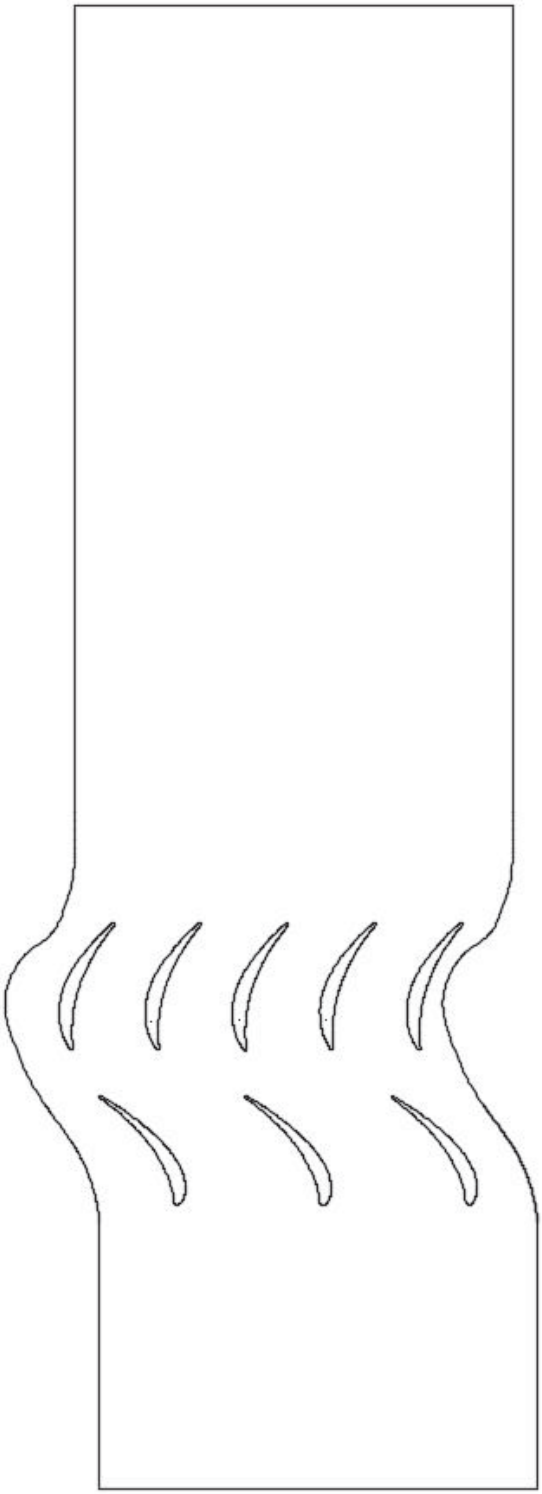

Figure 3.9: Domain geometry with rotor 2.[OE]

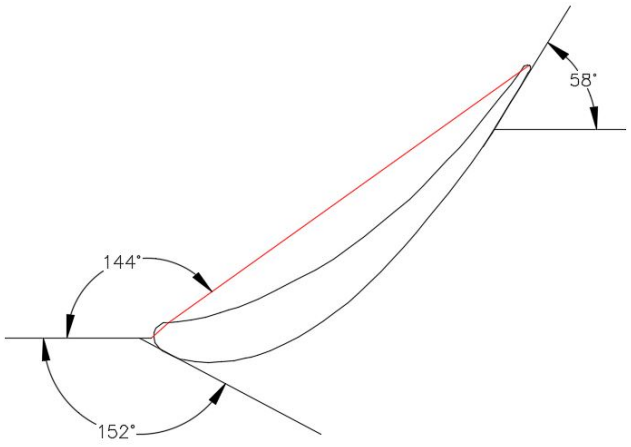

Figure 3.10: Stator close up.[OE]

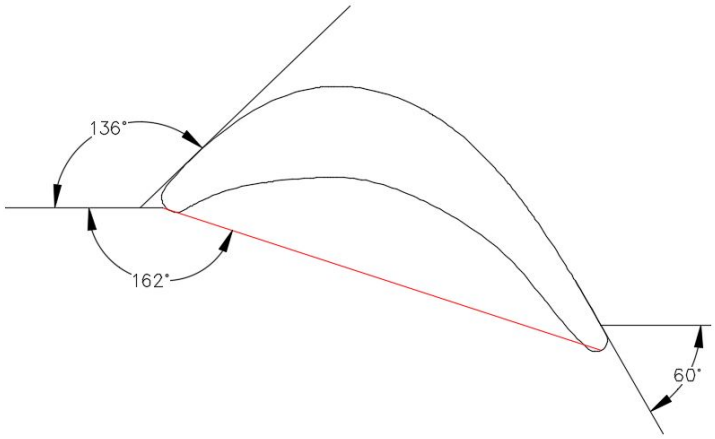

Figure 3.11: Rotor 1 close up.[OE]

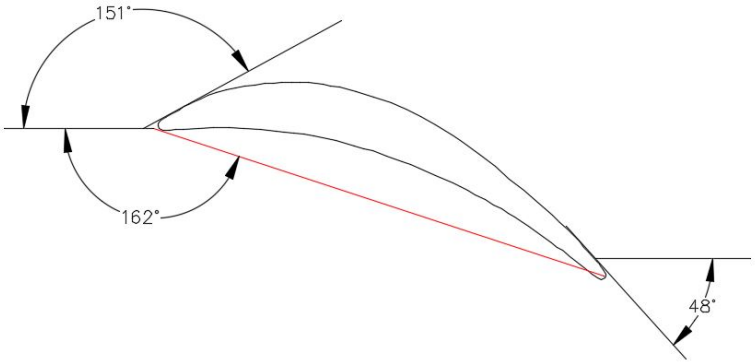

Figure 3.12: Rotor 2 close up.[OE]

More geometries have been considered interesting for this study after the first results, they are presented in the next chapters of the development.

The programs used for the obtainment of the different geometries have been Autodesk Fusion 360 and AutoCAD 2017. Fusion has been very helpful for extracting the aifoil profile of the rotor from the 3D CAD provided and for scaling the stator vane obtained form Reference [20]. AutoCAD has been employed for the disposition and creation of the geometry of domains that have been introduced in STAR CCM+ for the CFD simulation.

4. Mesh Generation

4.1 Mesh Importance

The mesh of a geometry represents the physical domain in a discrete form. It is an utterly relevant part when talking about the numerical solution of partial differential equations by finite-element or finite-difference methods. It is on the grid where continuous quantities are described by discrete functions and where the differential equations are approximated by algebraic relations for discrete values. Afterwards these values are analysed by the application computational code and a solution arises.

The efficiency of the solution of a problem is usually measured by the cost and time the computation takes, apart from its accuracy. It is obvious that then, the mesh number of cells and its shape and distribution will directly affect the cost and time of a numerical solution. Nevertheless, the accuracy needs a deeper investigation that is centred on the calculation errors appearing. The main errors arising in a computed solution are five:[23]

- Errors due to the fact that the mathematical models do not represent physical phenomena occurring in a 100%.
- Errors appearing because of numerical approximations of mathematical models.
- Errors caused by the incorrect shape and size of the mesh cells.
- Errors due to the computation of the discrete physical quantities satisfying the equations of the numerical approximation.
- Errors caused by the inaccuracy of the interpolation process.

As can be observed, points three, four and five are related to the mesh. Therefore, it can be stated that mesh quality is an important factor in a CFD calculation. A correct distribution of the points inside a mesh can lead to lower computational costs. Moreover, a good mesh can lead to the obtainment of a more accurate solution without convergence problems. However, accurate meshes usually tend to involve a great number of cells that penalise the computational time and require more computer memory. Achieving a trade-off between these factors is the main function of meshing operators and several mesh researches are focusing on this aspect.

4.2 Mesh Type Definition

The type of mesh selected for this project is the unstructured 2D mesh. In this kind of meshes the organization of the grid points and the form of the cells are not defined by a general rule, instead the connection of the neighboring grid nodes varies from point to point. This selection has been done due to the easiness of its construction in STAR CCM+.

The selected option has been Automated Mesh (2D) with Polygonal Mesher and Prism Layer Mesher.

The available volume meshers at STAR CCM+ are Polygonal, Quadrilateral or Triangular Meshers. The selection depends mainly on the shape of the domain that is needed to be meshed and the computational efficiency. While triangular cells are the ones that fit better any type of domain, the integration of the physical equations become in them a fewer times more expensive than quadrilateral cells. Quadrilateral cell option is frequently used in structured meshes but it can be used in unstructured ones providing accurate solutions. However, the fitting is not as good as the polygonal one, specially if the domain contain curves. Therefore, polygonal cells are selected which usually have hexagonal or pentagonal shape.

The Prism Layer Mesher is set near the wall boundary surfaces of the airfoils that will be specified in the next chapter. These cells are quadrilateral shaped and are highly efficient for treating boundary layers, since they can be established with a high aspect ratio in order to resolve the layers but without small angles as happens with triangular cells.[23]

In addition, some Custom Controls have been applied to the mesh, so apart from these volume meshers a Surface Control and a Volumetric Control have been defined. The Surface Control is employed in order to increment the number of cells near the blades, so accurate solutions near the boundary layer can be obtained. The Volumetric Control is defined as a square which comprises the stator an rotor cascade. It reduces the cells near the stage for a better wake and interaction computation.

4.3 Mesh Quality Analysis

In this part a mesh quality analysis is performed in order to verify the quality of the cells of the mesh.The software STAR CCM+ incorporates some field functions that enable to measure the mesh quality. This is applied to all the meshes that will be involved in the independence analysis appearing in the next section. However, the results shown in here are those regarding the selected mesh which parameters are explained in detail in the next section. At this point it must be highlighted the fact that it is constituted by 180 243 cells with a base value of 10^{-3}m and with 8 prism layers. [24]

- **Face Validity**

The face validity is an area-weighted measure of the correctness of the face normals relative to their attached cell centroid. If a mesh has good quality cells, the normals of those cells point outwards the centroid. If the cell is a bad quality cell, then it can have some faces with the normals pointing inwards.

A face validity value of 1 indicates that all face normals are pointing outwards and thus, those cells are good quality ones. Lower values indicate that some of the cell faces have normals pointing inwards, what means concavity. Cells bellow face validity values of 1 are considered bad, Figure 4.1.

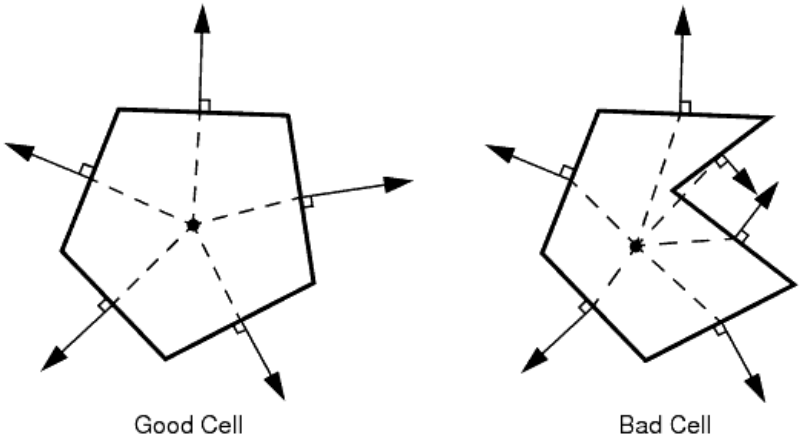

Figure 4.1: Face validity cells comparison.[24]

As can be seen on Figure 4.2 all the cells have a face value of 1, indicating that are valid cells.

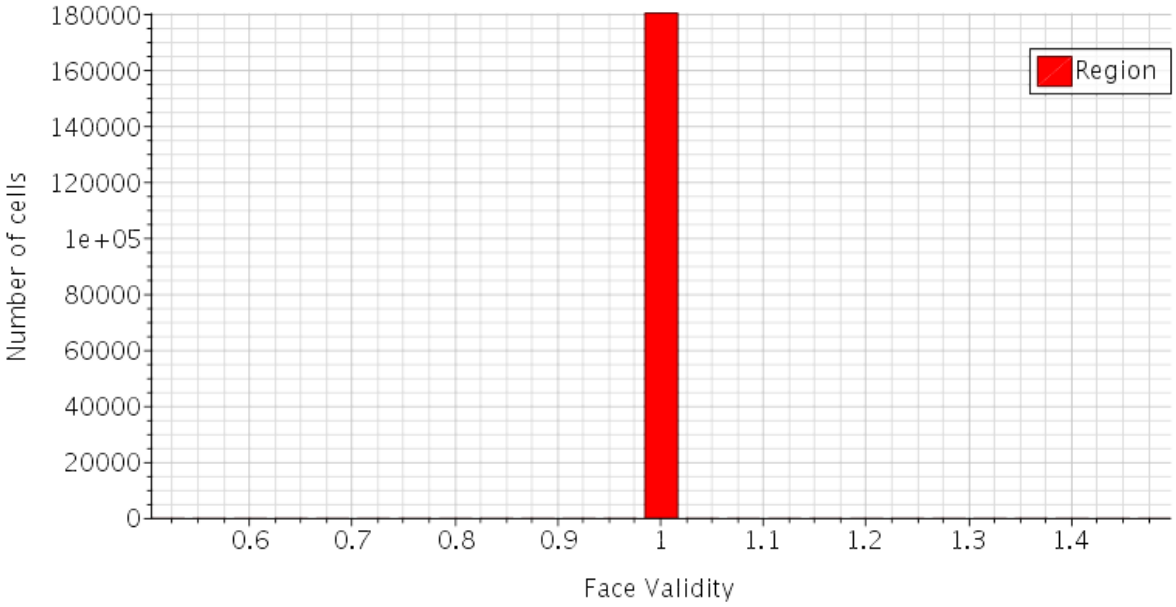

Figure 4.2: Face validity result. [OE]

- **Volume Change**

The volume change metric describes the ratio of the volume of a cell to that of its largest neighbour.

A volume change value of 1 indicates that the cell has at least the same volume as the neighbour cell. As the cell volume decreases with respect to its neighbour, the volume change value is reduced. If this difference in volume is large, potential inaccuracies and instability in the solvers may appear. Therefore, cells with a volume change lower than 0.01 are considered bad cells, Figure 4.3.

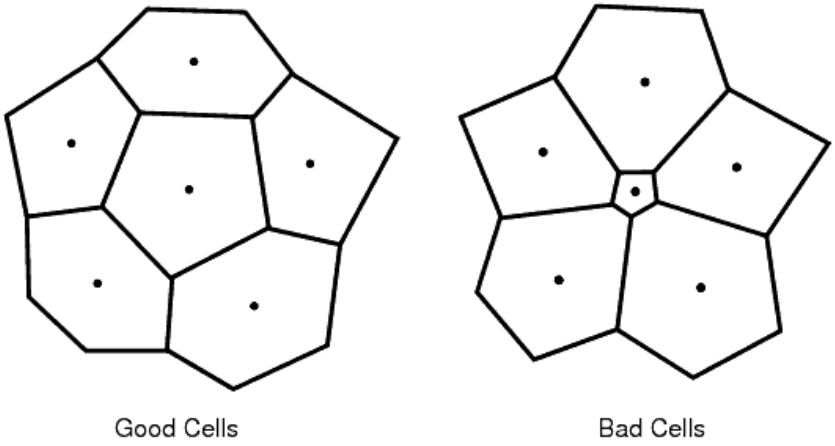

Figure 4.3: Volume change cells comparison.[24]

As can be seen on Figure 4.4 all the cells have a volume change greater that 0.01, indicating that are valid cells.

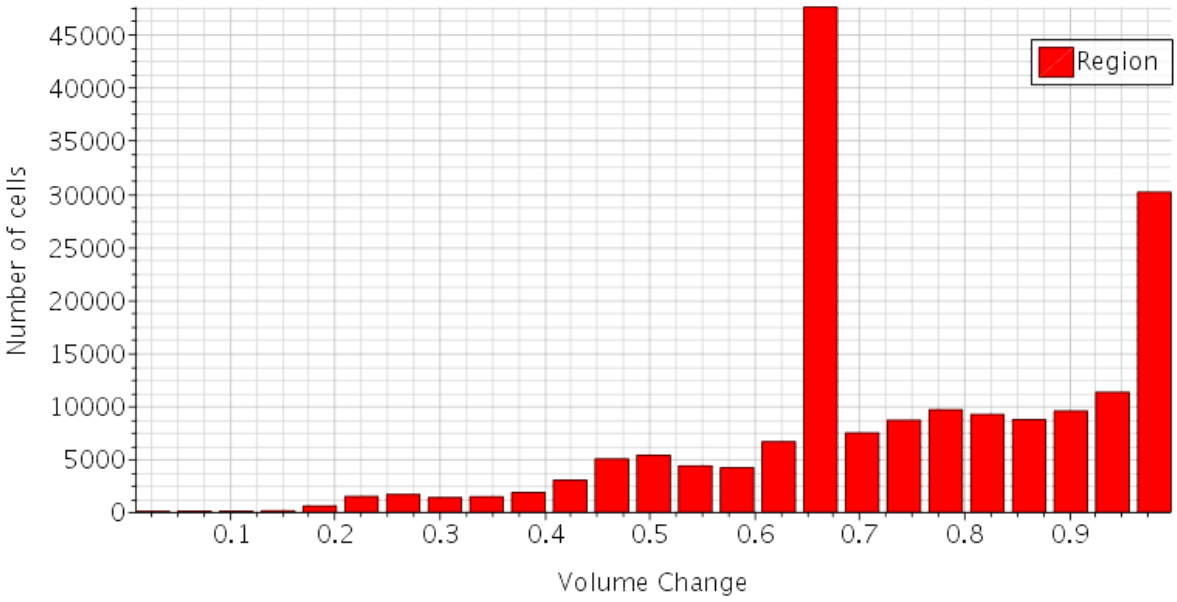

Figure 4.4: Volume change result. [OE]

- **Cell Skewness Angle**

The skewness mesure reflects whether the cells on either side of a face are formed in such a way as to permit diffusion of quantities without these quantities becoming unbounded.

A more visual meaning of the skewness angle is shown on Figure 4.5. The skewness angle θ is the the angle between the line that connects both cells centroids, ds, and the face area vector, a. If this angle is 0º it means that the mesh is perfectly orthogonal. Cells with a skewness angle greater than 85º are considered bad cells. Moreover, if the angle takes 90º, convergence issues may appear due to the fact that the diffusion term formulation contains the dot product $a \cdot ds$ in the denominator. This dot product becomes zero and a

divide-by-zero error arises.

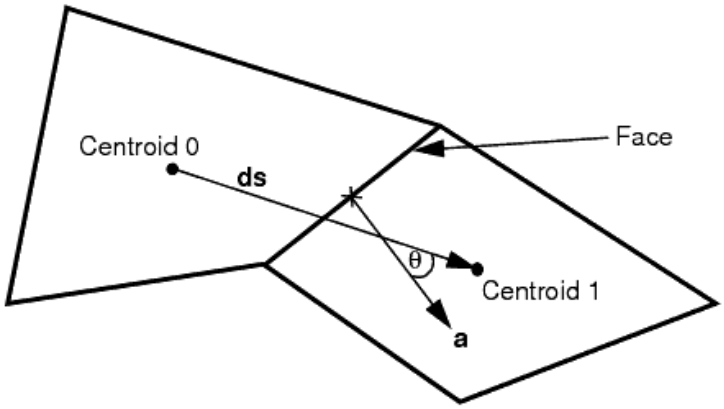

Figure 4.5: Cell skewness angle scheme.[24]

As can be seen on Figure 4.6 all the cells have a skewness angle lower than 75°, indicating that are valid cells.

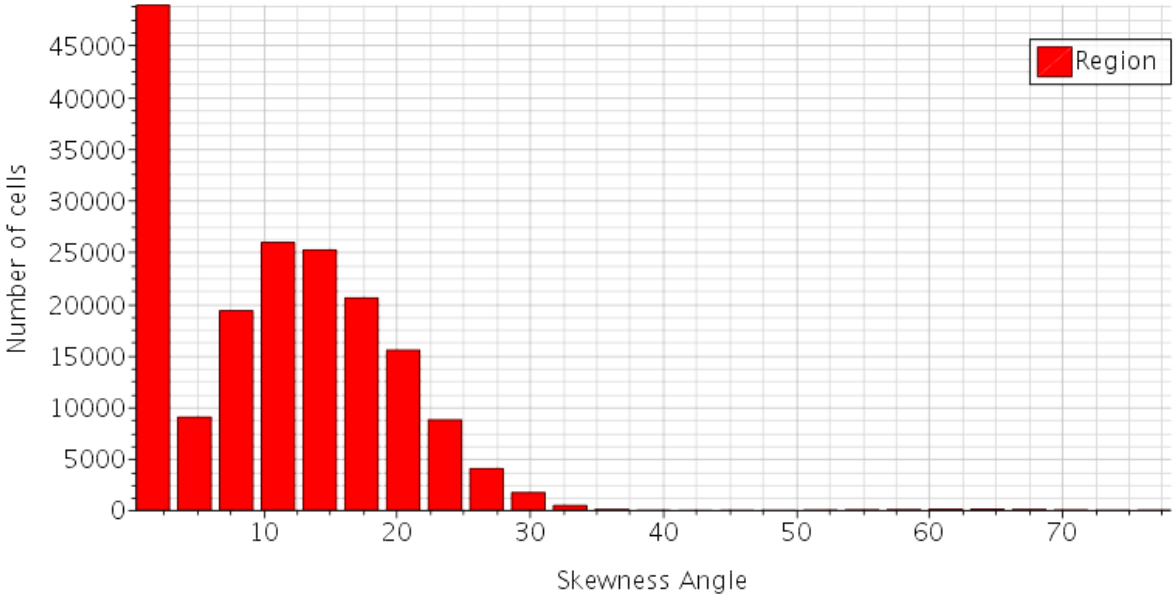

Figure 4.6: Skewness angle result. [OE]

- **Chevron Quality Indicator**

Chevron cells are pairs of thin slender cells which meet at a common face at an angle such that the line joining the cell centers does not pass through the common face, Figure 4.7.

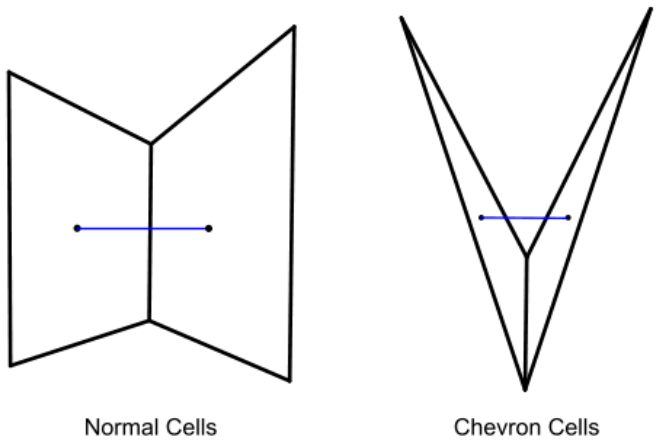

Figure 4.7: Chevron cell comparison.[24]

Chevron cells have a value of 1 being considered as bad cells, while any other cell has a value of 0 and is accepted as a good cell. As can be seen on Figure 4.8 all the cells have a value of 0 indicating that are good cells.

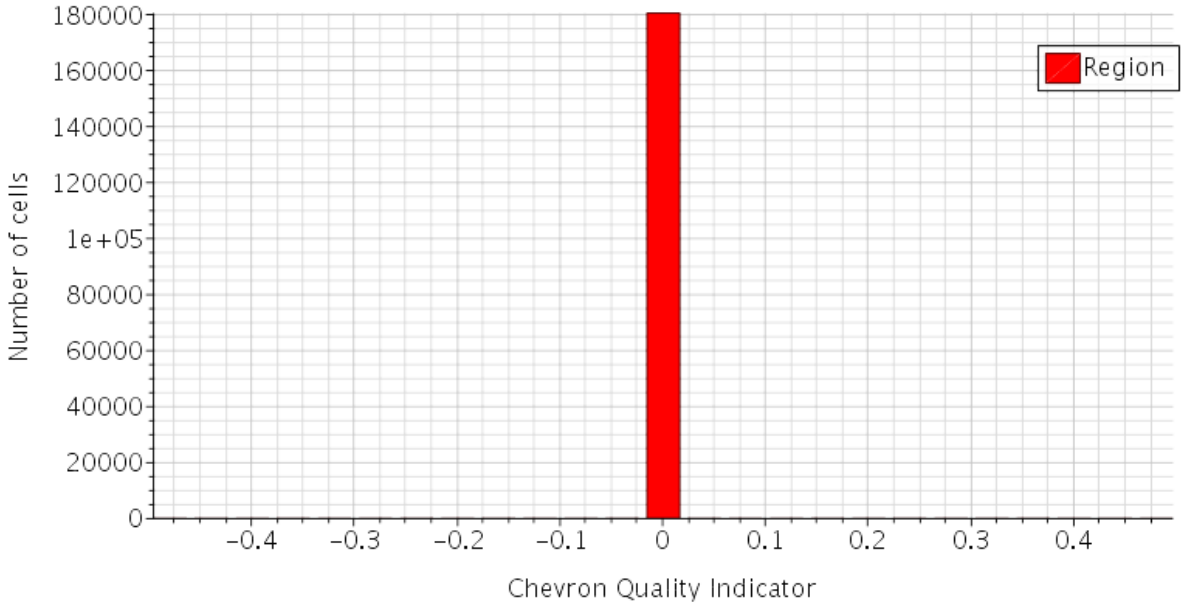

Figure 4.8: Chevron quality result. [OE]

- **Least Squares Quality**

The last mesh quality method is the least squares quality one. This method calculates the quality of the cell by comparing the position of its centroid with the physical position of the centroid of the neighbour cells, Figure 4.9.

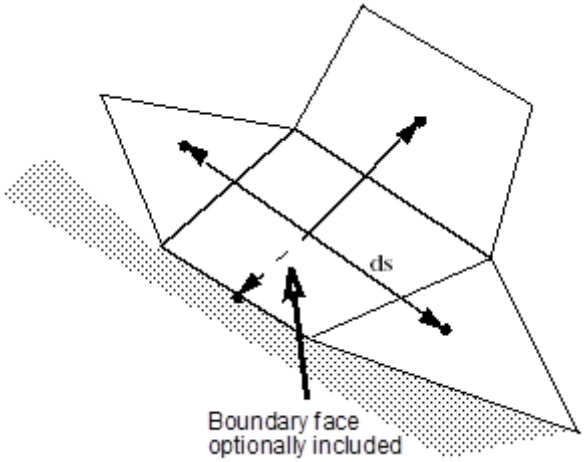

Figure 4.9: Least square scheme.[24]

The least square value for a perfect cell in a 2D domain is 0.5. Cells with a least squares quality less than $1{\cdot}10^{-3}$ are considered bad. As can be seen on Figure 4.10 all values are above 0.26 indicating a good quality mesh.

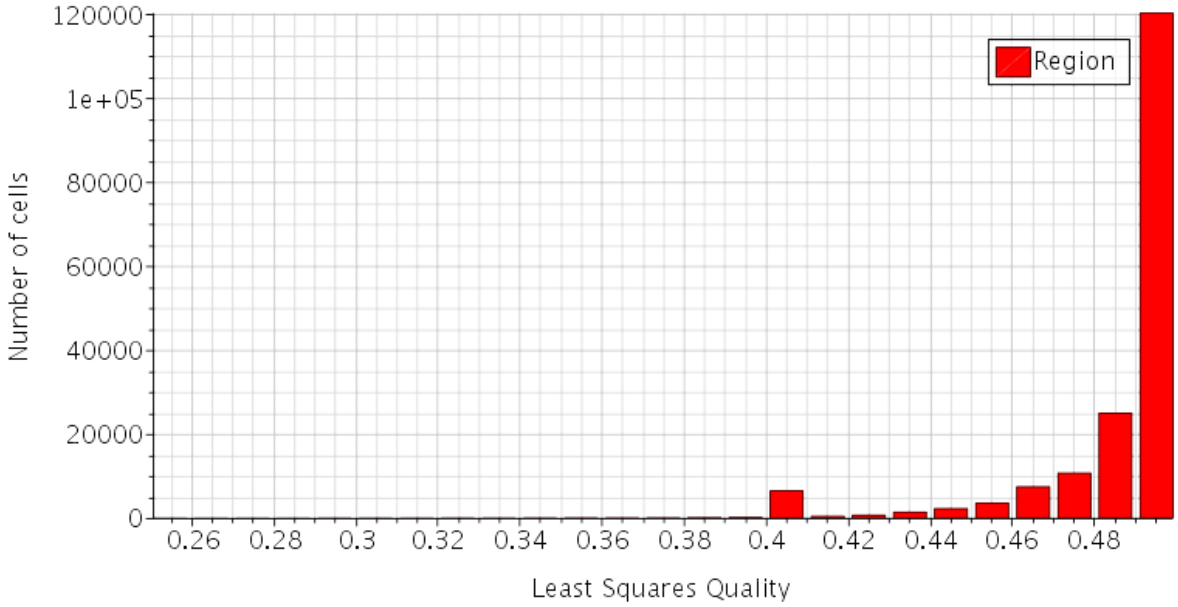

Figure 4.10: Least square quality result. [OE]

4.4 Mesh Independence

Once the type of mesh is chosen, the last step is to introduce the values of the different meshing parameters in order to see how many cells will constitute the grid. Per contra, this is not a direct task. As said in 4.1 the number of cells highly influences the computational cost, the convergence and accuracy of the results, thus, a mesh independence research should be done. The mesh independence is realized over the geometry domain containing Rotor 1, the rotor with the most curved airfoil.

Three meshes have been analysed. Each time the cells have been increased approximately by doubling the previous number of cells, that means incrasing a 40% the number of cells in each direction. Some relevant data like the isentropic efficiency, the velocities and densities upstream and downstream and the mass flow, among others, have been compared once the different cases where converged. The computational convergence criteria followed has been checking that the continuity residual was under 10^{-3} and that the rest where at least under 10^{-4}. However, this is not the only criteria. It must be highlighted that it is needed to check that the result of the relevant variables have achieved a constant value with the iterations.

The convergence criterion between meshes, what means the mesh independence validation is achieved once the values of the variables analysed does not change in more than 1% between consecutive meshes. [25].

Tables 4.1, 4.2 and 4.3 show the number of cells of each mesh and the variables analysed for the independence validation.

Name	**Nº cells**	**Isentropic Efficiency (%)**	**Velocity Upstream (m/s)**	**Velocity Downstream (m/s)**
Mesh 1	90 251	0.9041	184.2018	629.1196
Mesh 2	180 243	0.8837	184.2142	622.8953
Mesh 3	342 470	0.8821	184.2241	621.5738

Table 4.1: Mesh independence (1).[OE]

Name	**Nº cells**	**Density Upstream (kg/m^3)**	**Density Downstream (kg/m^3)**	**X Force on Rotor (N)**
Mesh 1	90 251	0.7218	0.3953	1 402.3523
Mesh 2	180 243	0.7218	0.3925	1 395.5592
Mesh 3	342 470	0.7218	0.3924	1 395.8183

Table 4.2: Mesh independence (2).[OE]

Absolute Error (%)	**Isentropic Efficiency**	**Velocity Upstream**	**Velocity Downstream**	**Density Upstream**	**Density Downstream**	**X Force on Rotor**
Mesh 1-2	2.25	0.0067	0.98	19.23	0	0.48
Mesh 2-3	0.18	0.0053	0.21	0	0	0.02

Table 4.3: Mesh independence error.[OE]

As can easily be deduced, the mesh selected is Mesh 2 with 180 243 cells, since the error of several variables with respect to Mesh 3 is lower than 1%. This means that the greater computational cost that Mesh 3 requires is not worth it when talking about solution precision. The specific meshing parameters are shown on Table 4.4. It must be stated that the prism layer related parameters are calculated in a way that the y+ value in the boundary layer is lower than 5 (y+<5). This is, as observed in Figure 4.11, the recommended value for an enhanced wall treatment simulation which involves the viscous sublayer resolution. This sublayer is dominated by viscous effects, therefore, there we get

much more dissipation than production of turbulent kinetic energy. When phenomena occur near the wall boundaries the effect of this sublayer must be solved with a near wall model approach instead of bridging it (y+<30), Figure 4.12, so a more accurate solution is obtained.

The equations needed for the y+ calculation are Equation 4.1 for the skin friction, Equation 4.2 for the shear stress at the wall, Equation 4.3 for the friction velocity and, finally, Equation 4.4 for the y+ value. All these values have been calculated for an estimated Reynolds of $2{\cdot}10^5$, the chord of the rotor, a density of 0.722 kg/m^3 and an average velocity of 390 m/s.

$$C_f = [2 \cdot \log_{10}(Re_x) - 0.65]^{-2.3} \qquad for Re_x < 10^9 \tag{4.1}$$

$$\tau_w = C_f \cdot \frac{1}{2} \cdot \rho \cdot u_\infty^2 \tag{4.2}$$

$$u_\tau = \sqrt{\frac{\tau_w}{\rho}} \tag{4.3}$$

$$y^+ = \frac{y \cdot u_\tau}{\upsilon} \tag{4.4}$$

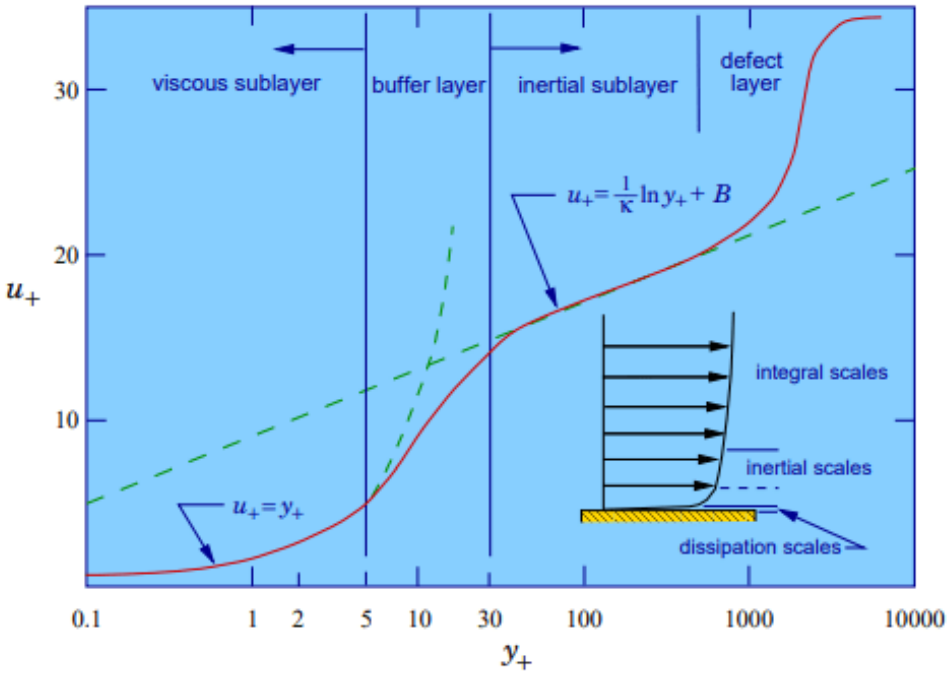

Figure 4.11: y+ values for different layers.[26]

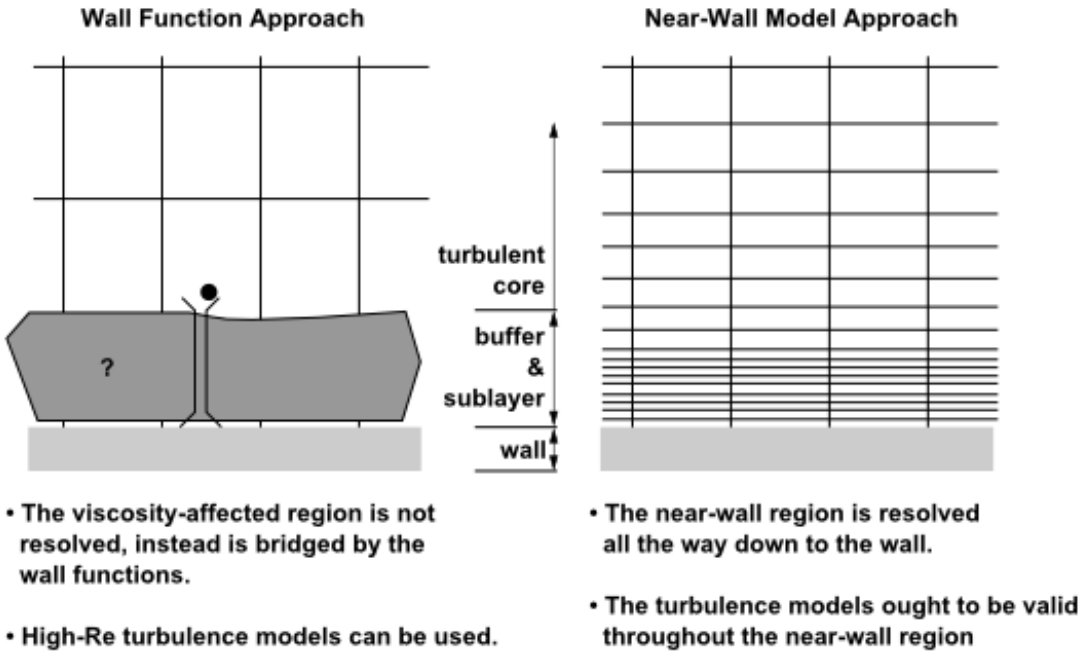

Figure 4.12: Wall function approach vs near wall model approach.[26]

Meshing Parameters		Value	Unit
Basic Cell Mesh	Cell base size	$1{\cdot}10^{-3}$	m
	Target Surface Size (Relative to Base)	100	%
	Minimum Surface Size (Relative to Base)	0.1	%
	Surface Growth Rate	1.1	-
Prism Layer Mesh	Number of Prism Layers	8	-
	Prism Layer Stretching	1.5	-
	Prism Layer Total Thickness	$4.66{\cdot}10^{-4}$	m
	y+	1.56	-

Table 4.4: Meshing parameters.[OE]

The mesh regarding the flatter rotor airfoil (Rotor 2) contains 170 865 cells. The same meshing parameters values have been used. All the meshes that have been generated for the rest of the analysis are also set with the same values as in Table 4.4.

4.5 Mesh Pictures

In this section some figures of the final mesh for the Rotor 1 case are shown. Figure 4.13 shows a global view of the mesh. It can be effortlessly distinguished the block generated with the Volumetric Control that comprises the rotor and the stator stage. In Figure 4.14 a close up of the airfoils is presented. It can be seen the Surface Control previously defined that enables that the cells near the boundary layer acquire lower sizes. Finally, Figure 4.15 shows the prism layer.

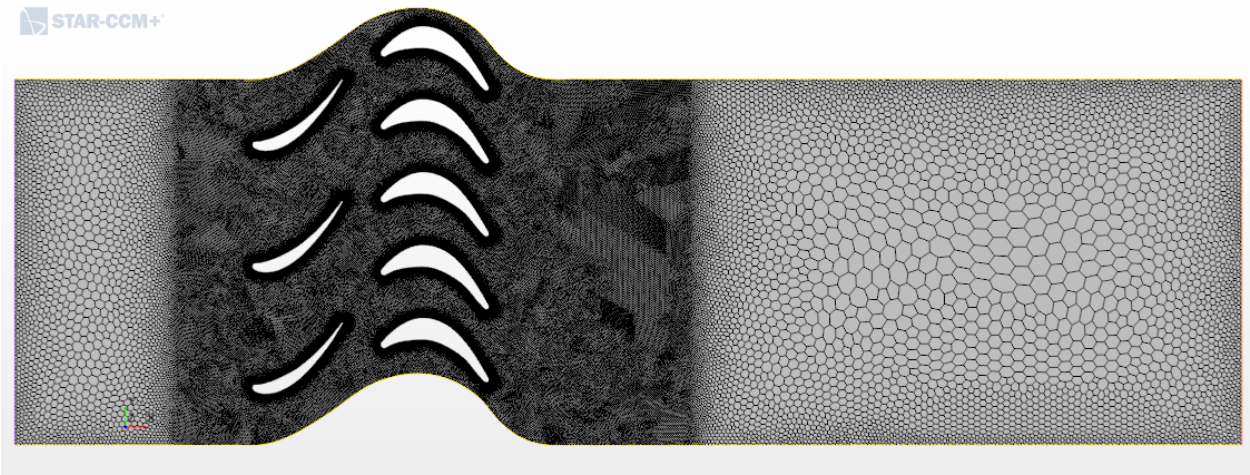

Figure 4.13: Final mesh obtained with STAR CCM+.[OE]

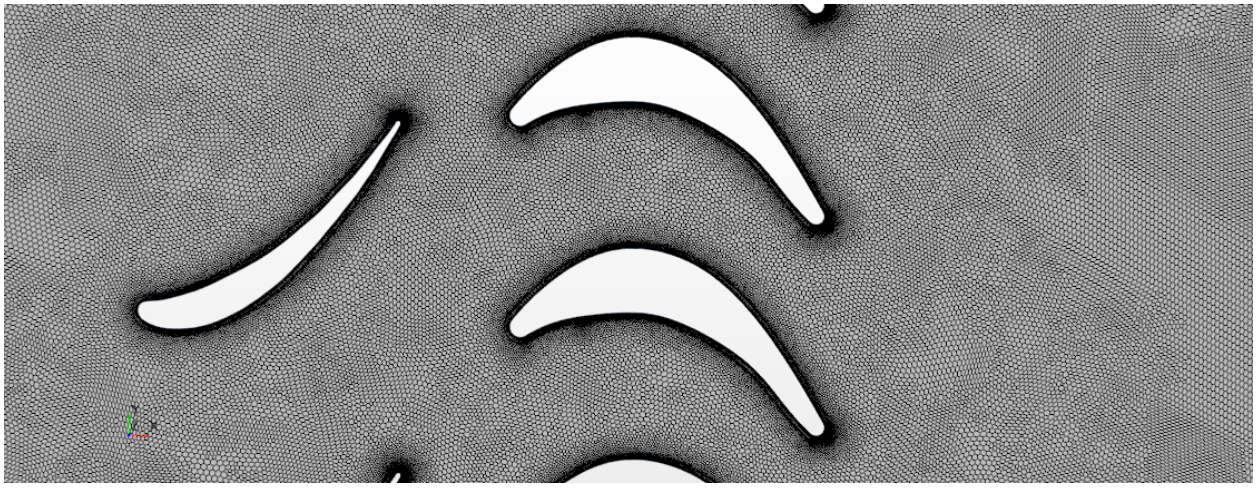

Figure 4.14: Final mesh close up.[OE]

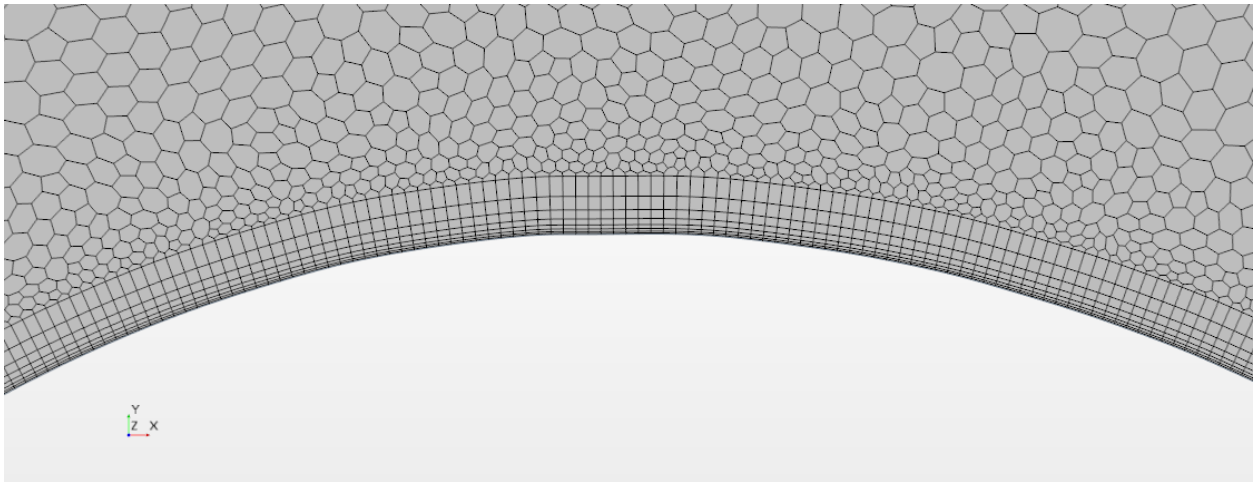

Figure 4.15: Prism layer.[OE]

Finally, it can be concluded that the designed mesh is a good quality one so the study can performed on it.

5. CFD Methodology

Once the geometry design and the mesh are set, the last step in the pre-processing is the definition of the problem, Figure 5.1. This last step involves the physical models selection and the definition of the boundary conditions applied in order to compute the solution. Nevertheless, some important concepts regarding the posterior solver procedure must be previously introduced for a better understanding of the future physical models that will be required.

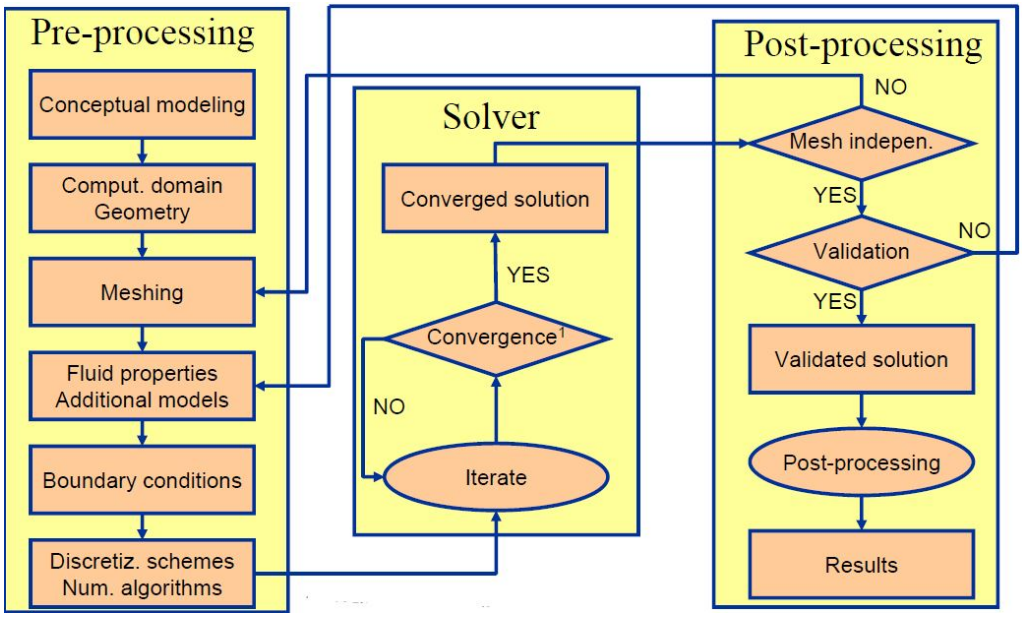

Figure 5.1: CFD simulation process.[25]

5.1 Finite Volume Method and Equations

There are four techniques for numerical solution calculation: finite difference, finite volume, finite element and spectral methods. The CFD software STAR CCM+ employs the finite volume method. This method is based on the integral form of the conservation equations of the fluid flow. The discretization of these equations leads to an algebraic system of equations, which is solved by some iterative process.

The control volume integration enables the conservation of the relevant properties for each finite cell. Therefore, the relationship between the numerical algorithm and the underlying physical conservation principle makes this method easier to understand to the engineers that the other two and makes it more attractive. [27]

The conservation of a general flow variable is expressed as the balance between the processes that tend to increase it and the ones that decrease the variable, Figure 5.2.

$$\begin{bmatrix} Rate\ of\ change \\ respect\ to\ time \end{bmatrix} = \begin{bmatrix} Net\ rate\ of \\ increase\ due \\ to\ convection \end{bmatrix} + \begin{bmatrix} Net\ rate\ of \\ increase\ due \\ to\ diffusion \end{bmatrix} + \begin{bmatrix} Net\ rate \\ of\ creation \end{bmatrix}$$

Figure 5.2: Conservation of a general flow variable.[28]

This balance is applied to the governing equations of the flow of a compressible Newtonian fluid, which are a mathematical representation of the conservation laws of physics. These equations include (stated in their integral form):

- Mass conservation (continuity) equation, which states that the rate of increase of mass in a fluid element is equal to the net rate of flow of mass into the fluid element, Equation 5.1.

$$\frac{\partial}{\partial t}\iiint_{V_c} \rho dV + \iint_{S_c} \rho \mathbf{u} \cdot d\mathbf{A} = 0 \tag{5.1}$$

- Momentum equation, which states that the rate of increase of momentum of a fluid element equals the sum of forces on a fluid element (surface and body forces), Equations 5.2, 5.3 and 5.4.

$$\frac{\partial}{\partial t}\iiint_{V_c} \rho u dV + \iint_{S_c} \rho u \mathbf{u} \cdot d\mathbf{A} = \iint_{S_c} \Gamma_\mu \nabla u \cdot d\mathbf{A} + \iiint_{V_c} S_x dV \tag{5.2}$$

$$\frac{\partial}{\partial t}\iiint_{V_c} \rho v dV + \iint_{S_c} \rho v \mathbf{u} \cdot d\mathbf{A} = \iint_{S_c} \Gamma_\mu \nabla v \cdot d\mathbf{A} + \iiint_{V_c} S_y dV \tag{5.3}$$

$$\frac{\partial}{\partial t}\iiint_{V_c} \rho w dV + \iint_{S_c} \rho w \mathbf{u} \cdot d\mathbf{A} = \iint_{S_c} \Gamma_\mu \nabla w \cdot d\mathbf{A} + \iiint_{V_c} S_z dV \tag{5.4}$$

- Energy equation which states that the rate of increase of energy of a fluid element is equal to the net rate of heat added to the element and the net rate of work done on it, Equation 5.5

$$\frac{\partial}{\partial t}\iiint_{V_c} \rho e dV + \iint_{S_c} \rho e \mathbf{u} \cdot d\mathbf{A} = \iint_{S_c} \Gamma_k \nabla T \cdot d\mathbf{A} + \iiint_{V_c} S_e dV \tag{5.5}$$

5.2 Models and Boundary Conditions

5.2.1 Model Set-Up

There are several physical models available in STAR CCM+. Its selection depends on the type of study performed and the characteristics it requires. A summary of the models selected and the argumentation of its selection are shown below in the order they have been selected.

- **Two Dimensional**

As was proposed at the beginning of the document, for the study of a turbine stage, a 2D domain provides accurate solutions when talking about rotor-stator interaction and shock wave development. So a 2D study is appropriate for the analysis of the influence of the geometry on the aerodynamic efficiency of a turbine stage.

- **Steady**

The study of the flow development between the stator and the rotor can be performed initially as an steady case if a constant rotation of the turbine is assumed. The unsteady phenomena that could appear, like buffeting, cannot be predicted with this study, but the cases that are more favourable to having it can be distinguished, so further studies involving unsteady simulations should be done on them. Moreover, the computational cost required for an unsteady simulation is such great that would have made impossible to perform this study with the resources that a laptop computer offers. Therefore the steady simulation is valid for the aim of the project.

In addition, for simplicity, the rotation of the rotor blades has not been simulated.

- **Gas**

The outgoing gases from the combustion chamber can contain some fuel particles. Nevertheless, the majority of the composition exiting from it is in gaseous form. Thus, gas model is selected.

- **Ideal Gas**

The behaviour of the gases involved in this expansion process can be considered as ideal. This model enables the calculation of any desired value of pressure and temperature at any point of the axial turbine by the simple application of isentropic relations and the state equation of the ideal gases.

- **Coupled Flow**

Segregated (pressure-based) and coupled (density-based) flow models differ in the way they solve the conservation equations of mass, momentum, and energy. While the segregated solver solves these equations sequentially, the coupled model solves them simultaneously using a pseudo-time-matching approach. Furthermore, the segregated model was designed for incompressible flows while the coupled one was designed for compressible flows.[28]

Gases can be treated as incompressible for Mach numbers under 0.3. In the further subsection a more detailed exposition of the conditions of the problem is shown, but if it is considered an outlet combustion chamber temperature, T, of 990 K and a possible inside channel speed, u, of 390 m/s, assuming the ideal gas consideration (constant of ideal gases, R, of 286 and ratio of specific heat, γ, 1.4), the mach number obtained is around 0.6 as can be seen in Equation 5.7. Therefore, the need of using a density-based model arises.

$$a = \sqrt{\gamma \cdot R \cdot T} \tag{5.6}$$

$$M = \frac{u}{a} = 0.62 \tag{5.7}$$

- **Turbulent**

The Reynolds number of a flow compares the relative importance of the inertia forces with respect to the viscous ones. It has been experimentally proved that if the flow remains under a so called critical Reynold number, Re_{cr}, the flow is described as smooth and the adjacent layers of fluid slide past each other in an orderly manner. This regime is called laminar. While the flow is in this regime, it is governed by the flow equations mentioned above (Equations 5.1, 5.2, 5.3, 5.4 and 5.5).

Once the flow surpasses the Re_{cr} it transforms into a chaotic and random state called turbulent regime. In this regime the flow properties change continuously with time across some temporal and length scales, being interconnected and interacting in a dynamically complex way. The threshold to determine transition from laminar to turbulent flow, Re_{cr}, depends on the application and the characteristic length. In this project it is expected to obtain important flow interactions between the stator and the rotos channel, therefore, turbulent flow will appear.

The importance of the turbulence in the engineering applications has made that several numerical methods were developed in order to calculate its effects. These methods can be grouped in three categories: DNS (Direct Numerical Simulation) which solves all turbulent scales and has a high computational cost, SRS (Scale-Resolving Simulations) in which only big scales are solved and the small ones are modeled, it has high computational cost too, and RANS (Reynolds Average Simulations) in which all turbulent scales are modeled and has lower computational cost.

The turbulent numerical method employed by STAR CCM+ when selecting turbulence is directly RANS. In this method the attention is focused on the mean flow and the effects of the turbulence on its properties. In RANS before the application of numerical methods the Navier–Stokes equations are time averaged. Therefore, extra terms appear in the time-averaged flow equations due to the interactions between various turbulent fluctuations. These extra terms are modelled with turbulence models such as k-ϵ model, k-ω model, Spalart-Allmaras model or Reynolds stress model.

The equations solved by RANS model are the previous ones but now taking into account fluctuations (the overbar indicates a time-averaged variable and the tilde indicates a density-weighted variable):

- Continuity equation

$$\frac{\partial \overline{\rho}}{\partial t} + \nabla \cdot \left(\overline{\rho} \tilde{\mathbf{U}} \right) = 0 \tag{5.8}$$

- Reynolds equations

$$\frac{\partial \left(\overline{\rho} \widetilde{U} \right)}{\partial t} + \nabla \cdot \left(\overline{\rho} \widetilde{U} \widetilde{\mathbf{U}} \right) = -\frac{\partial \overline{P}}{\partial x} + \nabla \cdot \left(\mu \nabla \widetilde{U} \right) + \left[-\frac{\partial \overline{\left(\overline{\rho} u'^2 \right)}}{\partial x} - \frac{\partial \overline{\left(\overline{\rho} u' v' \right)}}{\partial y} - \frac{\partial \overline{\left(\overline{\rho} u' w' \right)}}{\partial z} \right] + S_{M,x} \tag{5.9}$$

$$\frac{\partial\left(\overline{\rho}\widetilde{V}\right)}{\partial t}+\nabla\cdot\left(\overline{\rho}\widetilde{V}\widetilde{\mathbf{U}}\right)=-\frac{\partial\overline{P}}{\partial y}+\nabla\cdot\left(\mu\nabla\widetilde{V}\right)+\left[-\frac{\partial\overline{(\overline{\rho}u'v')}}{\partial x}-\frac{\partial\overline{\left(\overline{\rho}v'^{2}\right)}}{\partial y}-\frac{\partial\overline{(\overline{\rho}v'w')}}{\partial z}\right]+S_{M,y} \tag{5.10}$$

$$\frac{\partial\left(\overline{\rho}\widetilde{W}\right)}{\partial t}+\nabla\cdot\left(\overline{\rho}\widetilde{W}\widetilde{\mathbf{U}}\right)=-\frac{\partial\overline{P}}{\partial z}+\nabla\cdot\left(\mu\nabla\widetilde{W}\right)+\left[-\frac{\partial\overline{(\overline{\rho}u'w')}}{\partial x}-\frac{\partial\overline{(\overline{\rho}v'w')}}{\partial y}-\frac{\partial\overline{\left(\overline{\rho}w'^{2}\right)}}{\partial z}\right]+S_{M,z} \tag{5.11}$$

- Scalar transport equation

$$\frac{\partial\left(\overline{\rho}\widetilde{\Phi}\right)}{\partial t}+\nabla\cdot\left(\overline{\rho}\widetilde{\Phi}\widetilde{\mathbf{U}}\right)=\nabla\cdot\left(\Gamma_{\Phi}\nabla\widetilde{\Phi}\right)+\left[-\frac{\partial\overline{(\overline{\rho}u'\varphi')}}{\partial x}-\frac{\partial\overline{(\overline{\rho}v'\varphi')}}{\partial y}-\frac{\partial\overline{(\overline{\rho}w'\varphi')}}{\partial z}\right]+S_{\Phi} \tag{5.12}$$

- **Spalart-Allmaras**

When the decomposition is applied to Navier-Stokes equation an extra term known as the Reynolds Stress Tensor arises and a modelling methodology is needed to close the equations. The available models in STAR CCM+ were the four above mentioned (k-ϵ, k-ω, Spalart-Allmaras and Reynolds stress). From these four the Spalart-Allmaras turbulence model has been selected.

It is a simple one-equation model which solves a modelled transport equation for kinematic eddy viscosity parameter ν. It was designed for aerospace applications, specially for external aerodynamic flows. The model has been proved to give good performance in boundary layers that present adverse pressure gradients, thus on predicting stalled flows. Its appropriateness to airfoil applications has made the Spalart-Allmaras model an attractive turbulence model for simple turbomachinery purposes.[27]

The fact that only one transport equation is solved, gives this model and advantage over the k-ω and SST k-ω models which will also be very effective at this application but involve a higher computational effort. Moreover, its specifically development for aerospace applications has also contributed to its election.

In references [29], [30] and [31] the validity of its application in turbomachinery can be observed.

5.2.2 Boundary Conditions

In order to run the simulations some boundary conditions need to be applied on the geometrical boundaries. The selected conditions are the following ones:

- **Wall**

The wall boundary option is set for the rotor and stator blades since they must be impermeable to the fluid. Therefore, no flow crosses inside them acting as an obstacle to the fluid displacement.

- **Stagnation Inlet**

The stagnation inlet option is a pressure inlet option. It is applied at the entry of the domain, left-hand side, Figure 5.3. In this boundary condition the flow direction must be specified together with the total pressure and total temperature at the inlet.

- **Pressure Outlet**

The pressure outlet is set at the end of the domain, right-hand side, Figure 5.3. This condition asks for the static pressure and static temperature at the outlet. A static pressure value has been introduced, however the static temperature has been set as a field function that the program calculates in each iteration. This gives the velocity solution an extra degree of freedom. Furthermore, the non-reflecting mode specification has been set. This option prevents spurious numerical reflection of the solution into the solution domain. This function is activated in order not to obtain convergence problems arising due to the shock waves that could appear.

- **Periodic Interface**

Finally, for the top and bottom boundaries a periodic internal interface has been created. This interface allows to simulate a turbine stage with a reduced number of blades. The flow entering at the bottom boundary will give the flow exiting at the top all its properties (velocity, pressure, temperature), simulating that the upper and lower geometrical limits are not bounded. It must be highlighted that this option will only be applicable if the top and bottom boundaries are geometrically equal.

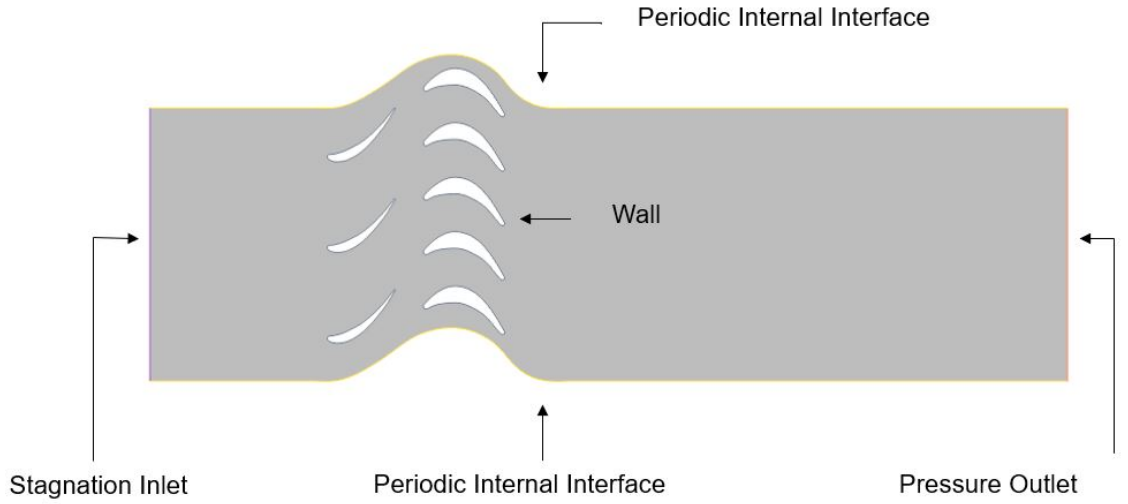

Figure 5.3: CFD boundaries disposition.[OE]

Some usual values of pressures and temperatures at the turbine inlet have been extracted from reference [20] and have been used as reference for Case 1, see Table 5.1. Moreover, at reference [13] it is said that typical pressure ratios (inlet to exit) across a turbine stage are around two. Therefore, with isentropic relations (Equation 5.13) and assuming an inlet Mach number of 0.4, a little bit lower than the one before (0.62), and γ of 1.4 as before, an approximation of the value of the stagnation inlet pressure is calculated. Then, the inlet to exit ratio is obtained, Equation 5.14. It is confirmed that the value is around

two. Thus, for the part of the study in which the same geometry is analysed but with a different pressure drop for the stage, it has been decided to analyse lower pressure ratios.

$$P_{Si} = P_{Ti} \cdot \left(1 + \frac{\gamma - 1}{2} \cdot M^2\right)^{\frac{-\gamma}{\gamma - 1}} \tag{5.13}$$

$$Stagnation \quad Pressure \quad Ratio = \frac{P_{Si}}{P_{Sf}} \tag{5.14}$$

Case	Total Inlet Temperature (K)	Total Inlet Pressure (Pa)	Stagnation Outlet Pressure (Pa)	Approx. Stagnation Inlet Pressure (Pa)	Stagnation Pressure Ratio
1	990	214 145	89 891	191 791	2.13
2	990	214 145	130 000	191 791	1.47
3	990	214 145	170 000	191 791	1.12

Table 5.1: CFD simulation values.[OE]

It must be highlighted the fact that calculations appearing on Table 5.1 are just approximations, and that the stagnation inlet pressure will vary with the variation of the outlet stagnation pressure due to variations in Mach number, however it is a good initial approximation. For the part of the study in which some geometric parameters have been modified, Case 2 has been used as base data. In all the simulations the flow has a 0^o inlet angle, thus, going in the X direction.

6. Results

In this chapter the obtained results are analysed. As was introduced at Section 1.2, this project can be divided in different parts in which the shock wave development, the rotor-stator interaction and the isentropic efficency variations are studied.

- In the first part, the geometry that involves Rotor 1 is analysed. The static outlet pressure is incremented in order to obtain lower static pressure ratios. Therefore three cases are simulated, as was shown on Table 5.1.

- In the second part, the same study as before is performed but now a new geometry is involved, the rotor blades are changed to Rotor 2 shape. Again the three simulated cases are are the ones appearing on Table 5.1. The aim of this second case is to compare the differences among the fist initial curved geometry rotor airfoil and a flatter one.

- The next part focuses on the study of the rotor-stator number of blades ratio. The first two studies were analysed using a rotor-stator ratio of 1.67. In this part it is variated to 2.5 and 1 by the variation of the number of stator vanes. Thus, the influence of the number of stator blades, or, in another words, the separation between them, is studied.

- The last part is centered on the comparison of different rotor solidities. Hence, it is changed form 1.55 to 1, the reference value of the bibliography, [13].

6.1 Pressure Ratio Study

This section is intended to analyse the effect that the pressure ratio selection of a stage has on its performance. All the studies may be analysed through tables and images with color contours of different field functions. The figures shown along the whole chapter may present difficulties for those with colorblindness problems, thus, they are presented in suitable colors for them at Appendix A.

6.1.1 Pressure Ratio Study of Case 1

If looking at Figures 6.1 and 6.2, the Mach contour images of Case 1 can be observed. Figure 6.3 shows the pressure coefficient (c_p) along the absolute chord of the rotor located at the middle of the rotor row. For c_p the pressure, density and speed downstream has been set as reference.

Analysing the figures of Case 1, with an static pressure drop of 1.12 Bar, it can be seen how the combustion chamber outcoming gases (with X direction) are clearly subsonic. The flow is then accelerated in the stator vanes and is redirected to the rotor. It is in this middle region, between the stator an the rotor, where the flow starts having a mach number of 0.7. In this case the rotor-stator interaction is almost null. The only more relevant things is the fact that, as can be seen with the position of the stator vane that is closer to the bottom, in the rotor movement there is a position in which the alignment with the wake of the stator creates a loss pressure zone in the intrados of the rotor blade. However this zone has not a remarkable impact on the rotor performance since all of them

produce the same resutant wake.

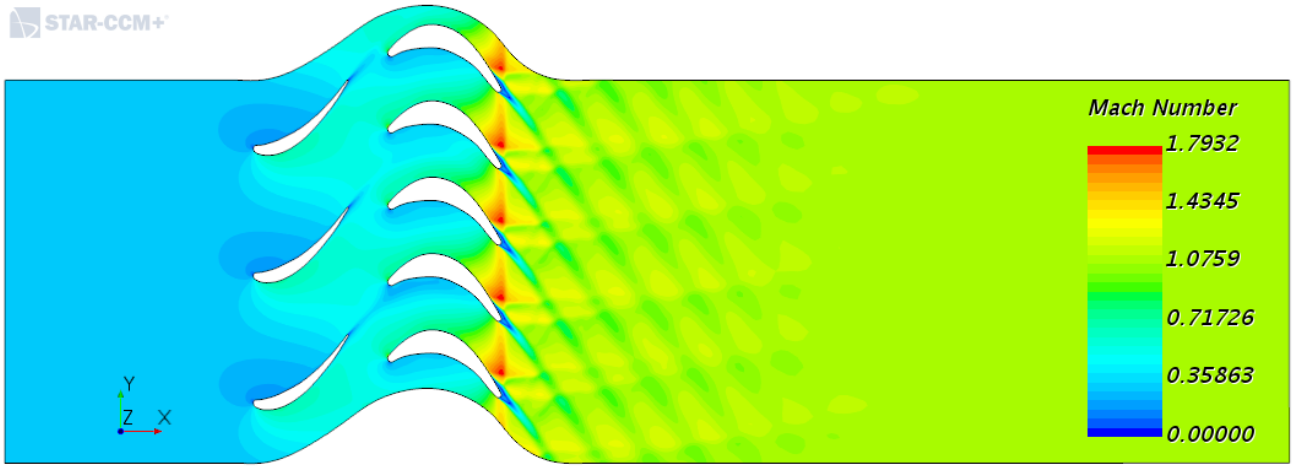

Figure 6.1: Mach number contour of Case 1.[OE]

Then, if focusing on the rotor, it can be seen how the flow follows perfectly its shape. Figure 6.3, shows how the flow after the initial acceletarion at the suction peak suffers a deceleration, however, as seen on Figure 6.2 this does not implies any flow separation.

At the 70% of the chord the flow starts taking supersonic values and at 87% a strong shock wave appears after the Mach has achieved a value 1.79. Then the separation of the flow starts. This separation of the flow after a shock wave means that if fluctuations of pressure on the boundary layer separation occur, buffeting could appear. Thus, it would be interesting to perform an unsteady simulation of this case in further investigations.

Furthermore, the shock wave generated is reflected creating a supersonic wake that will affect the next set of stator vanes.

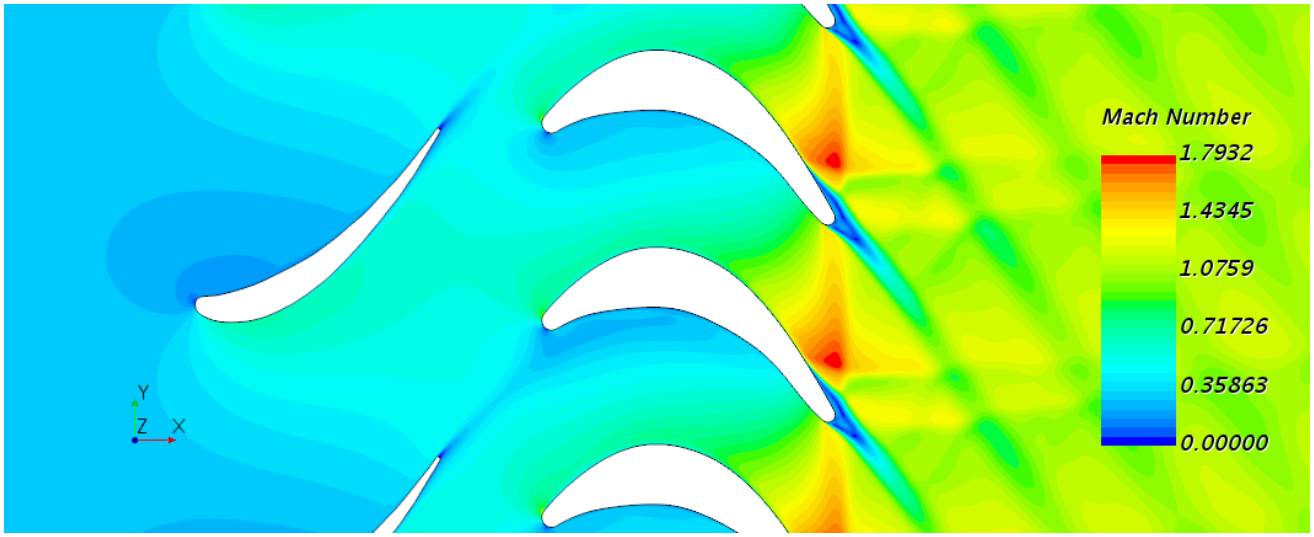

Figure 6.2: Zoom of the Mach number contour of Case 1.[OE]

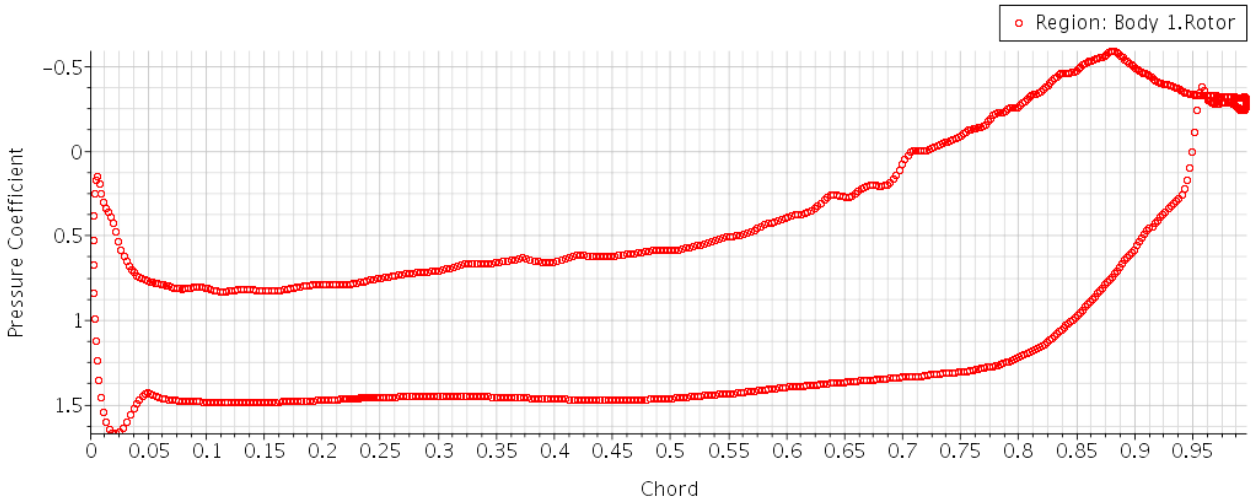

Figure 6.3: Pressure coefficient along the rotor chord for Case 1.[OE]

Since the Mach number and the static pressure drop at the stage obtained (Table 6.1) were big enough, it was decided, as mention in Table 5.1, to increase the static outlet pressure so lower pressure drops and lower Mach numbers could be obtained.

6.1.2 Pressure Ratio Study of Case 2

Figure 6.4 shows the Mach number contour resulting from Case 2 simulation. It must be stood out the fact that the color scale is not the same as before. In this case the static pressure drop has been reduced from 1.12 Bar to 0.72 Bar.

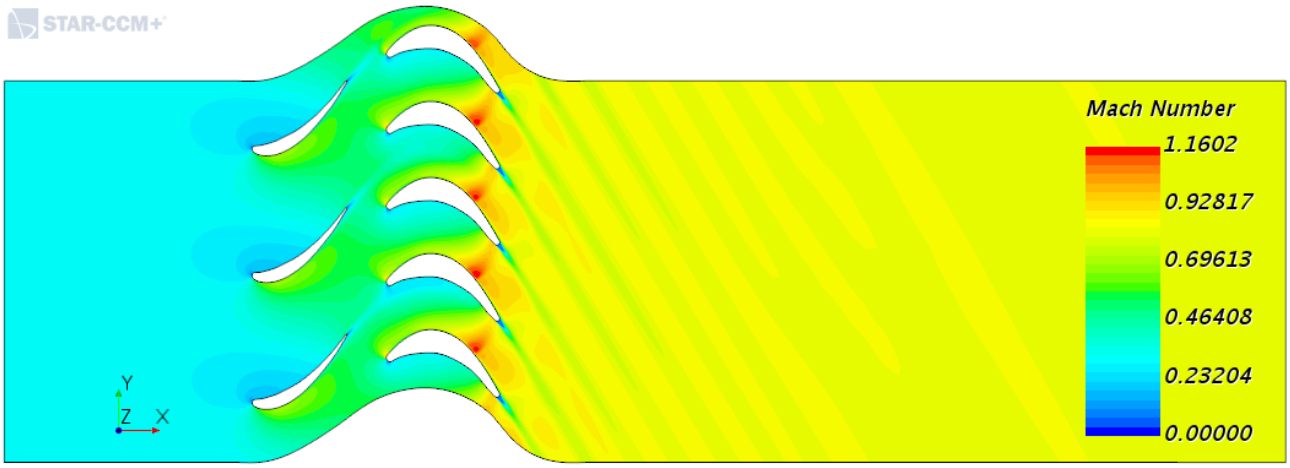

Figure 6.4: Mach number contour of Case 2.[OE]

In the figures obtained for Case 2 it can be seen how the velocity entering the stator is practically the same than in Case 1. This inlet velocity is around Mach 0.3, Figures 6.2 and 6.5. When the value of this velocity is measured half chord before the stator, a value of 184 m/s is obtained in both cases. In Case 2 the flow accelerates in the stator and is directed towards the rotor where again the suction peak is followed by deceleration. This

reduction in pressure is more accused in this case since the c_p plot shows a reduction of 0.6 while in the previous one it has a value of 0.5. This means that the flow has a lower speed after the suction peak.

The lower velocity leads to lower speed values along the airfoil generating a weak shock-wave. Figure 6.5 evidences that the supersonic effects start around 60% of the chord. The flow is accelerated, until 75%, Figure 6.6, where a weak shock wave appears. This shock wave is weaker that the one in Case 1 since the velocity decreases from Mach 1.16 until 0.9, while in Case 1 this reduction was from Mach 1.79 to 1.3. This weak shock wave does not reflect as the previous one neither produces a boundary layer separation, so buffet will never appear.

In addition, the c_p diagram shows that, as happened before, the shock wave affects the last part of the intrados of the upper rotor blade.

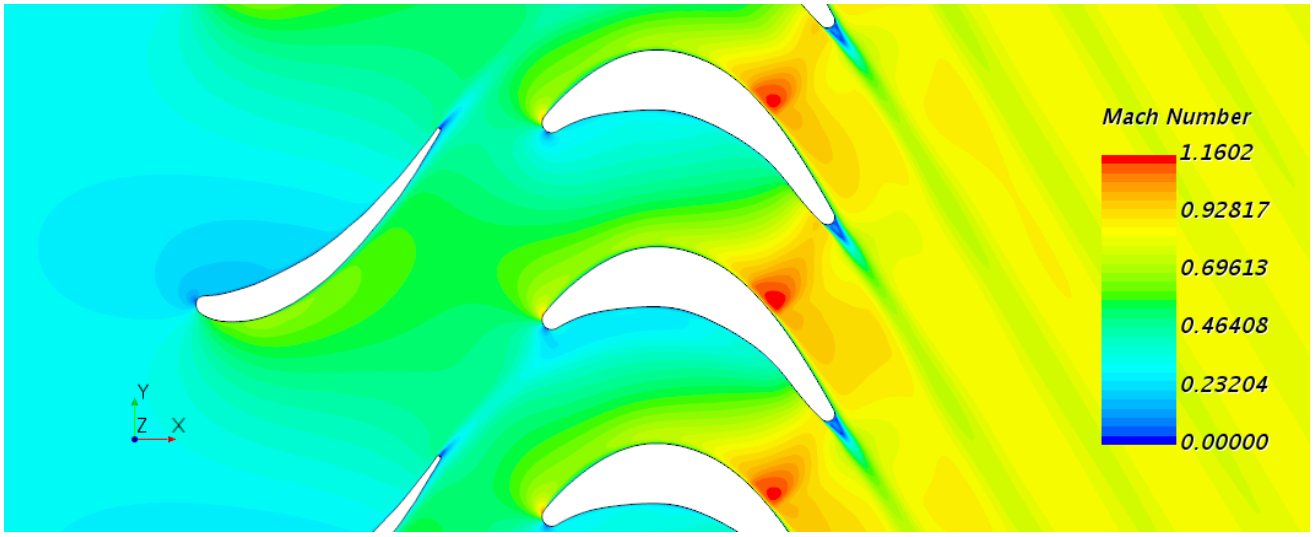

Figure 6.5: Zoom of the Mach number contour of Case 2.[OE]

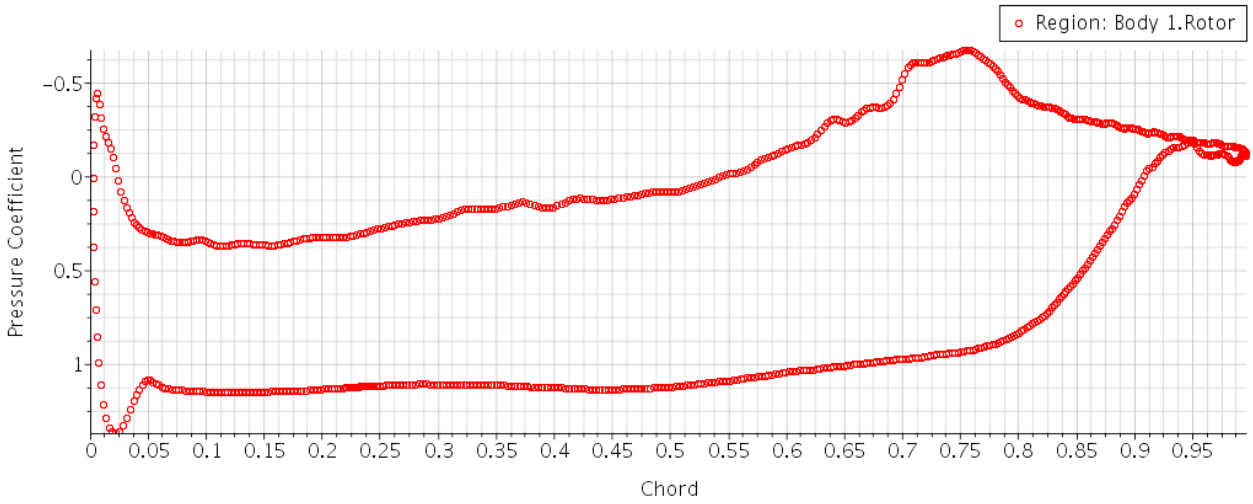

Figure 6.6: Pressure coefficient along the rotor chord for Case 2.[OE]

6.1.3 Pressure Ratio Study of Case 3

In the last case, Case 3, the static pressure at the exit is increased to 170 000 Pa, Table 5.1. If the static pressure drop is reduced to 0.35 Bar by the increment of the static pressure at the outlet, then, since the total pressure drop is not reduced in a big manner, it results in a decrease in the dynamic pressure that leads to lower velocities and lower Mach numbers, Figure 6.7. Again, pay attention to the scale.

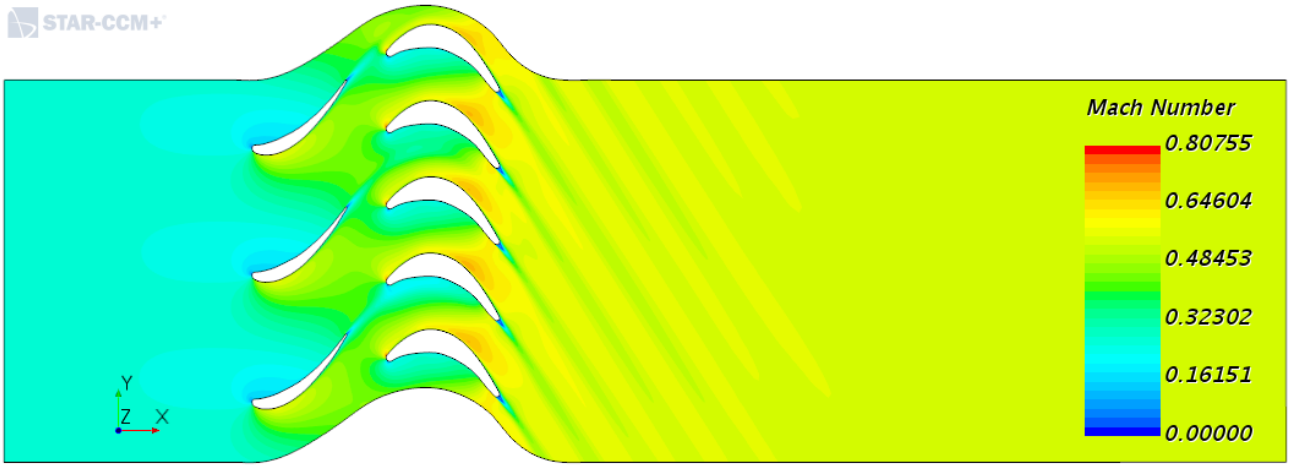

Figure 6.7: Mach number contour of Case 3.[OE]

This case starts with flow at 159 m/s, what means a Mach number around 0.2. Since the inlet value is lower due to the lower pressure difference between the inlet and the outlet, Table 6.1, the stator accelerates the flow only up to Mach number 0.4-0.5. The acceleration suffered at the rotor and the later deceleration has the same magnitude as before, however, since the flow velocity is lower it is not capable of accelerating again to reach sonic conditions. Therefore, in this case no transonic conditions are reached.

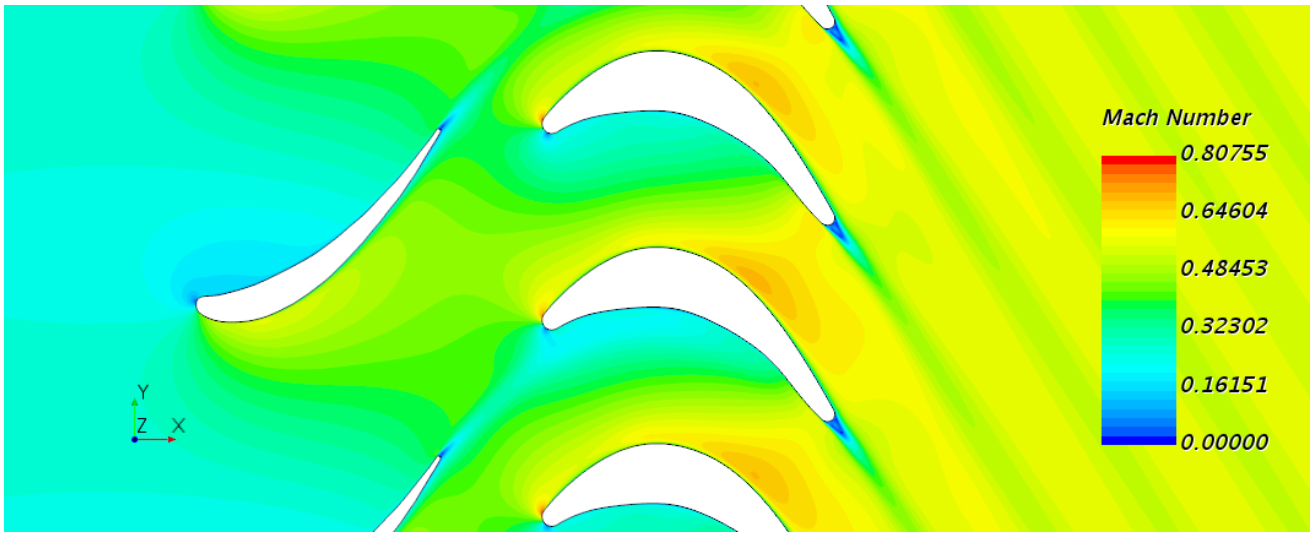

Figure 6.8: Zoom of the Mach number contour of Case 3.[OE]

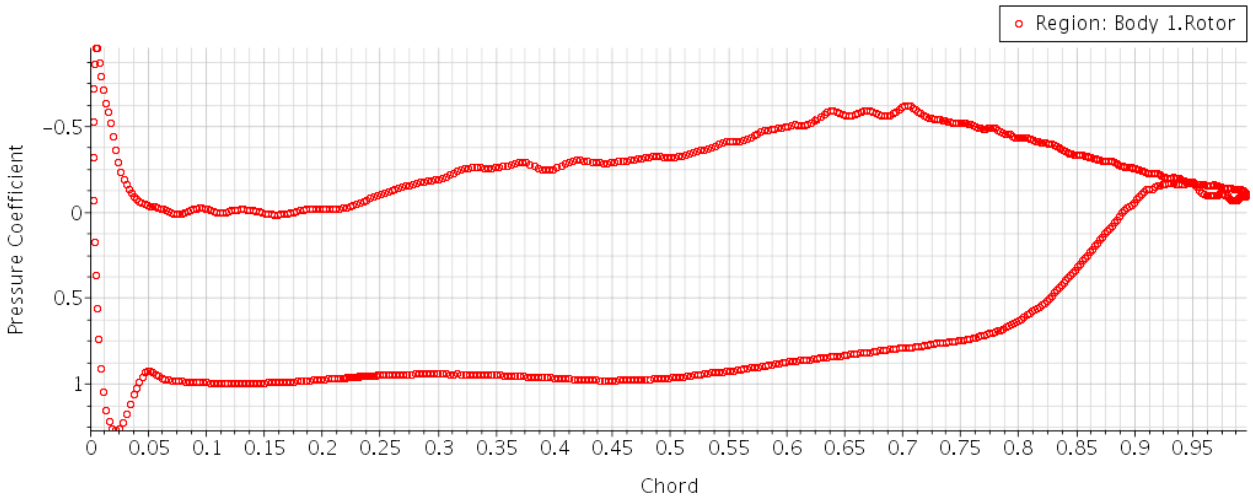

Figure 6.9: Pressure coefficient along the rotor chord for Case 3.[OE]

Table 6.1 shows a summary of some important data collected from these three simulations. One of the principal values analysed, apart form the pressure drop, is the isentropic efficiency of the turbine. This value is the ratio of the work output of the turbine to the work output of it if the process is totally isentropic. It is internally computed by the software and gives an idea of how efficient is the stage aerodynamically talking.

As a result, it can be seen how if the static pressure drop in a stage is too high, Case 1, supersonic conditions are achieved. Thus, shcok waves and boundary layer separation, that can lead to buffet, may appear, repercuting on the isentropic efficiency of the stage.

Per contra, if the pressure drop is too low, as in Case 3, maybe the required work for moving the compressor is not achieved and the velocities are not enough high for ensuring the maximum performance. Moreover, since the pressure drop is too low too many rotor-stator stages will be required along the turbine to achieve the total pressure drop desired. This would increment the weight of the engine which, in aeronautical applications, is a critical parameter that can make the difference between aircraft.

Specially, at some aeronautical applications like fighter aircraft, turbojets are designed only with two or three turbine stages in which high pressure drops are required. Then, even isentropic efficiency is sacrificed in order to obtain the higher expansions in lower stages and then lower engine weights. In this cases higher amounts of fuel are burned to compensate this effect and specially attention must be payed to turbine blade during maintenance.

Case	Static Pressure Ratio	Stage Static Pressure Drop ($Pa \cdot 10^5$)	Stage Total Pressure Drop ($Pa \cdot 10^5$)	Maximum Mach	Isentropic Efficiency (%)
1	2.24	1.12	0.23	1.79	88.37
2	1.55	0.72	0.10	1.16	91.82
3	1.20	0.35	0.05	0.8	90.01

Table 6.1: Rotor 1 simulation results.[OE]

From this study, Case 2 is selected as the best one regarding isentropic efficiency and will

be the basis of posterior studies.

6.2 Rotor Curvature Study

This part of the study focuses on the analysis of the curvature of the rotor. Therefore, in this part, the same geometry as in the last case is simulated but changing the rotor by the airfoil of Rotor 2. It is a flatter airfoil with less curvature what at first sight suggests that lower mach numbers should be reached. Again in this case the three pressure drop cases are simulated.

6.2.1 Rotor 2 Curvature Study of Case 1

The first one can be seen on Figures 6.10 and 6.11, where the Mach number contours are presented. It can be clearly seen how the flow achieves greater values at the stator surface, arriving until mach 0.8 or even 1 in some points while in the previous study, at Case 1 this flow only reached Mach 0.7. The reduced curvature of the new rotor airfoil and the increment of the velocity in the flow coming from the stator generates a strong oblique shock wave at the suction side of the rotor blades that passes form Mach 1.9 to 1.5. Therefore, the rotor-stator interaction is by far more accused than in the previous geometry.

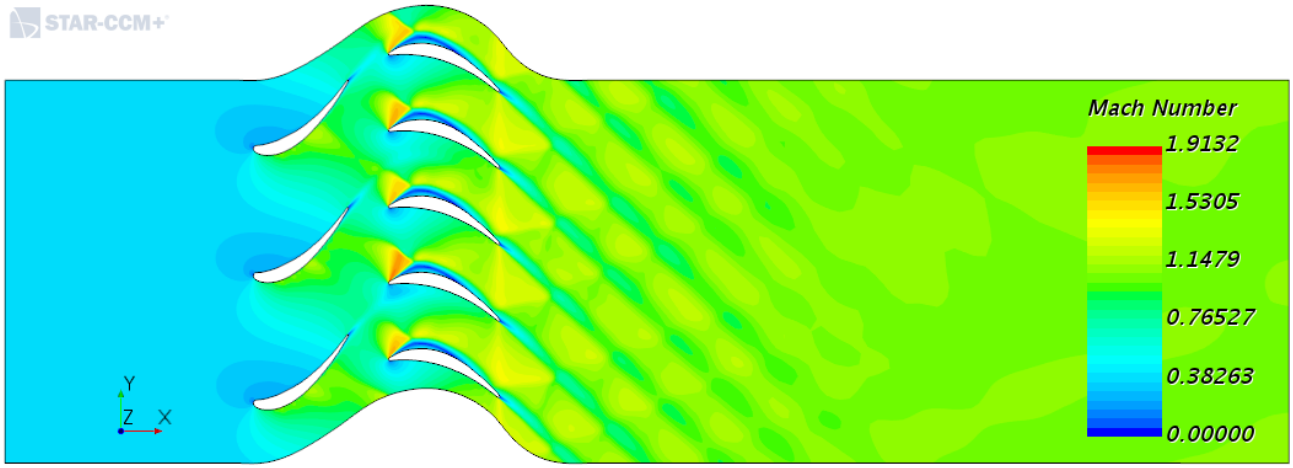

Figure 6.10: Mach number contour of Case 1 for Rotor 2.[OE]

If focusing on Figure 6.11, it is seen how this interaction generates greater stall wake at the trailing edge of the stator. Moreover, the greater velocity incoming in the rotor makes the flow unable to adapt to this new shape after the shock wave and creates a great boundary layer separation, Figure 6.12. However, at about half chord, the separation bubble reattaches due to the interaction with the external high velocity flow. At this last part some sonic conditions are achieved again in the channel due to the fact that the flow sees a thicker airfoil due to the thick boundary layer but no shock waves appear.

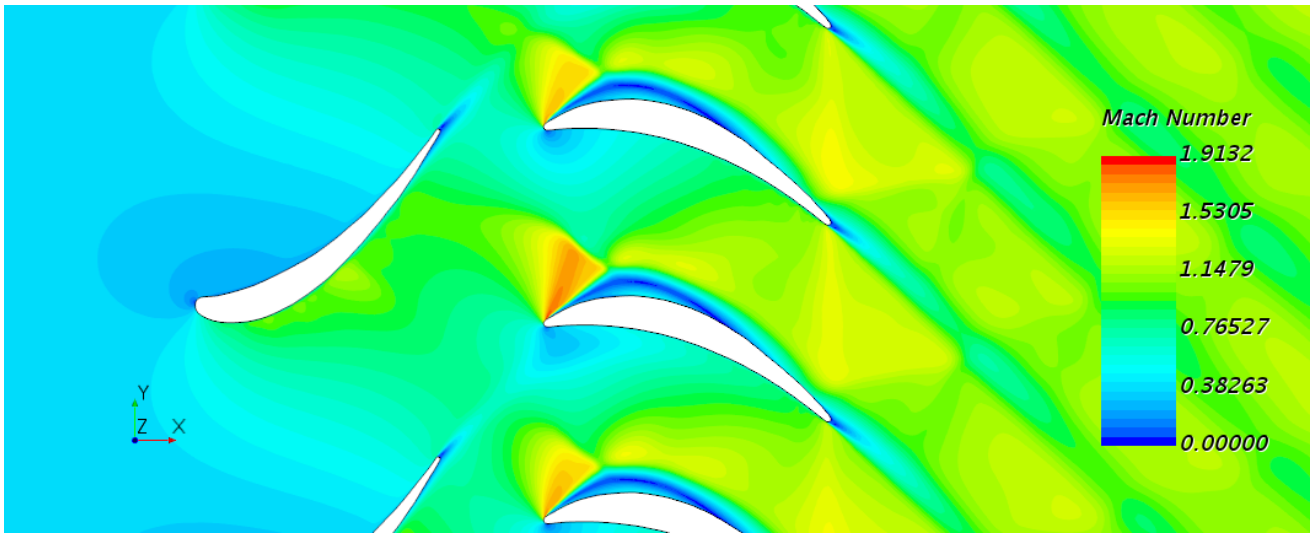

Figure 6.11: Zoom of the Mach number contour of Case 1 for Rotor 2.[OE]

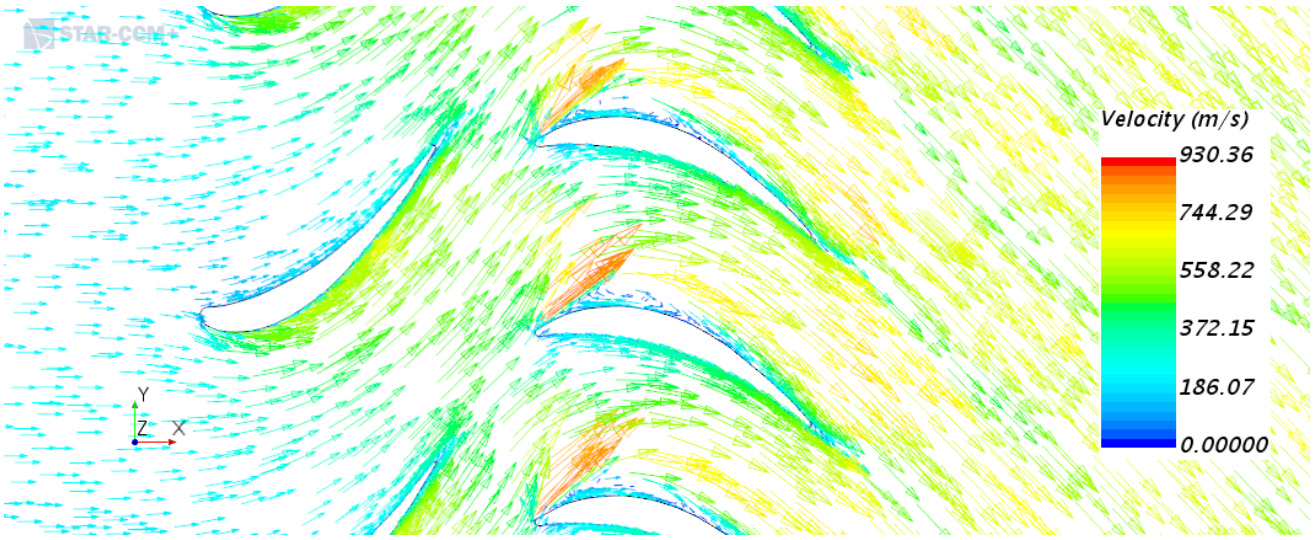

Figure 6.12: Velocity vector contour of Case 1 for Rotor 2.[OE]

Figure 6.12 shows that the flow separation is mostly due to the incoming flow direction, which comes out of the stator almost perpendicular to the chord, at a very high incidence.

The c_p plot, Figure 6.13, is unable to register the initial shock wave due to its position, at the very beginning of the airfoil, and the inmediate boundary layer separation. Moreover, despite the initial difference in pressure between the extrados and intrados, it can be observed that it is rapidly reduced due to the flow separation.

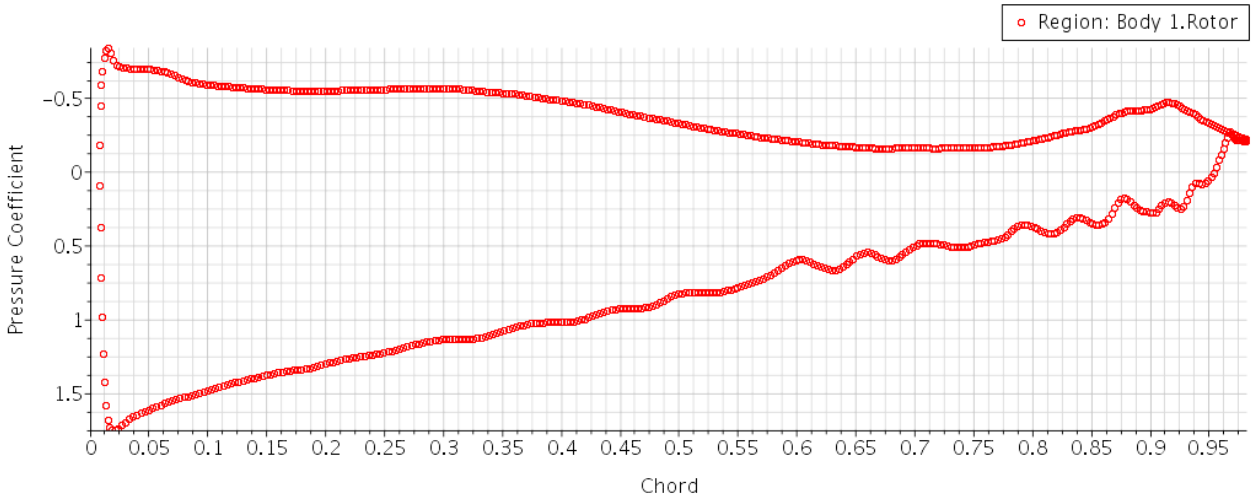

Figure 6.13: Pressure coefficient along the Rotor 2 chord for Case 1.[OE]

6.2.2 Rotor 2 Curvature Study of Case 2

The static pressure at the outlet is increased until 130 000 Pa in order to reduce the static pressure drop from 1.04 Bar to 0.66 Bar. Again, as in Case 1 the rotor-stator in between section achieves transonic speeds. Nevertheless, in this case the rotor-stator interaction is lover due to the lower velocities reached at the suction peak. Now the maximum Mach achieved is 1.34 and the shock wave is less intense.

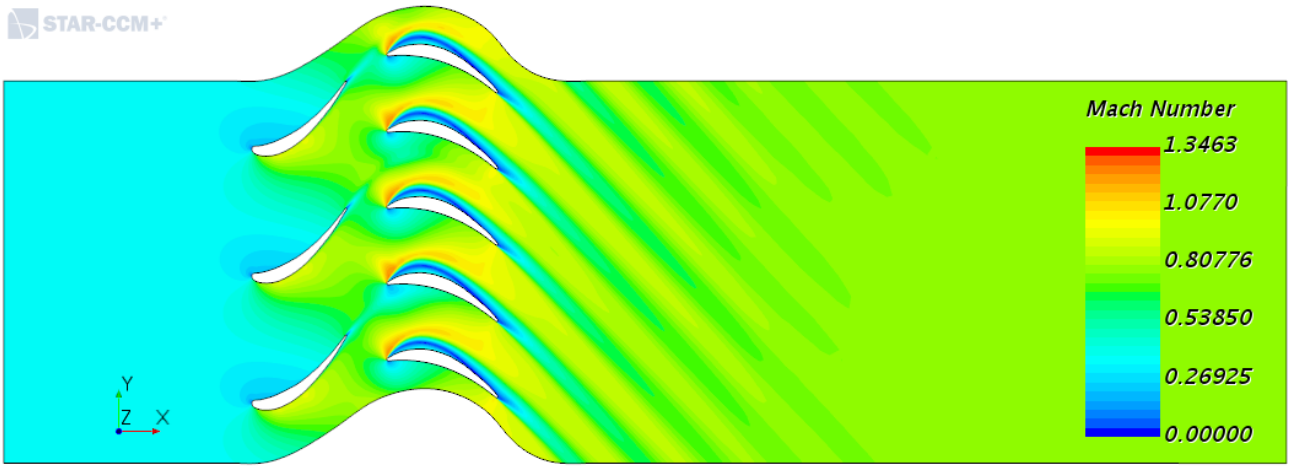

Figure 6.14: Mach number contour of Case 2 for Rotor 2.[OE]

The boundary layer still separates creating a high stall zone all along the extrados. Nevertheless, in Case 2 the flow does not manage to readapt to the airfoil, Figure 6.15, as occurred in Case 1, Figure 6.11. Hence, this geometry shows an inefficient disposition for the incoming flow from the stator that leads to a great stall wake that will seriously affect the next stage of blades.

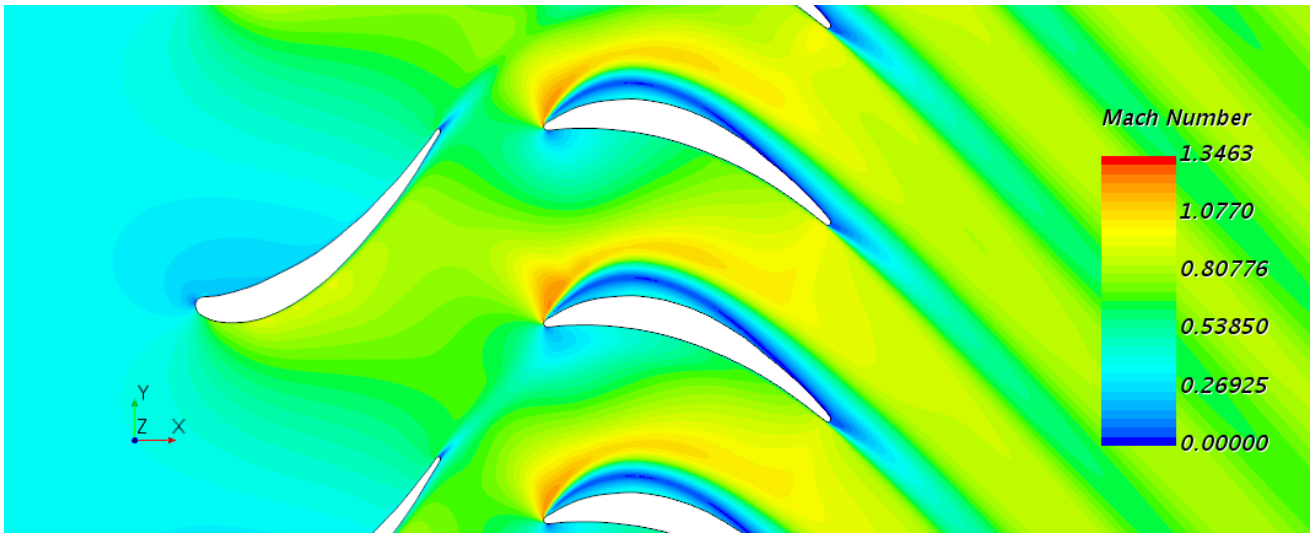

Figure 6.15: Zoom of the Mach number contour of Case 2 for Rotor 2.[OE]

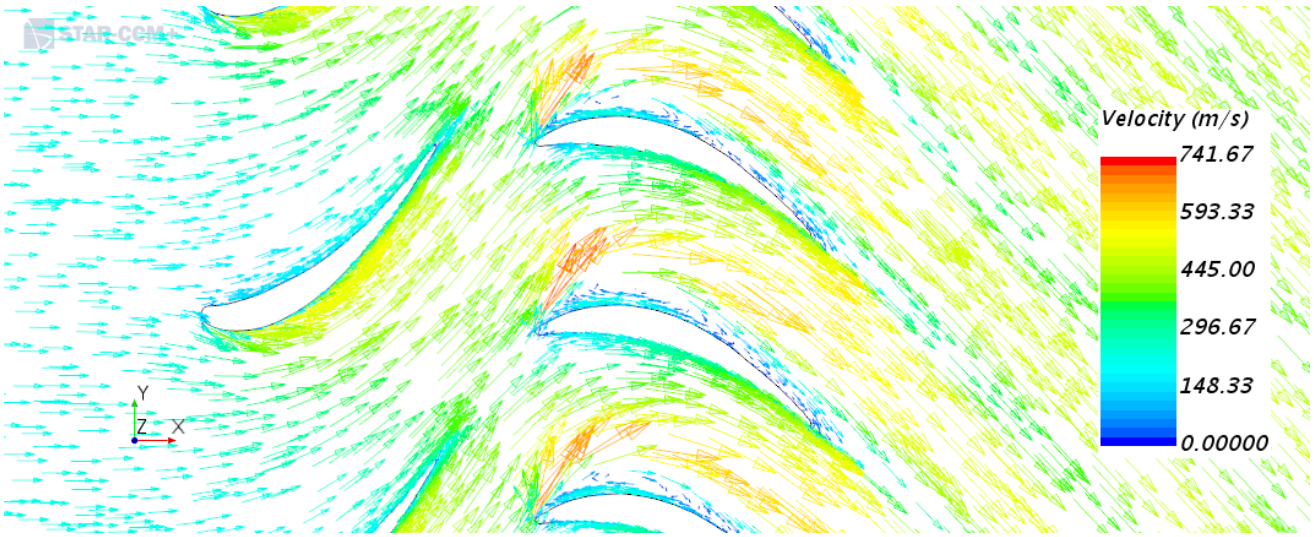

Figure 6.16: Velocity vector contour of Case 2 for Rotor 2.[OE]

Finally, when looking at the c_p plot, it can be observed that in this case since the flow does not adheres to the airfoil pressure remains more or less constant on the extrados, Figure 6.17.

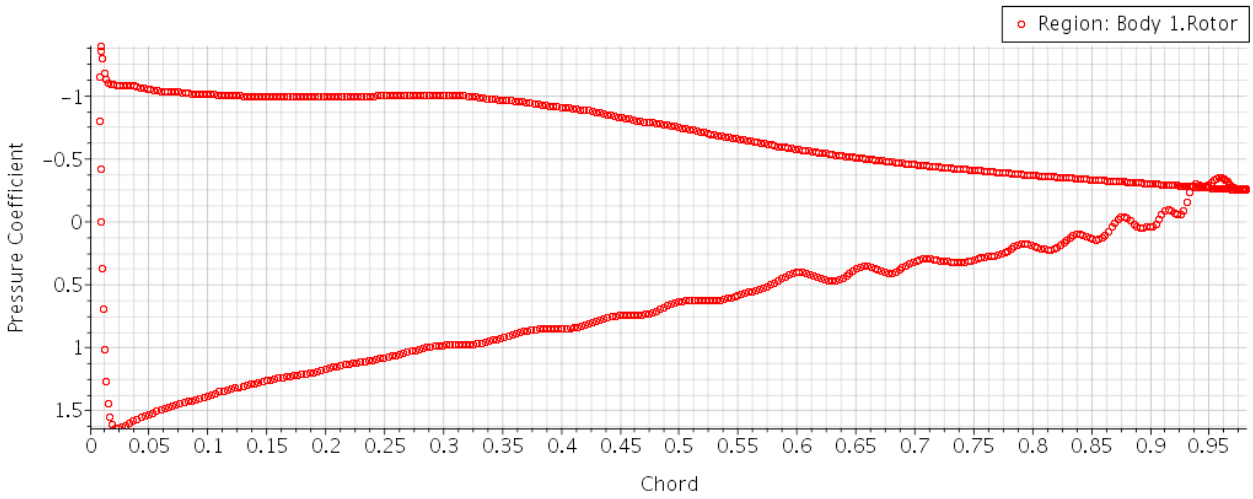

Figure 6.17: Pressure coefficient along the Rotor 2 chord for Case 2.[OE]

6.2.3 Rotor 2 Curvature Study of Case 3

When diminishing even more the pressure drop of the stage, the Mach is globally reduced but the same distributions of c_p and boundary layer separation arise, Figures 6.18, 6.19 and 6.20.

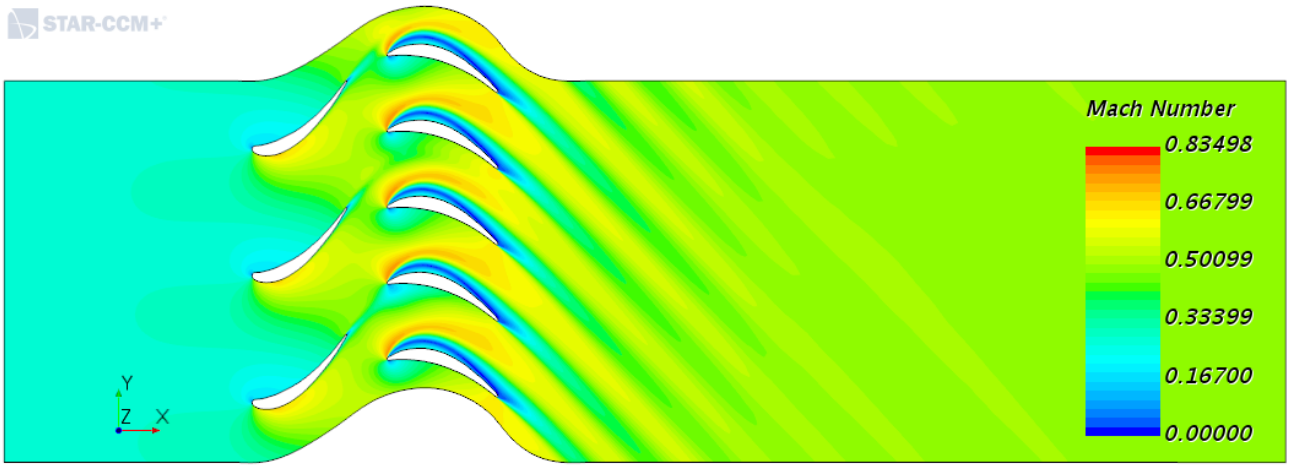

Figure 6.18: Mach number contour of Case 3 for Rotor 2.[OE]

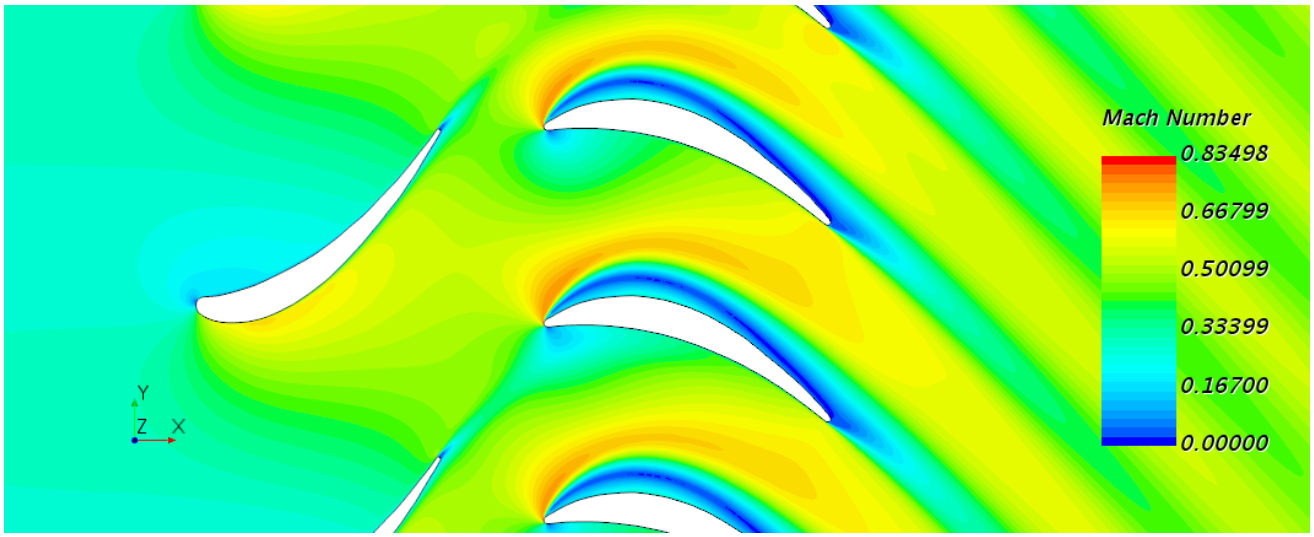

Figure 6.19: Zoom of the Mach number contour of Case 3 for Rotor 2.[OE]

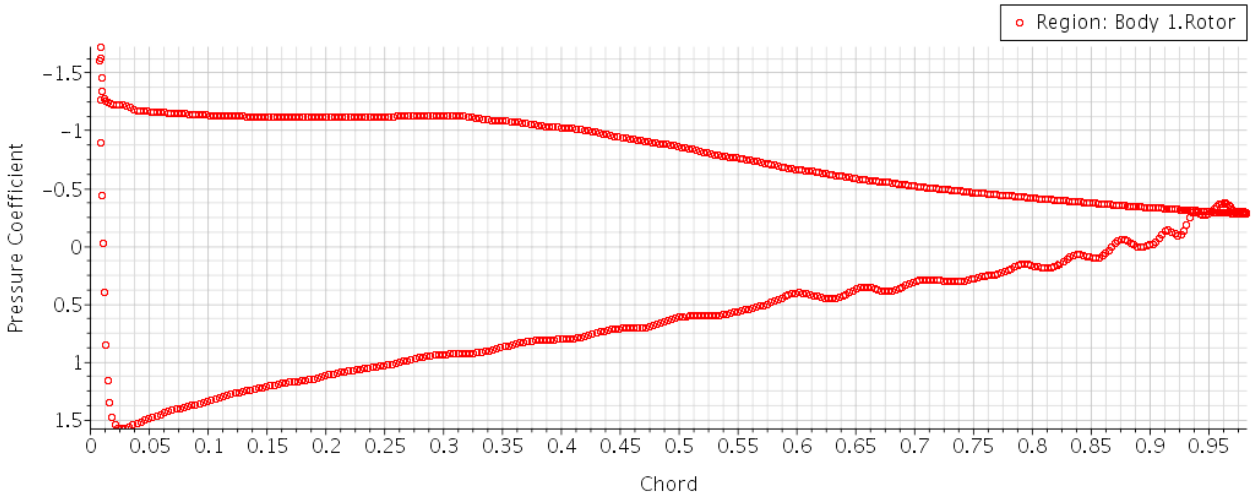

Figure 6.20: Pressure coefficient along the Rotor 2 chord for Case 3.[OE]

Finally, if the results of the three cases are analysed together, some conclusions can be extracted. While in the study involving the Rotor 1, it was Case 2 the most efficient one, in this study it is the Case 1 the one achieving the highest isentropic efficiency. This difference arises from the fact that in the curved rotor case, the efficiency was directly dependant on the shock wave generated at the end of the extrados of the rotor. Therefore, higher velocities involved higer efficiencies until the generation of a strong shock wave. However, in this study the most relevant factor is not the channel choking but the shock-geometry dependency. As can be seen Case 1, the case with the strong shock wave, is more efficient. The reason is that the highest velocities achieved at the shock wave enable that after the initial boundary layer separation the flux readheres to the blade generating a smaller stall wake.

In addition it must be highlighted the fact that in all the three cases that include Rotor 2, the boundary layer separation generates a shape that resembles the Rotor 1 curvature, indicating that a most curved airfoil is needed for an enhancement of the isentropic efficiency. The reason, as mentioned above, is that the flow exiting the stator has a higher

angle than the inlet one of the rotor.

Case	Static Pressure Ratio	Stage Static Pressure Drop ($Pa \cdot 10^5$)	Stage Total Pressure Drop ($Pa \cdot 10^5$)	Maximum Mach	Isentropic Efficiency (%)
1	2.16	1.04	0.29	1.91	85.08
2	1.51	0.66	0.23	1.34	78.27
3	1.19	0.32	0.13	0.83	72.82

Table 6.2: Rotor 2 simulation results.[OE]

6.2.4 Rotated Rotor 2 Curvature Study

This result introduces the a new case generation in which the Rotor 2 is rotated in order to make this inlet angle coincident with the one exiting the stator. For the highest pressure drop case, Case 1, the maximum Mach achieved at the extrados is greater than before, it passes form 1.91 to 2.18 when the rotor is rotated. The rotor-stator interaction becomes more accused and at the trailing edge of the rotor the sonic reflection zones appear with higher intensity, Figures 6.21 and 6.22.

Again the flow separates after the shock wave. It could be thought that it is the shock wave the cause of this adverse pressure zone, however, on the analysis of this geometry for Case 3, Figures 6.23 and 6.24, it can be clearly seen that the boundary layer separation is caused by the lack of curvature of the profile and the high angle of attack of the flow incoming the rotor. Therefore, since Case 2 does not contributes with any new conclusion, it has been decided not to show it but in Table 6.3.

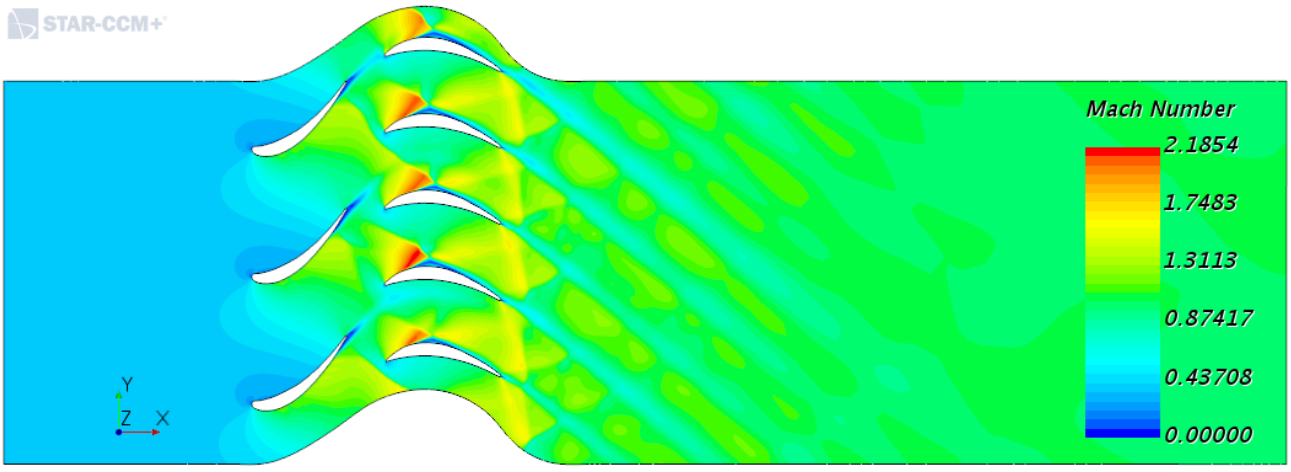

Figure 6.21: Mach number contour of Case 1 for Rotor 2 rotated.[OE]

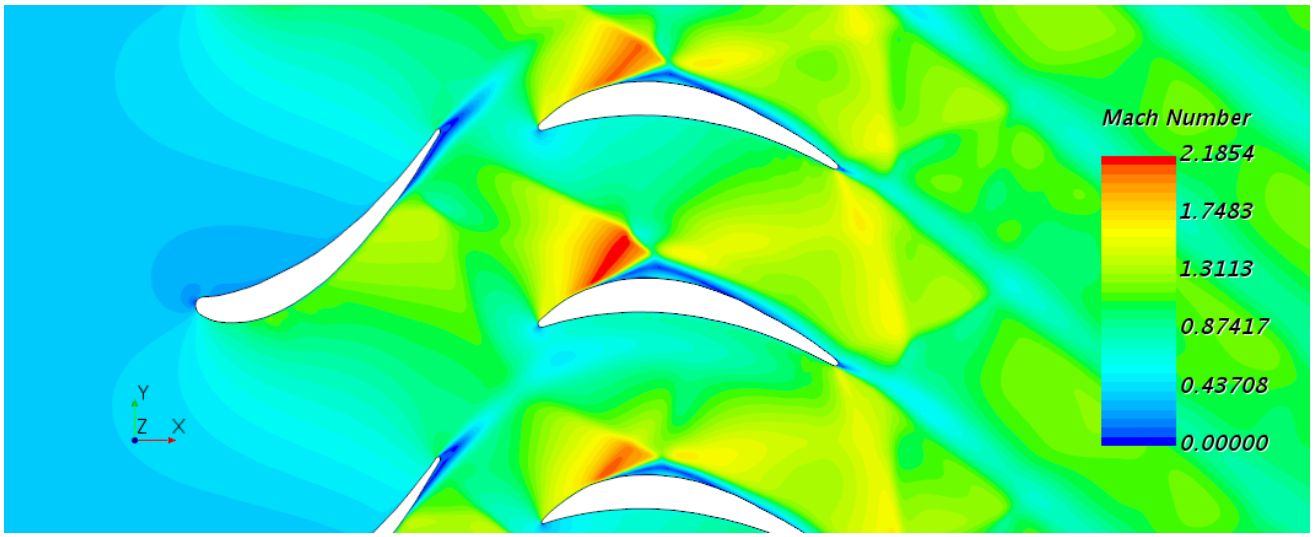

Figure 6.22: Zoom of the Mach number contour of Case 1 for Rotor 2 rotated.[OE]

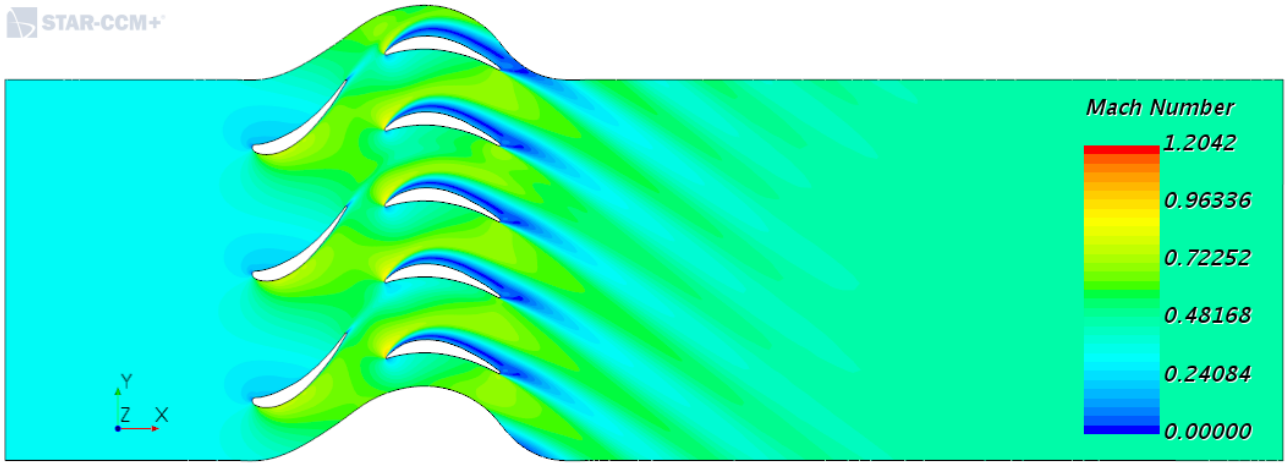

Figure 6.23: Mach number contour of Case 3 for Rotor 2 rotated.[OE]

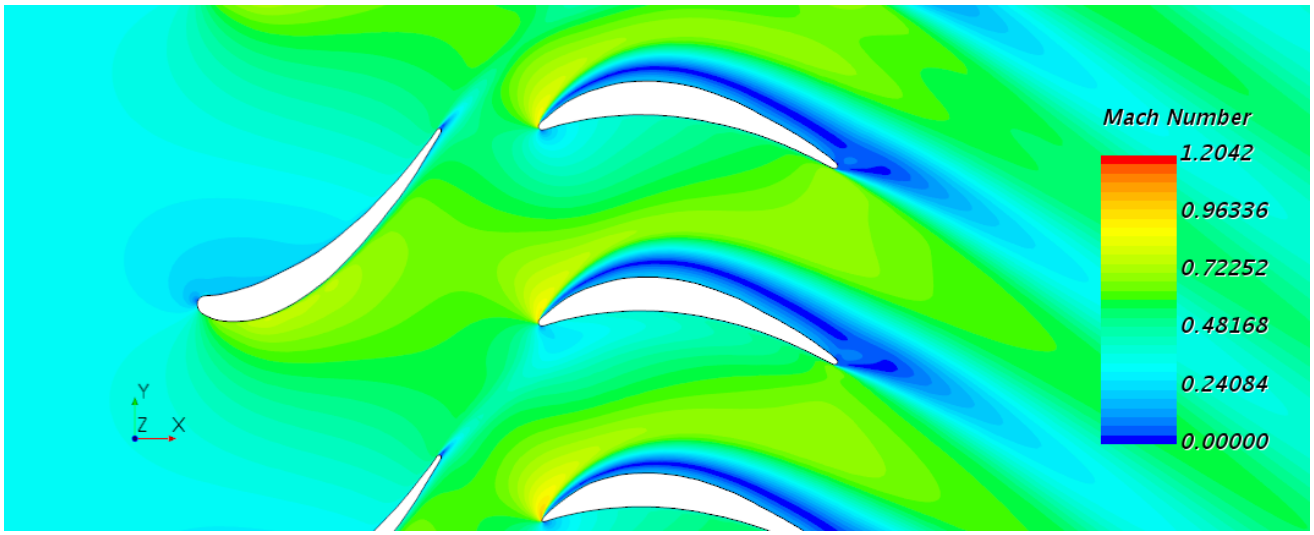

Figure 6.24: Zoom of the Mach number contour of Case 3 for Rotor 2 rotated.[OE]

Table 6.3 shows that even with the airfoil rotated, the isentropic efficency is not improved. This rotation produces an increase in the total pressure drop that also increases the Mach number and causes higher interactions of the flows that result in lower isentropic efficiency values.

Case	Static Pressure Ratio	Stage Static Pressure Drop ($Pa \cdot 10^5$)	Stage Total Pressure Drop ($Pa \cdot 10^5$)	Maximum Mach	Isentropic Efficiency (%)
1	2.15	1.02	0.40	2.18	77.55
2	1.49	0.64	0.33	1.8	68.08
3	1.17	0.29	0.17	1.2	63.96

Table 6.3: Rotated rotor 2 simulation results.[OE]

Once the curvature study has been set, the most efficient case is selected as the base of the rest of the performed analysis, Case 2 with Rotor 1, the curved geometry with transonic flow.

6.3 Rotor-Stator Number of Blades Ratio Study

In section 3.4 of Chapter 3, it was stated that the rotor-stator number of blades ratio selected was 1.67. This means that five rotor blades and three stator vanes are used in the previous simulations. This selection was made based on some bibliographic references. However, since this ratio selection does not follow any rule, some simulations are performed in order to see if the ratio selected could be improved.

Thus, this section considers a variation in the number of stator vanes in order to see how this number affects the stage efficiency. In this way, the blade ratio is varied but rotor solidity is not.

The ratios analysed can be seen on Table 6.4.

Ratio Study	Nº Rotor Blades	Nº Stator Vanes	Ratio
1	5	3	1.67
2	5	2	2.5
3	5	5	1

Table 6.4: Rotor-Stator blade ratios simulated.[OE]

6.3.1 Blade Ratio Study: 1.67

Figures 6.25 and 6.26 are the same figures obtained in section 6.1.1, Figures 6.1 and 6.2. They appear again in this section since they were computed for the rotor-stator ratio of 1.67 and for the middle pressure drop simulation conditions, called Case 2. Figures 6.29, 6.30, 6.33 and 6.34 present ratio studies of 2.5 and 1 respectively.

Figure 6.25 shows a good performance of the flow around the airfoils, if looking at an enlarged picture of this scene, Figure 6.26, it can be noted that no flow separation zones appear appart from the trailing edges what is normal due to its rounded shape.

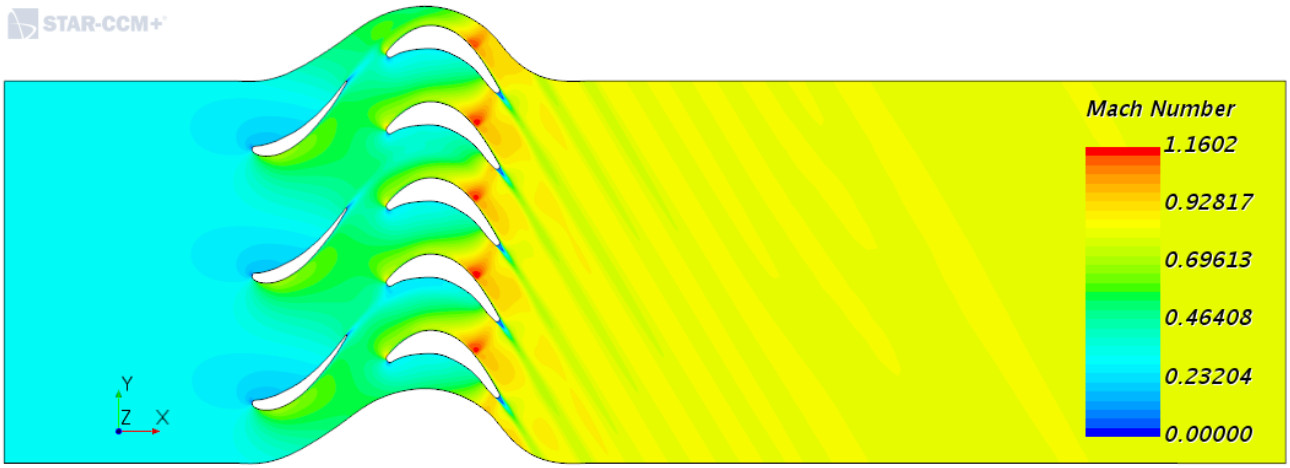

Figure 6.25: Mach number contour for blade ratio of 1.67 for Rotor 1.[OE]

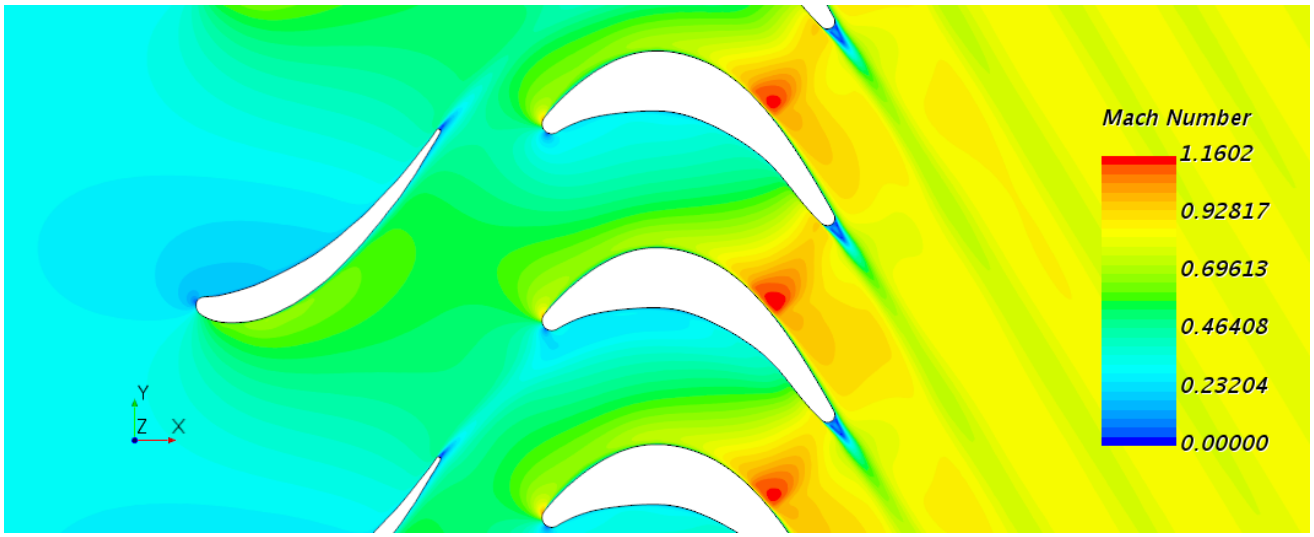

Figure 6.26: Zoom of the mach number contour for blade ratio of 1.67 for Rotor 1.[OE]

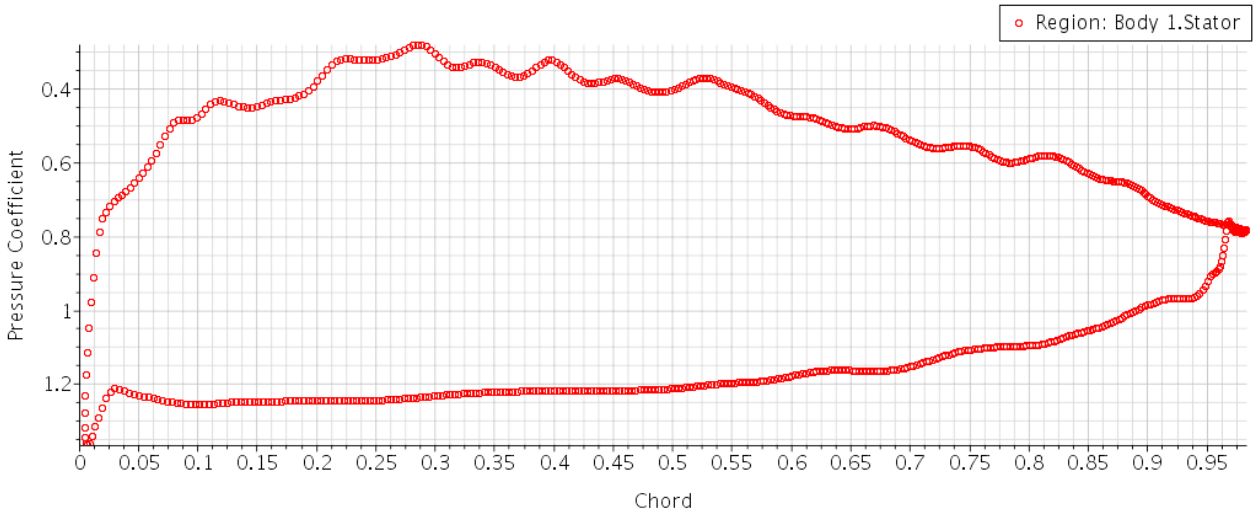

Figure 6.27: Pressure coefficient along the stator chord for blade ratio of 1.67.[OE]

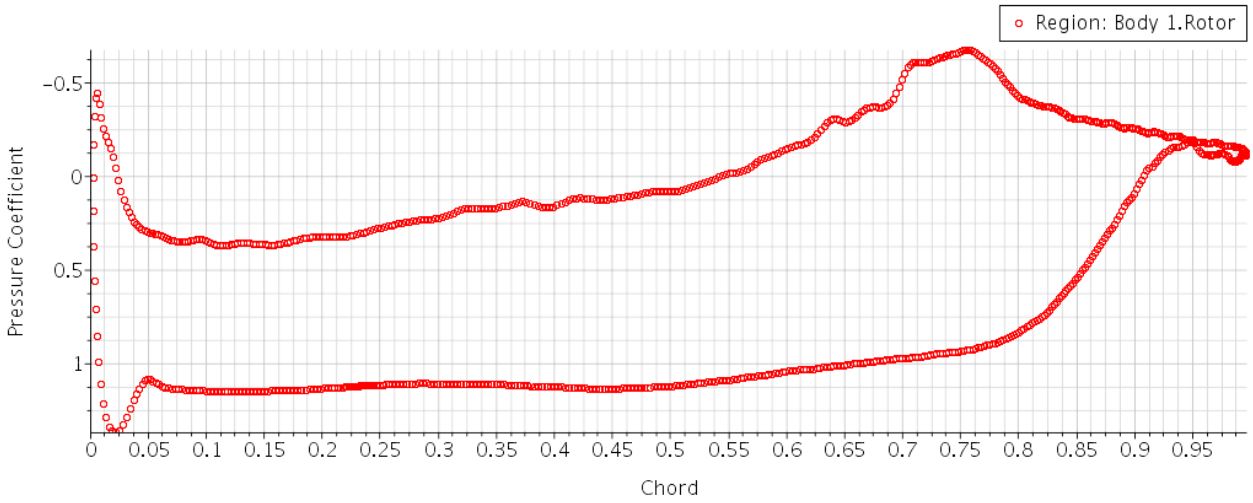

Figure 6.28: Pressure coefficient along the Rotor 1 chord for blade ratio of 1.67.[OE]

6.3.2 Blade Ratio Study: 2.5

Now, the rotor-stator blade ratio is incremented to 2.5, what means that if the number of rotor blades is maintained, a decrease in the number of stator vanes is applied. The geometry has two stator vanes intead of three.

The main differences in the flow appear in the c_p plots. The stator plot shows that for a higher blade ratio the diference in pressure at the first part of the stator becomes grater, thus the flow accelerates more, but not in an important quantity since the Mach numbers are very close. However the difference is greater in the last part of the stator. Figures 6.29 and 6.30 show a greater low pressure zone wake at the trailing edge. This is caused by the lack of stator vanes that poorly direct the flow making it to slip form the path.

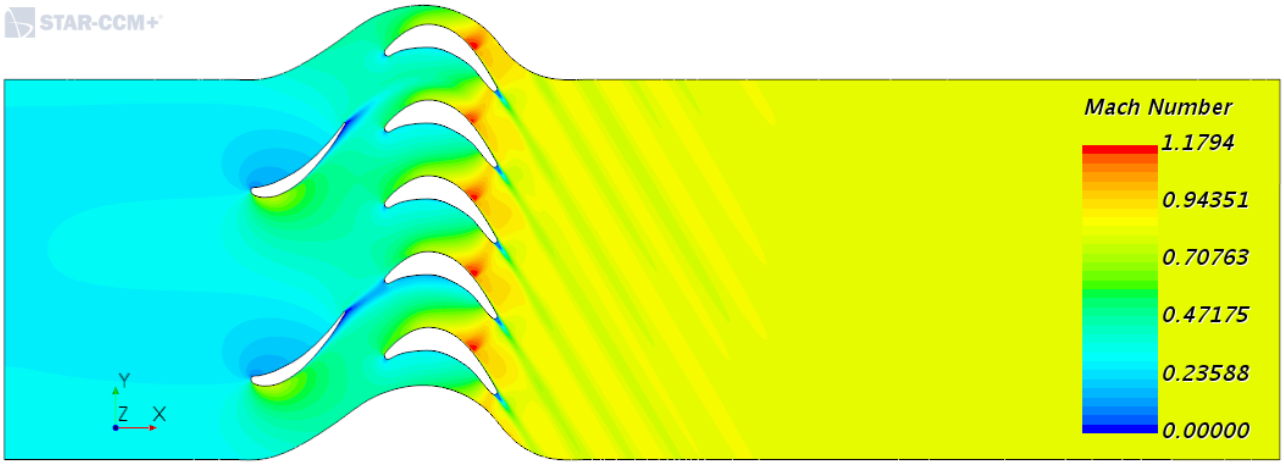

Figure 6.29: Mach number contour for blade ratio of 2.5 for Rotor 1.[OE]

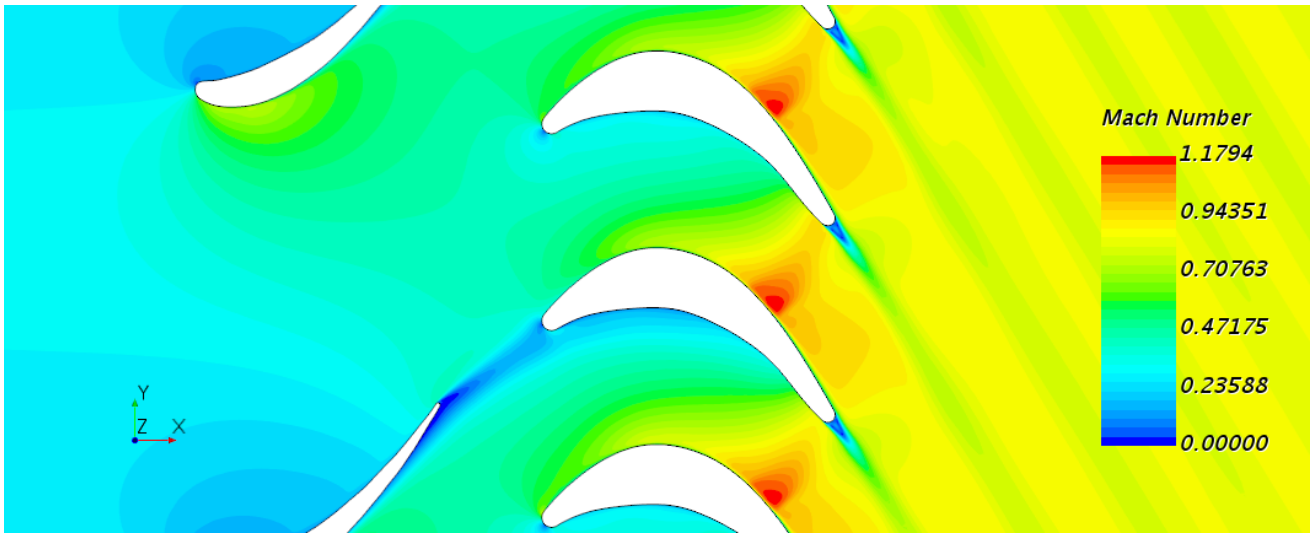

Figure 6.30: Zoom of the mach number contour for blade ratio of 2.5 for Rotor 1.[OE]

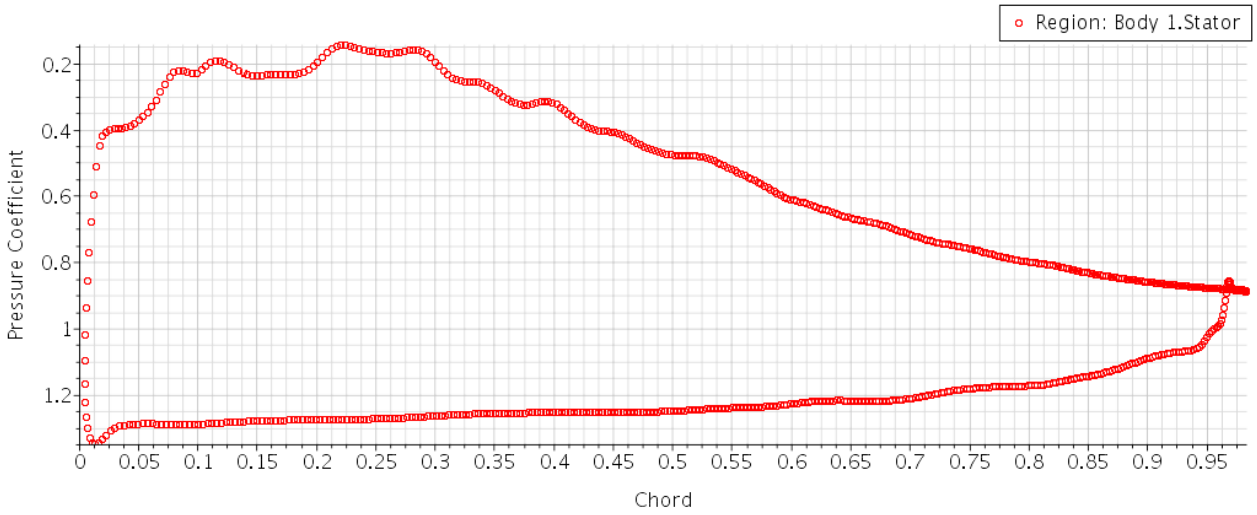

Figure 6.31: Pressure coefficient along the stator chord for blade ratio of 2.5.[OE]

If focusing on the rotor, the main differences appear at the suction peak where the flow accelerates much less for blade ratio of 2.5. It can be seen that for blade ratio of 1.67 the upper side achieves in Figure 6.28 a maximum peak of around -0.5 and the lower side arrives to 1.25. In Figure 6.32, for blade ratio of 2.5, the suction sides arrives to 0.3 and the pressure zone to 1.25. In Mach numbers it means that while with three stator vanes the flow arrives until Mach 1 in the suction peak, with two stator vanes it remains subsonic.

Nevertheless this does not prevent the flow from achieving supersonic Mach numbers at the end of the rotor blade, crating a diffuse and low shock wave at the 80% percent of the chord.

This indicates that this case is still efficient, what is proven in Table 6.5. What is more, this case appears to be even more efficient that the selected one, with an isentropic efficiency of 92.45% against the 91.82% of the base case. The reason, the subsonic flow at the leading edge of the rotor that adapts smoothly to the airfoil and the lower friction losses due to a less number of blades and lower speeds at the rotor blades. Moreover, lower quantity

of stator vanes will lead to less rotor-stator interference when the rotation of the rotor is considered.

However, the flow separation at the end of the stator vanes indicates that considering higher blade ratios than 2.5 could lead to a reduction in the efficiency due to considerable low pressure zones interacting with the rotor blades.

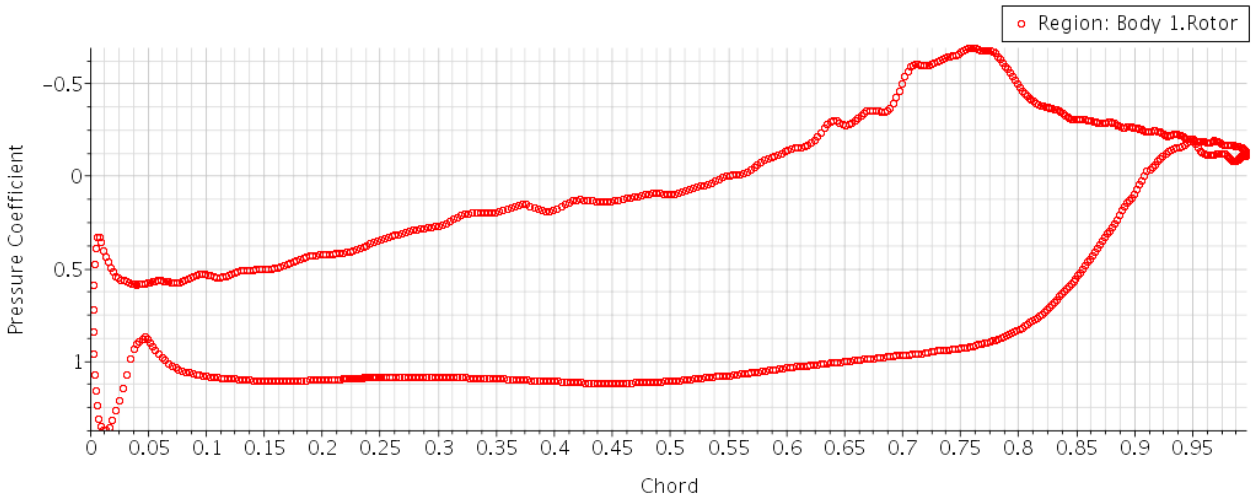

Figure 6.32: Pressure coefficient along the Rotor 1 chord for blade ratio of 2.5.[OE]

6.3.3 Blade Ratio Study: 1

Although it has been said that selecting the same number of stator vanes as rotor blades leads to resonance problems, since the aim of the study is not to analyse resonance effects but flow development, a blade ratio of 1 is simulated. The geometry consists of 5 rotor blades and 5 stator vanes and the obtained results are shown as Mach number contours and c_p plots on Figures 6.33, 6.34, 6.35 and 6.36.

The introduction of more stator vanes means that the flow is better directed into the rotor blades. Figures 6.33 and specially 6.34 show how the flow perfecly attaches to the whole stator and almost no low pressure zone is created at the trailing edge of the stators. This implies that the flow reaches the rotor with higher speeds and a supersonic zone appears at the leading edge of the rotor blades. This supersonic zone causes a thickening of the boundary layer at the first half of the airfoil chord. The acceleration at the last part of the rotor is not as great as with higher blade ratios so very low shock waves appear.

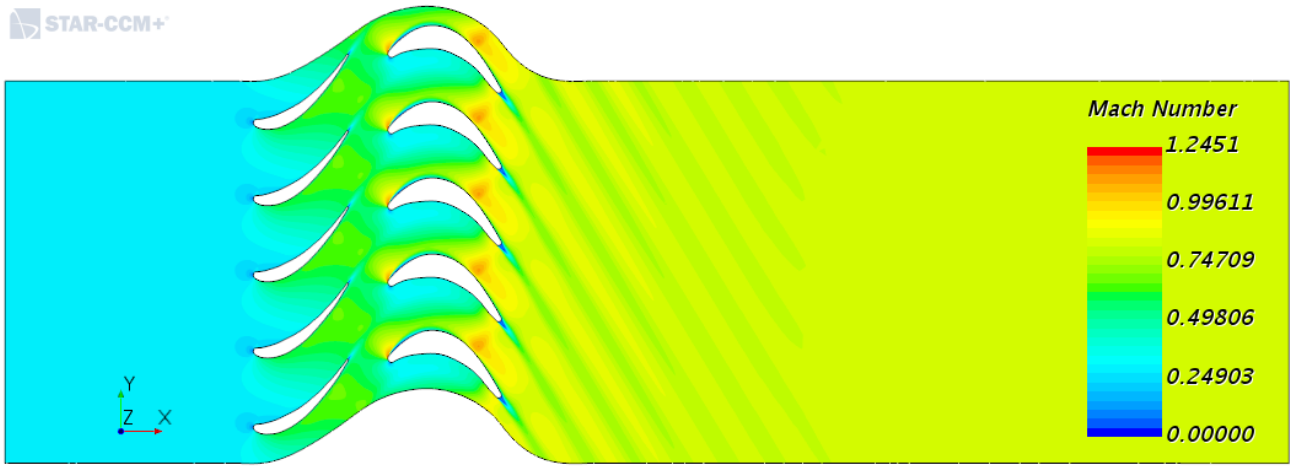

Figure 6.33: Mach number contour for blade ratio of 1 for Rotor 1.^{OE}

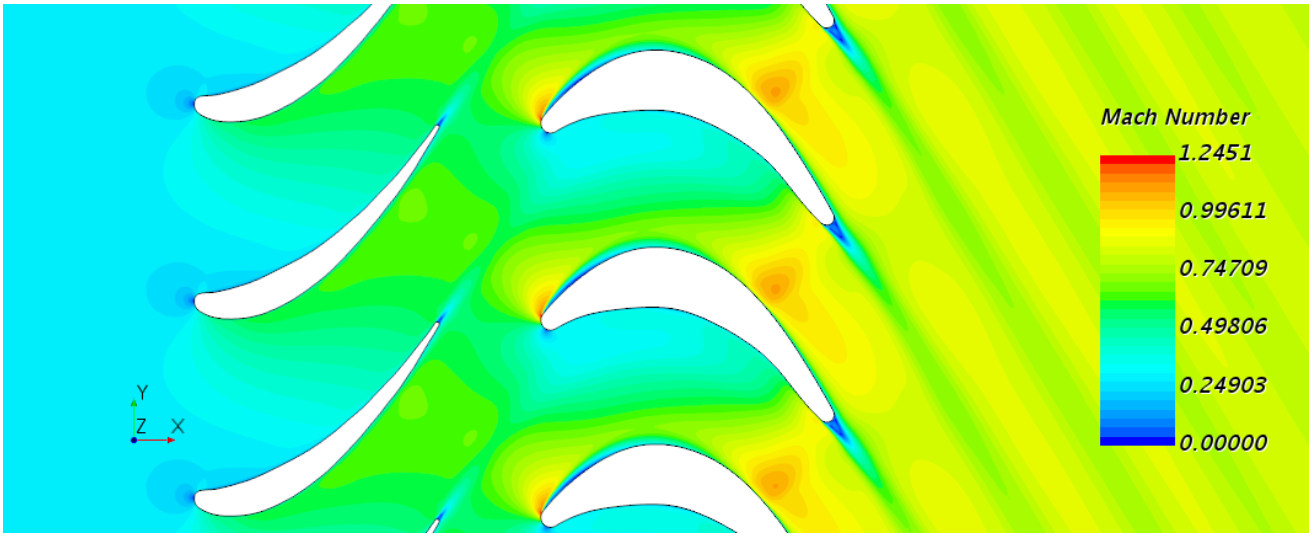

Figure 6.34: Zoom of the mach number contour for blade ratio of 1 for Rotor 1.^{OE}

Table 6.5 shows that with lower blade ratios the isentropic efficiency is reduced. This is caused due to the extra frictional losses and the fact that if the stator exit is not perfectly aligned with the rotor inlet angle, the flow outcoming the stator has less flexibility to adapt to the new shape of the rotor. Specially after the initial shock wave zone at the leading edge that does not appear in the other cases. Thus, the energy generated by the acceleration of the flow in the stator is lost in the low speed zone of the rotor and the channel is less efficient.

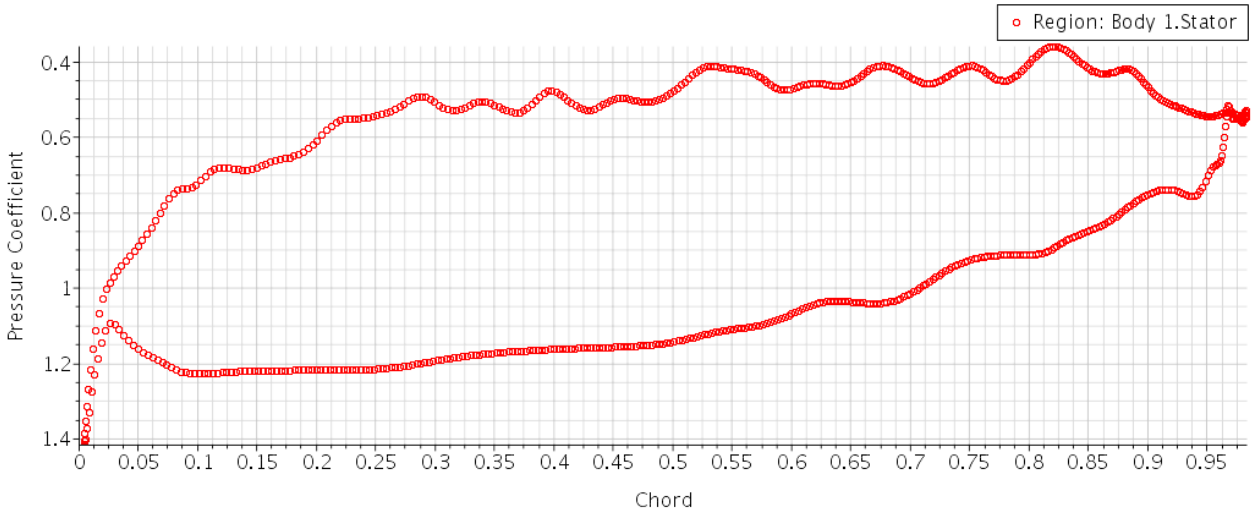

Figure 6.35: Pressure coefficient along the stator chord for blade ratio of 1.^{OE}

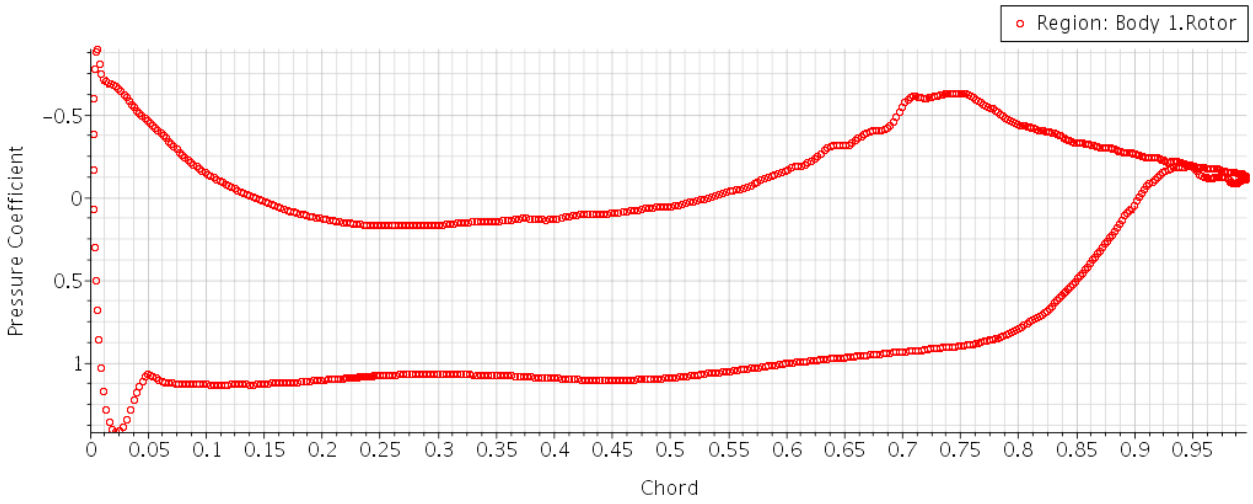

Figure 6.36: Pressure coefficient along the Rotor 1 chord for blade ratio of 1.^{OE}

Finally, it can be concluded that the rotor-stator blade ratio has a direct effect on the performance of a turbine stage. Its selection can lead to flow slip because of the poorly guidance of the flow into the correct direction if the ratio is too high. On the contrary, excess of frictional loses appear when the ratio is reduced. In addition, too many stator vanes can lead to bad adaptation of the flow to rotor blades if the stator exit and rotor inlet angles are not perfectly oriented and low pressure zones may appear over the rotor blades. For this case, the selected ratio has resulted to be a valid selection when talking about the stage performance, however, it can be improved.

Higher pressure cases are not analysed for this geometry. However, at the first study it was seen that higher pressure drops lead lo higher Mach numbers. Then, if the pressure drop is increased the effect of higher Mach at the leading edge would became more important, involving higher flow separations. In those cases, where military engine applications are included, the importance of setting a lower and more adequate number of stator vanes is enhanced.

Blade Ratio	Static Pressure Ratio	Stage Static Pressure Drop (Pa·105)	Stage Total Pressure Drop (Pa·105)	Maximum Mach	Isentropic Efficiency (%)
1.67	1.55	0.72	0.10	1.16	91.82
2.5	1.55	0.72	0.09	1.18	92.45
1	1.55	0.72	0.12	1.25	89.13

Table 6.5: Results for different rotor-stator blade ratios.[OE]

6.4 Solidity Study

The number of stator vanes is kept constant in this part and the number or rotor blades is changed. Then, the spacing between rotor blades is modified and if it is related with the rotor chord length, solidity (C/s) is obtained. As introduced in Chapter 3, the selection of this parameter is essential in a turbine blade stage design. Usually in turbines, as in compressors, solidity takes values of unity.[13] The base geometry includes a value of 1.55 that was directly extracted from the 3D CAD model supplied by the CMT. This part of the project aims to analyse the effects of the solidity if it is changed from 1.55 to 1, the value suggested by the bibliography.

6.4.1 Solidity Study: 1.55

Once more the base case is shown in order to compare both cases easier.

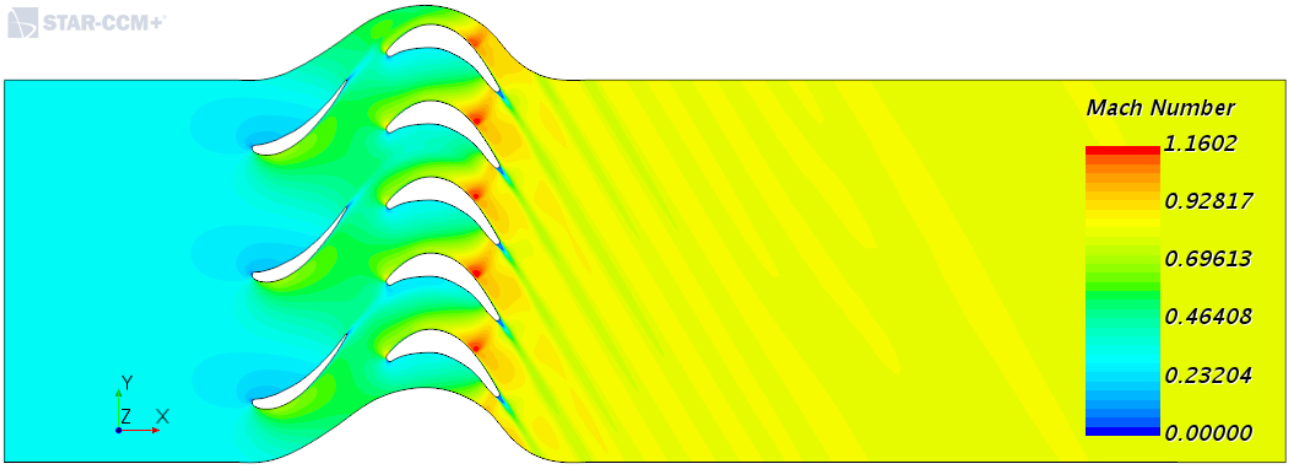

Figure 6.37: Mach number contour for solidity value 1.55 for Rotor 1.[OE]

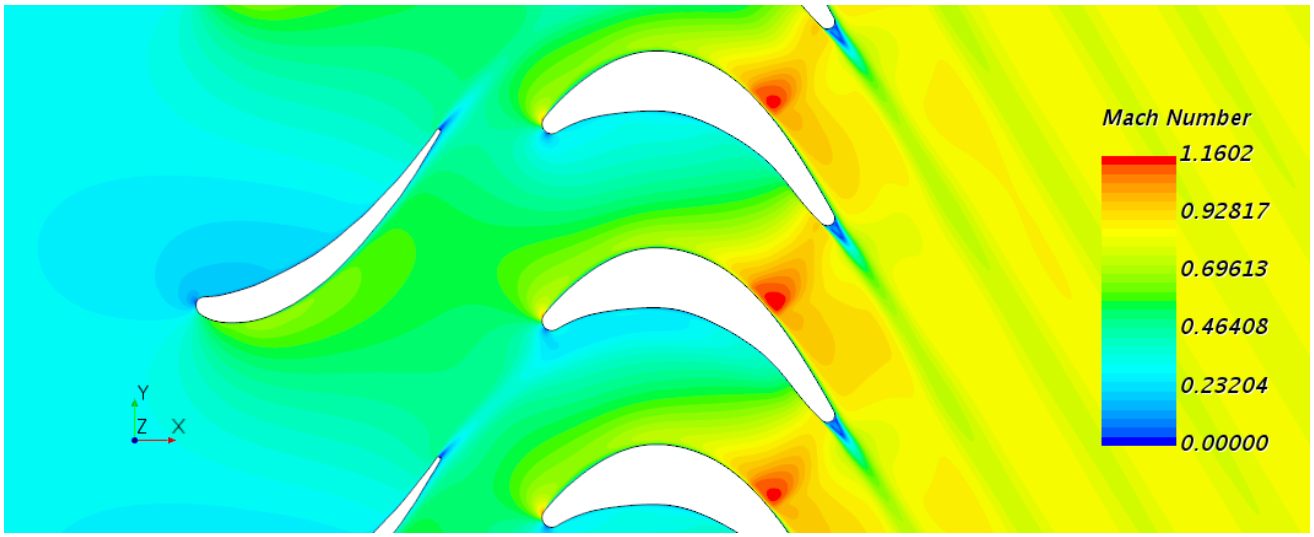

Figure 6.38: Zoom of the mach number contour for solidity value of 1.55 for Rotor 1.[OE]

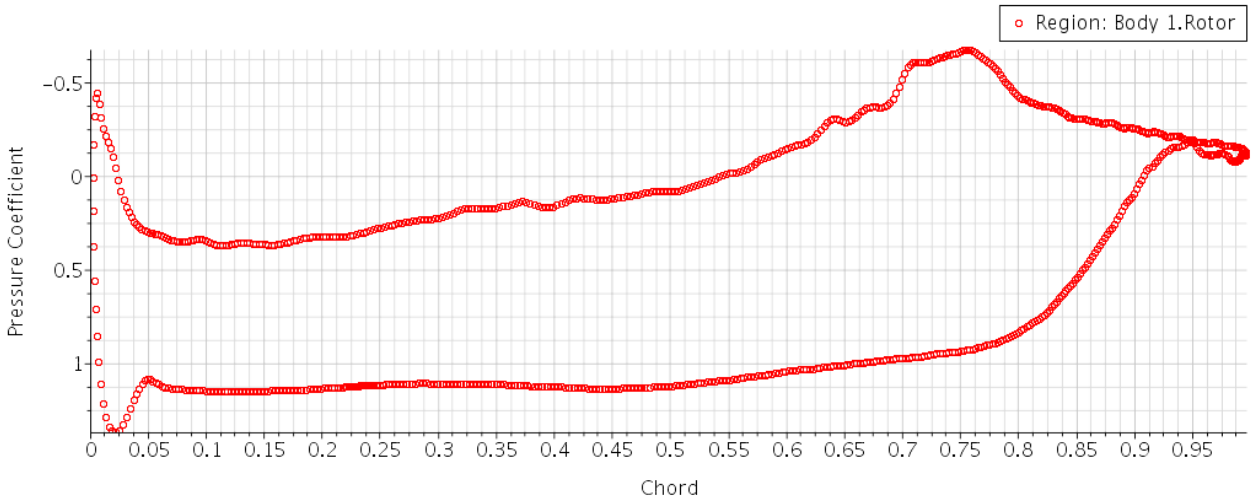

Figure 6.39: Pressure coefficient along the Rotor 1 chord for blade ratio ofsolidity value 1.55.[OE]

6.4.2 Solidity Study: 1

It can be seen by the comparison of Figures 6.37 and 6.40 that if solidity is too large the flow clearly behaves in a very different manner. With unitary solidity the flow accelerates too much at the rotor inlet, causing a strong rotor-stator interaction that creates a shock wave at the 20% of the chord.. After the initial shock wave the flow starts detaching from the rotor surface and the lack of a narrow channel that directions the flow creates a great boundary layer separation from the 60% of the chord. The considerable adverse pressure gradient zone generates a great wake that will negatively affect the next stator row. On the intrados, the pressure side, lower Mach numbers are reached. The cause is again the higher amplitude of the channel that is not able to correctly direct the flow.

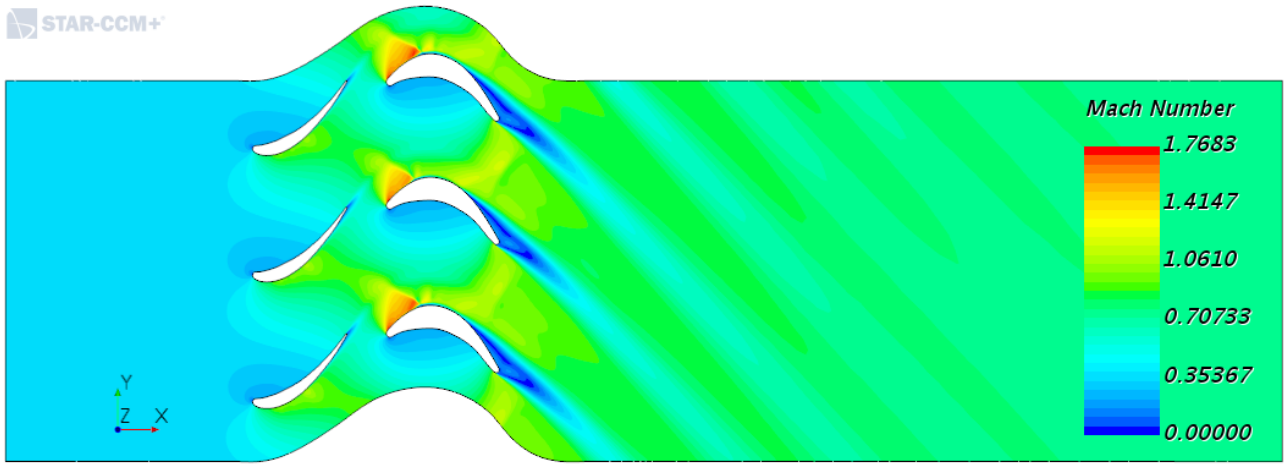

Figure 6.40: Mach number contour for solidity value 1 for Rotor 1.[OE]

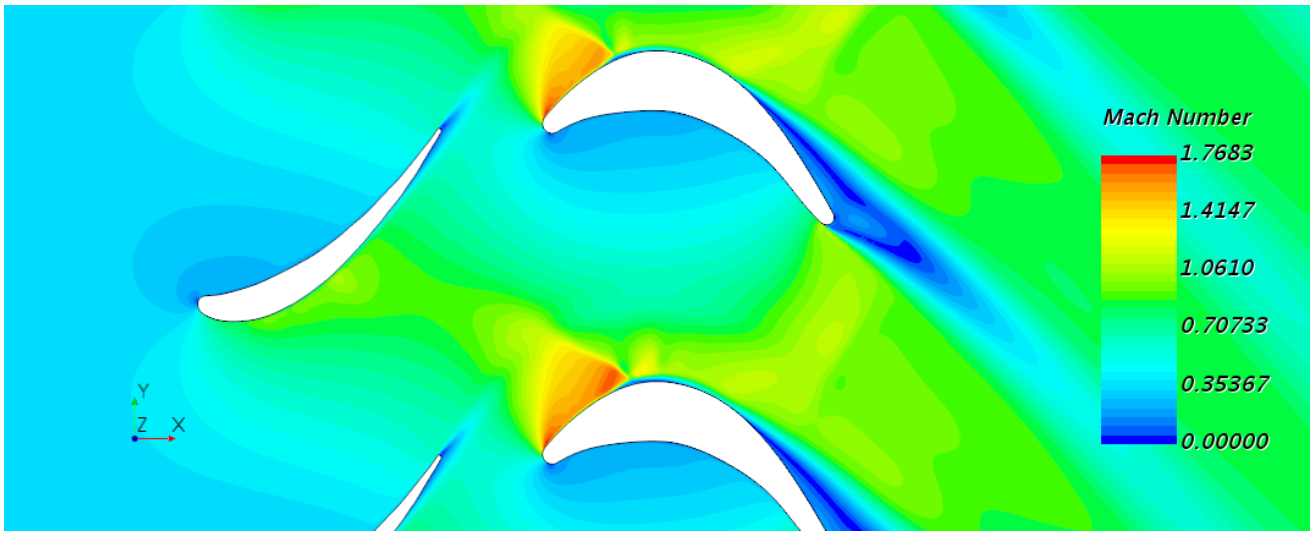

Figure 6.41: Zoom of the mach number contour for solidity value of 1 for Rotor 1.[OE]

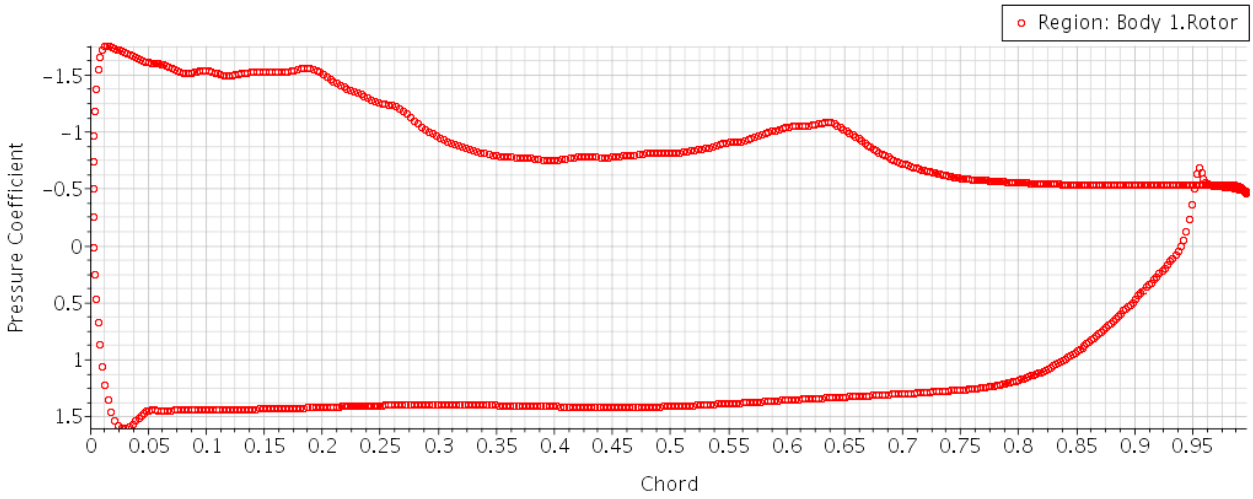

Figure 6.42: Pressure coefficient along the Rotor 1 chord for solidity value 1.[OE]

Table 6.6 reflects that in this case, a lower solidity value is not effective since the isentropic efficiency is reduced in a 12%. The lack of rotor blades makes impossible the flow to correctly adapt to the rotor and thus the expansion is not performed in an efficient way crating a considerable low pressure wake where flow recirculation appears.

Solidity	**Static Pressure Ratio**	**Stage Static Pressure Drop (Pa·105)**	**Stage Total Pressure Drop (Pa·105)**	**Maximum Mach**	**Isentropic Efficiency (%)**
1.55	1.55	0.72	0.10	1.16	91.82
1	1.50	0.66	0.22	1.76	79.17

Table 6.6: Results for different solidities.[OE]

Finally, it can be stated that the results obtained all along the document agree the initial assumptions proposed by Reference [13] in Chapter 3, Geometric Design, and that the best geometry selection is the one constituted by two stator vanes and fife rotor blades, thus the one with a blade ratio of 2.5.

7. Conclusions and Future Studies

Along this project two of the most important things to take into account while designing a turbine have been analysed, the secondary flows and the efficiency of a turbine stage. The importance of obtaining more efficient turbines has become more important as fuels have increased its price. That is why CFD studies have become utterly important in an engine design process. The use of these software enables the possibility of performing different and more variate studies over several turbine parameters.

In this project a performance of a 2D study of the first IGV(stator)-rotor stage of a turbine of what could be a jet engine has been carried out. The simulations have been executed in an steady state and the rotation of the rotor has been neglected. This assumptions enable a preliminary study of what will happen in a real stage, although it must be highlighted that since the rotor is not moving, the extraction of energy due to its rotation is not simulated and further more complex studies must be performed.

This simplicity involves that the time required both to implement the model and for computational calculation is significantly reduced but interesting results are still obtained.

7.1 Conclusions

These are the results that can be concluded.

- The study of different pressure drops show that increasing the static pressure drop of a stage results in higher velocities over the blades that can lead to the generation of shock waves that choke the inter-blade channel and reduces the isentropic efficiency of the stage. Moreover, the cases involving stronger shock waves generate a boundary layer separation after them that could lead to buffeting that will negatively affect the flow by making it more chaotic.

  Moreover, in application where high pressure drops for a stage are required in order to obtain smaller turbines (with less stages), turbine's efficiency is sacrificed for reducing weight. Then this lose is tried to be compensated by the use of higher amount of fuel. Then, special attention must be payed to blades while inspections in order to prevent from corrosion. On the other hand, if the pressure drops are too low it could lead not to extract the desired work due to low expansions or to the requirement of too many stages that would affect negatively to an aircraft's weight.

- The curvature study exhibits the necessity of a curved airfoil for the rotor blade in order not to obtain important boundary layer separation. In addition, curved rotor blades present lower rotor-stator interaction due to the fact that they present a more appropriate inlet angle that easily accommodates the flow outcoming from the stator. It has been also highlighted the effect of more rounded leading edges, with higher radius, contributing to flow adaptation.

- The analysis of the impact of the number of stator vanes shows that these number must be selected in such a way that the leading edge of the rotor blades keeps in subsonic Mach numbers in order to reduce the rotor-stator interaction. However, this subsonic numbers must not be very far from the transonic speeds so flow still

perfectly attaches to the rotor and stator surfaces. This is achieved with a low quantity of stator vanes.

A high number would imply higher frictional losses and losses due to the fact that the flow accelerates to much at the very beginning of the rotor blades achieving supersonic speeds and a thickening of the boundary layer after it that reduces the efficiency of the stage.

- Finally, the rotor solidity study shows that in order to be selected, a CFD simulation needs to be performed since little variations can lead to flow separation caused by an inefficient in-between rotors channel. In this case the initial value (1.55) which was not the recommended at the bibliography (1) resulted in a better option.

7.2 Future Studies

Further 2D studies may be done over different aspects. First of all the introduction of the movement of the rotor in order to extract work. The rotational movement of the rotor should give a better and more accurate approach to transonic flow development. New phenomena could appear since the upwards velocity direction would lead to a change in the velocity triangle incoming the rotor.

Moreover, unsteady simulations could be performed in order to check if in the cases where boundary layer separation occurs due to high shock waves, buffeting truly appears. This could also involve some frequency studies in order to check if buffeting can conduce to flutter. If it appears, stress studies would also be interesting in order to select the better material composition of the blade.

In addition, several parameters have been studied but some are still remaining like the influence of the shape of the tip at trailing edge or the effect of the length of the blades.

Finally, these studies could be performed in 3D in order to take into account things like the torsion angle of the blades, blade tip phenomena, or the interaction of the blades with the motor casing.

8. Budget

8.1 Description

This section contains an economical estimation of the cost of this project. On one hand, there must be considered the human time hours as engineer and mesh modeling specialist. On the other hand, material resources including informatic equipment and software licence are considered.

This budget is calculated by the computation of the cost per worked hours. Thus, the duration of each activity that has been carried out must be estimated. After the analyse of the breakdown of the activities a final cost of the whole project, in Euros, is showed.

8.2 Breackdown of Activities

The different activities performed can be divided in six parts that directly depend on the information explained in each chapters of the study.

1. **Bibliography Research**

   This part includes the research done in order to obtain information about the turbine stage performance, the parameters involved in its design and the flow phenomena development. Several books about turbomachinery performance and turbomachinery in CFD where consulted. In addition, studies carried out by researches on buffeting, flutter and CFD simulations over turbine stages where considered.

2. **Geometric Design**

   This activity includes the obtainment of the geometry. First of all, the rotor blade geometry was extracted from a 3D CAD and the stator from a 2D one with Autodesk Fusion 360. AutoCAD software was employed for the arrangement of the blades and the domain draft. Finally Excel was used for saving the points of the blade geometries in a CSV file that the STAR CCM+ could read.

3. **Mesh Generation**

   This is one of the most important parts since the quality of the mesh determines the accuracy of the results that are obtained during the simulation. Therefore, several quality mesh analyses are done to it and a mesh independence study is carried out.

4. **CFD Set-Up and Computation**

   This process implies the configuration of physical models, solvers and boundary conditions. Moreover, once the case starts being run it requires from monitorization in order to control that no convergence errors arise. Therefore it will be the most expensive part.

5. **Analysis of the Results**

   Once a valid solution is obtained, it must be post-processed. The analysis of the

results comprises the comparison of all the solutions obtained. Then, conclusions about the geometric changes that are made can be extracted.

6. **Project Report**

   The writing of the project aims to record the study carried out and the conclusions drawn from it.

8.3 Budget per Activities

The cost per hour for an aeronautical engineer has been extracted from the Spanish BOE Bulletin.[32] It has been supposed that the modelling technician pertains to group 5 (Graduate) and the engineer is part of the so called group 6 (Superior Technician or Enabling Master). For this calculation is has been taken as annual salaries 35 945 € and 50 911 € respectively. The annual worked hours are 1 685h.

Software licenses employed have a cost of 7 €/month fot the Microsoft 365 Personal that includes Excel, 61 €/month for the Autodesk Fusion 360, 279 €/month for the AutoCAD and 4 000 € for 1 000h for the STAR CCM+. Months of 31 days and 253 annual working days have been supposed for these calculations.

The informatic equipment used is calculated from the computer cost that was around 600 € and it has been supposed an amortization in one and a half years.

Resource	**Time [h]**	**Unitary Cost [€/h]**	**Value[€]**
Engineer	30	30.21	906.3
Modeling Technician	10	21.33	213.3
Informatic Equipment	40	0.06	2.4
		TOTAL	**1 122.4**

Table 8.1: Budget for activity 1: Bibliography Research^{OE}

Resource	**Time [h]**	**Unitary Cost [€/h]**	**Value[€]**
Engineer	20	30.21	604.2
Modeling Technician	10	21.33	213.3
Informatic Equipment	30	0.06	1.8
Microsoft Software License	5	0.01	0.05
Fusion Software License	5	0.08	0.40
Autocad Software License	5	0.38	1.9
		TOTAL	**821.65**

Table 8.2: Budget for activity 2: Geometrical Design^{OE}

Resource	**Time [h]**	**Unitary Cost [€/h]**	**Value[€]**
Engineer	10	30.21	302.1
Modeling Technician	40	21.33	853.2
Informatic Equipment	50	0.06	3
STAR Software License	50	4	200
		TOTAL	**1 358.3**

Table 8.3: Budget for activity 3: Mesh Generation^{OE}

Resource	Time [h]	Unitary Cost [€/h]	Value[€]
Engineer	60	30.21	1 812.6
Informatic Equipment	80	0.06	4.8
STAR Software License	80	4	320
		TOTAL	**2 137.4**

Table 8.4: Budget for activity 4:CFD Set-Up and Computation[OE]

Resource	Time [h]	Unitary Cost [€/h]	Value[€]
Engineer	50	30.21	1 510.5
Informatic Equipment	20	0.06	1.2
Microsoft Software License	10	0.01	0.1
		TOTAL	**1 513.1**

Table 8.5: Budget for activity 5:Analysis of the Results[OE]

Resource	Time [h]	Unitary Cost [€/h]	Value[€]
Engineer	30	30.21	906.3
Modeling Technician	15	21.33	319.95
Informatic Equipment	45	0.06	2.7
Microsoft Software License	45	0.01	0.45
		TOTAL	**1 229.4**

Table 8.6: Budget for activity 6: Project Report[OE]

8.4 Final Budget

Activity	Value[€]
1. Bibliography Research	1 122.4
2. Geometric Design	821.65
3. Mesh Generation	1 358.3
4. CFD Set-Up and Computation	2 137.4
5. Analysis of the Results	1 513.1
6. Project Report	1 229.4
TOTAL	**8 182.25**

Table 8.7: Total budget.[OE]

The project has a final cost of: **8 182.25 €**

Eight thousand one hundred and eighty-two euros with twenty-five cents

A. Appendices

A.1 Pressure Ratio Study

A.1.1 Pressure ratio study of Case 1

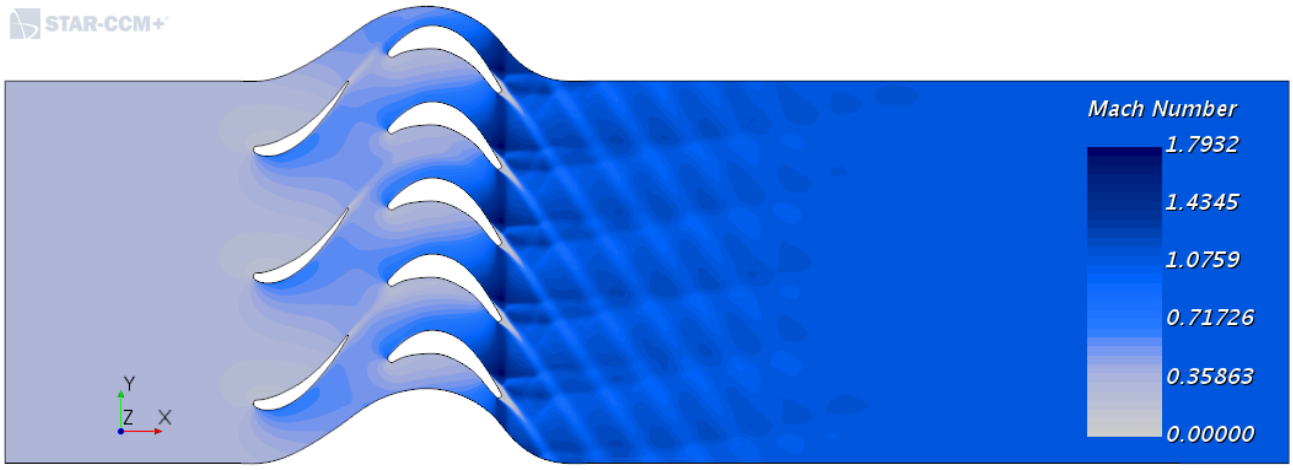

Figure A.1: Mach number contour of Case 1.[OE]

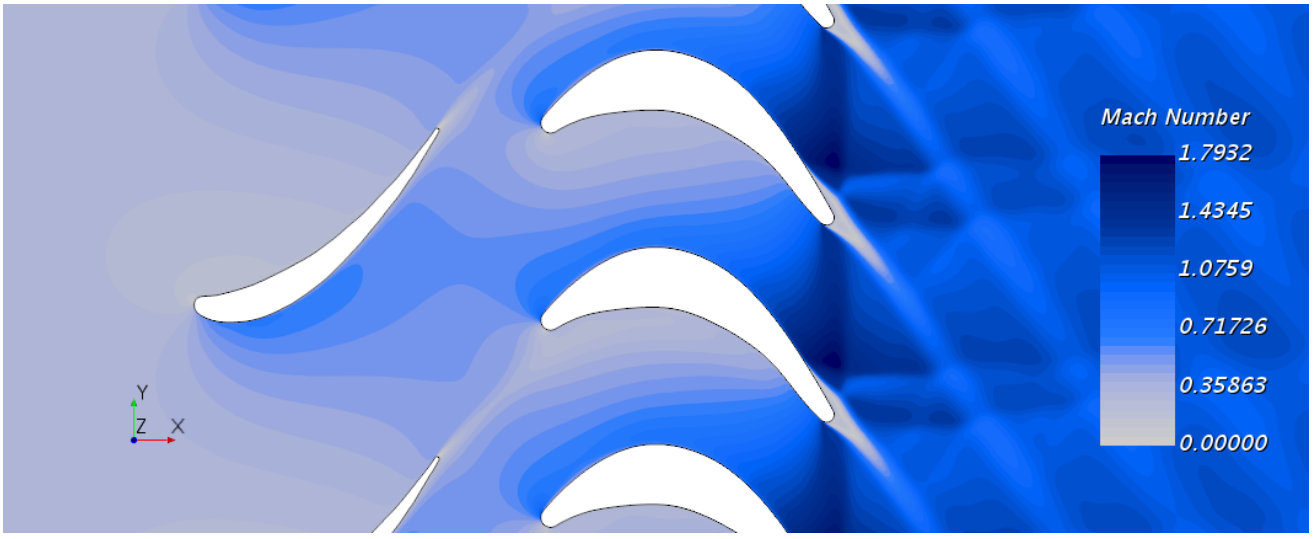

Figure A.2: Zoom of Mach number contour of Case 1.[OE]

A.1.2 Pressure ratio study of Case 2

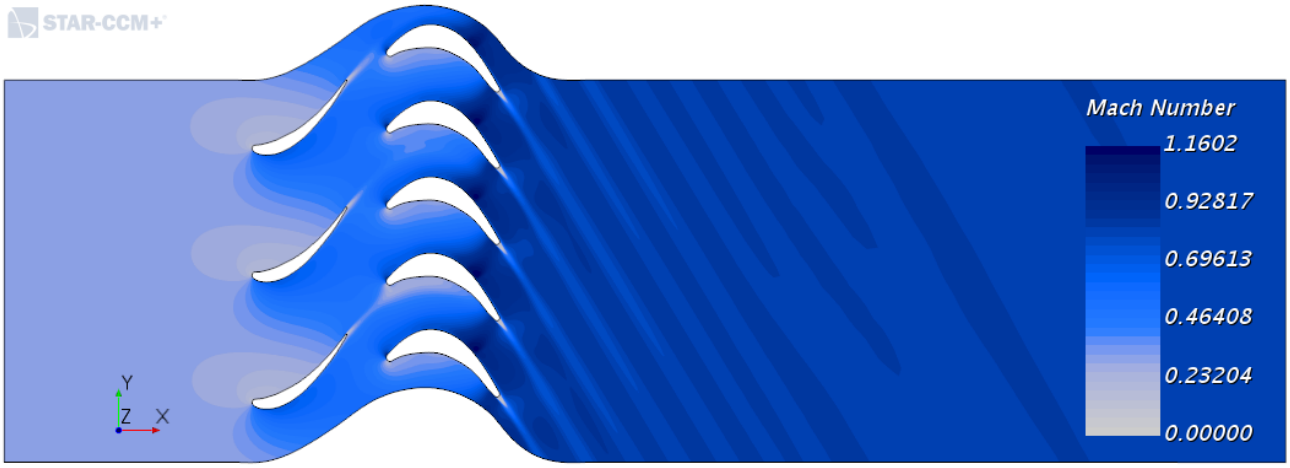

Figure A.3: Mach number contour of Case 2.[OE]

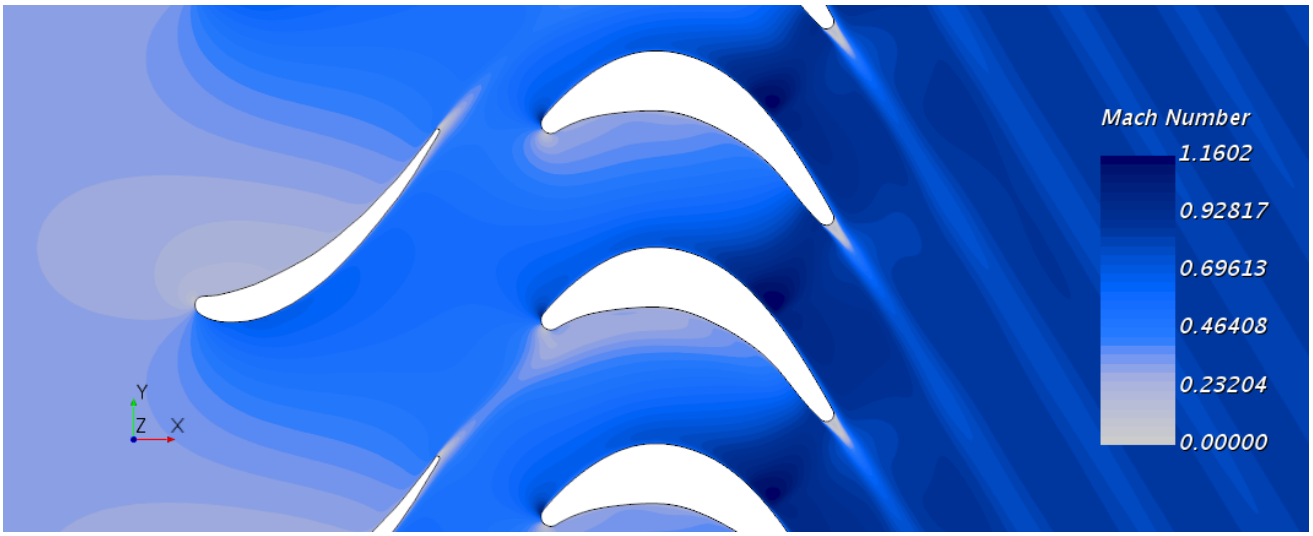

Figure A.4: Zoom of Mach number contour of Case 2.[OE]

A.1.3 Pressure ratio study of Case 3

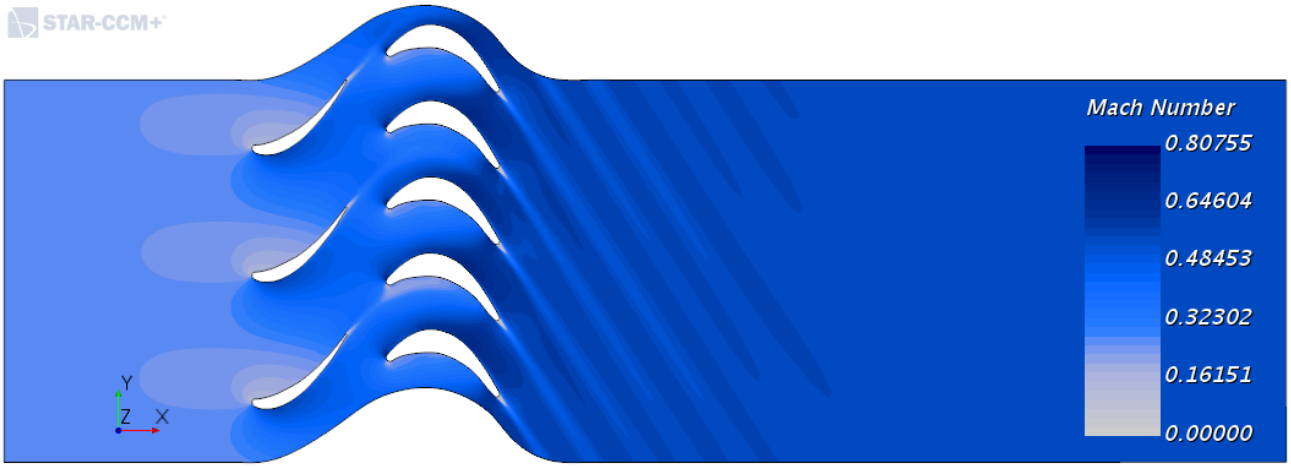

Figure A.5: Mach number contour of Case 3.[OE]

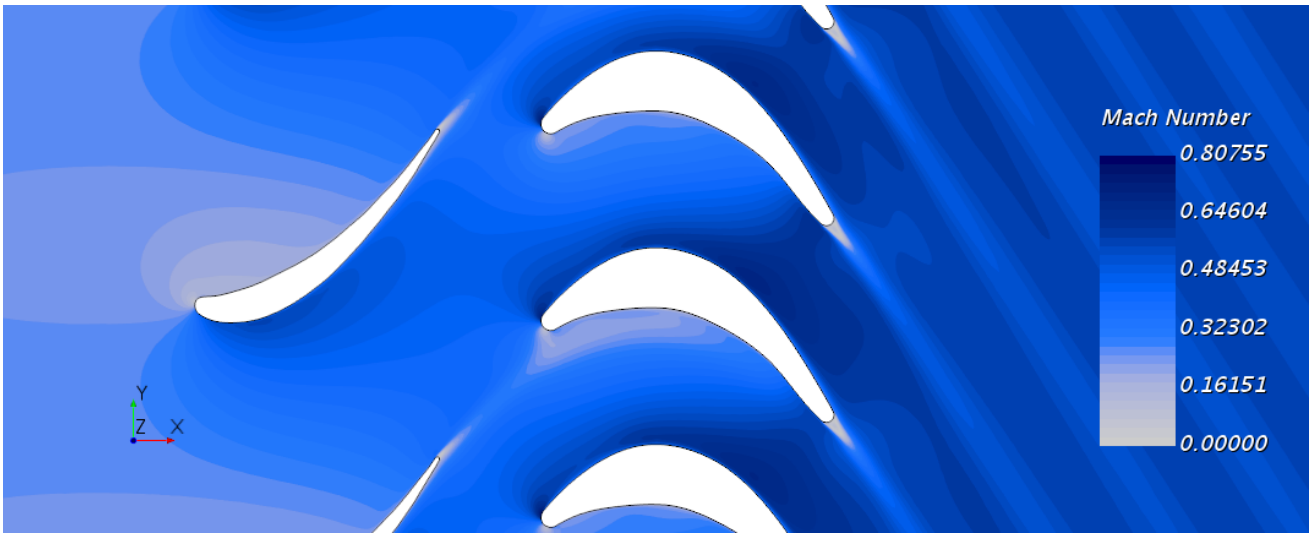

Figure A.6: Zoom of Mach number contour of Case 3.[OE]

A.2 Rotor Curvature Study

A.2.1 Rotor 2 curvature study of Case 1

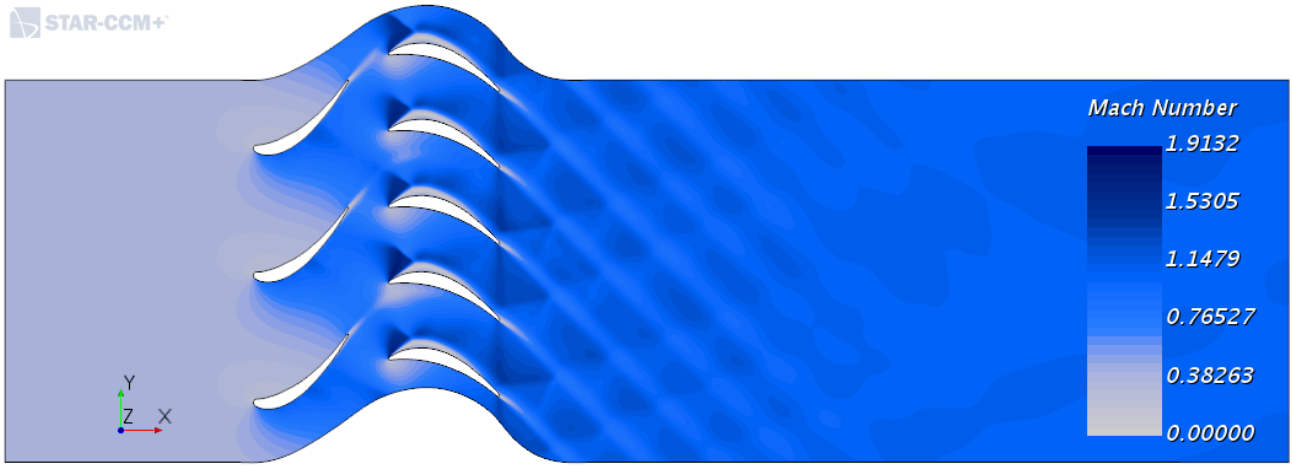

Figure A.7: Mach number contour of Case 1 for Rotor 2.[OE]

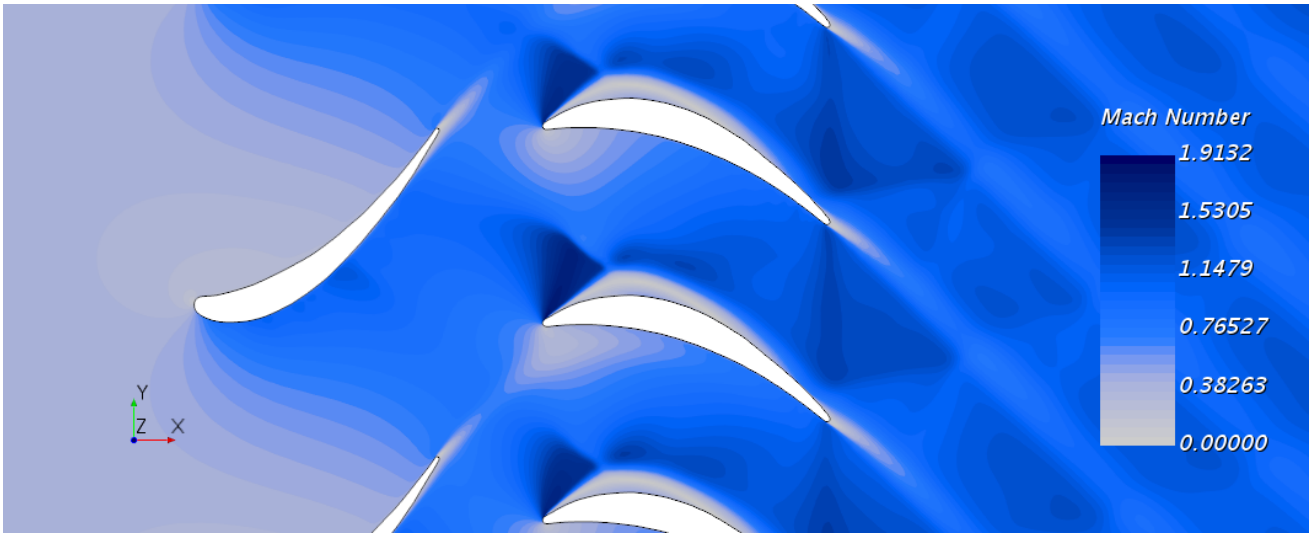

Figure A.8: Zoom of the Mach number contour of Case 1 for Rotor 2.[OE]

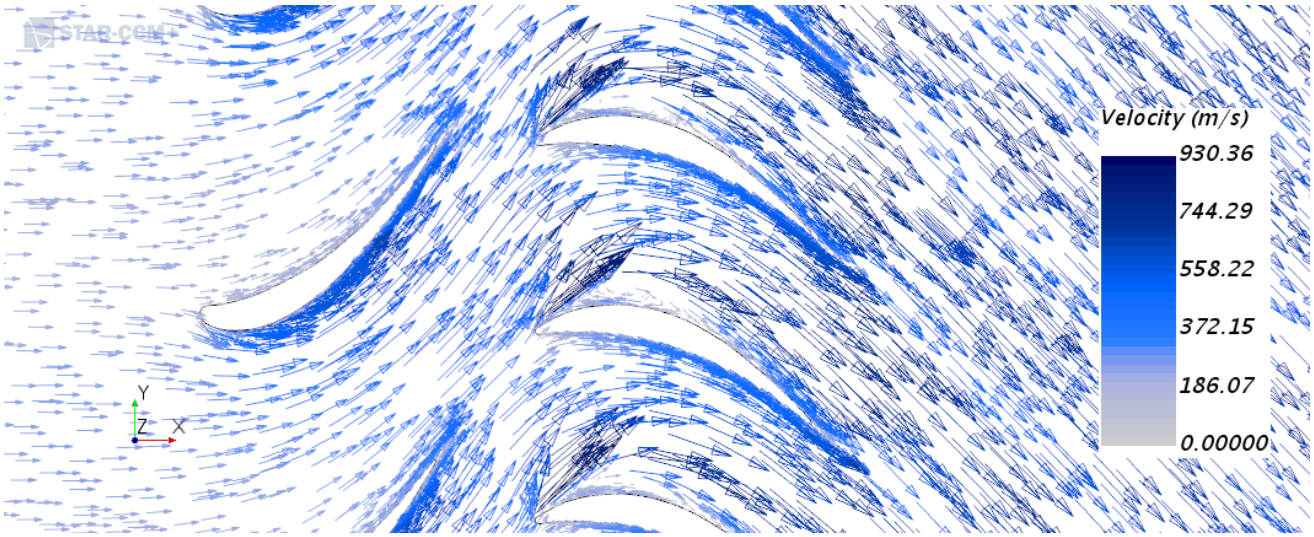

Figure A.9: Velocity vector contour of Case 1 for Rotor 2.[OE]

A.2.2 Rotor 2 curvature study of Case 2

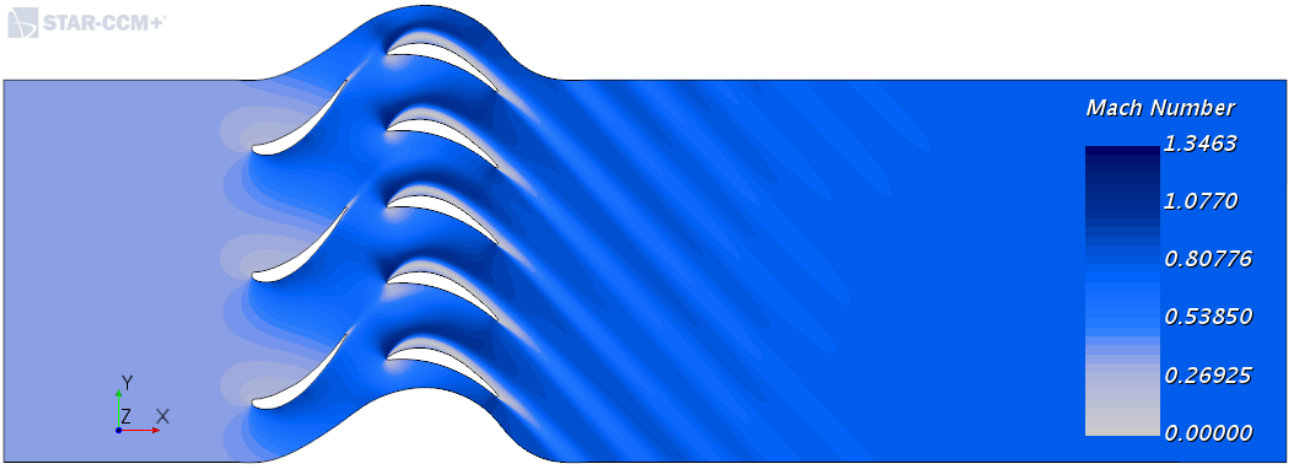

Figure A.10: Mach number contour of Case 2 for Rotor 2.[OE]

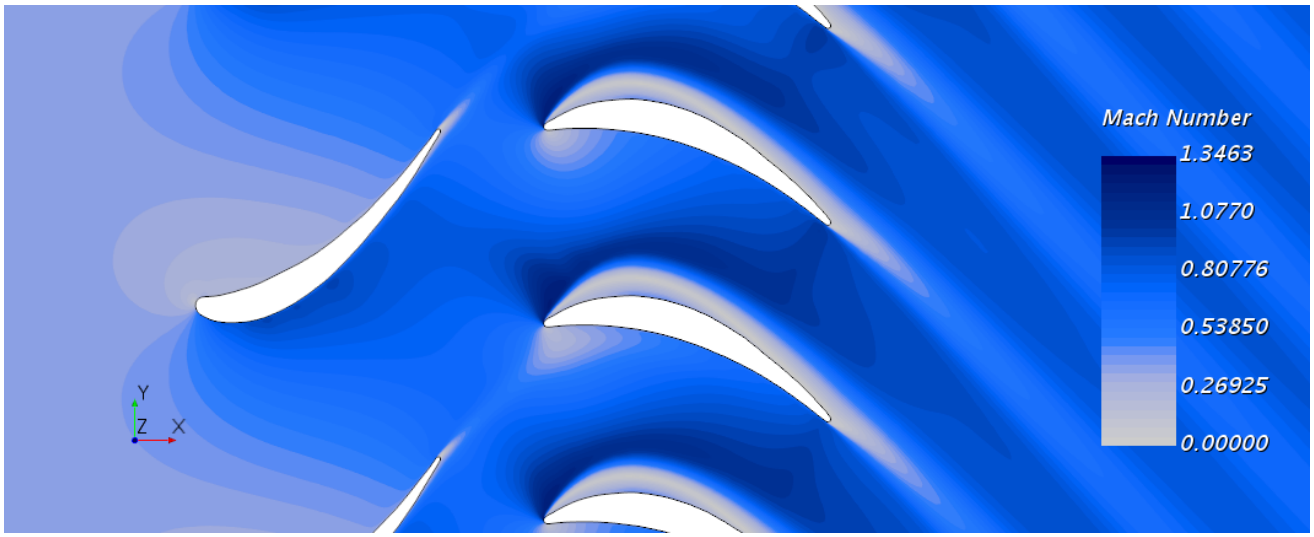

Figure A.11: Zoom of the Mach number contour of Case 2 for Rotor 2.[OE]

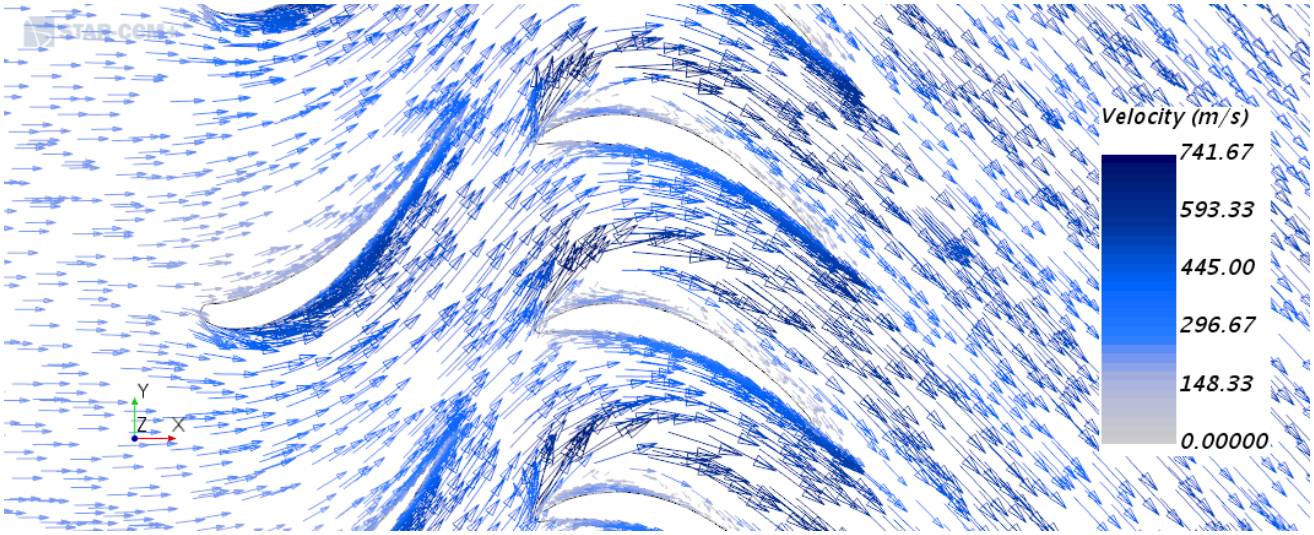

Figure A.12: Velocity vector contour of Case 2 for Rotor 2.[OE]

A.2.3 Rotor 2 curvature study of Case 3

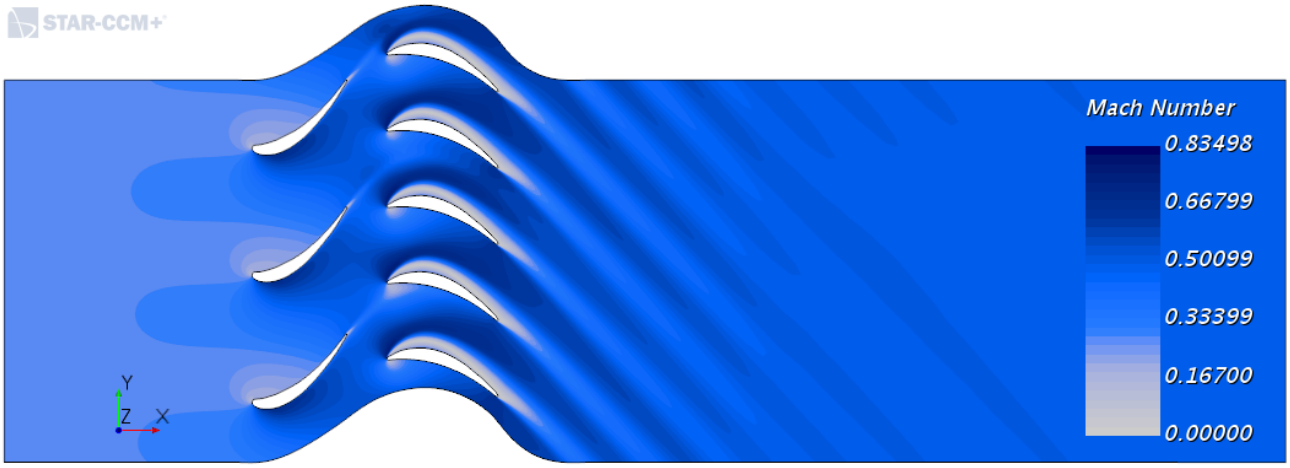

Figure A.13: Mach number contour of Case 3 for Rotor 2.[OE]

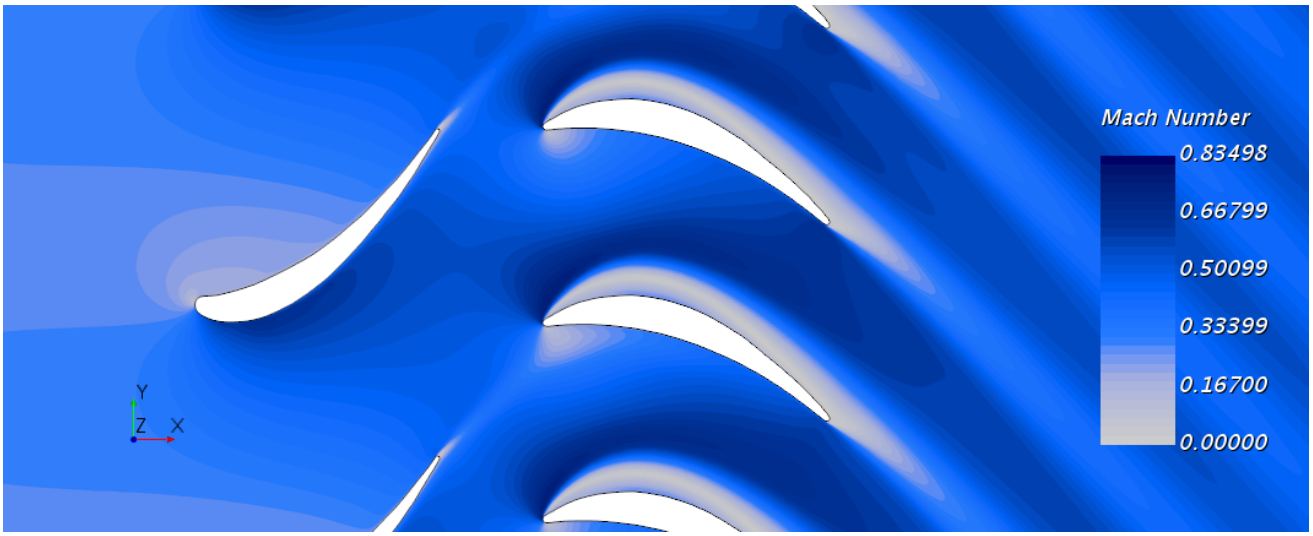

Figure A.14: Zoom of the Mach number contour of Case 3 for Rotor 2.[OE]

A.2.4 Rotated Rotor 2 curvature study of Case 1

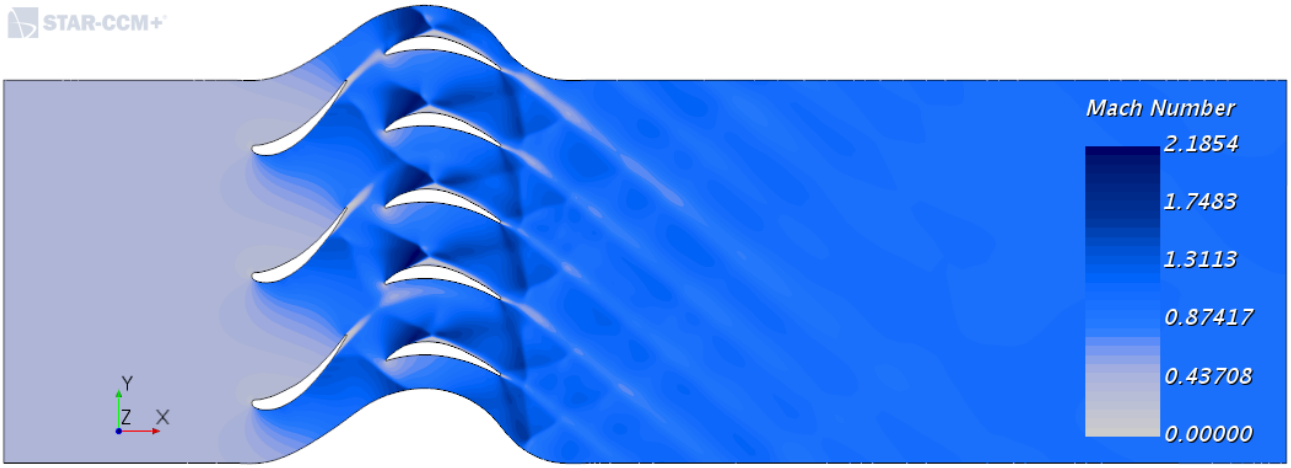

Figure A.15: Mach number contour of Case 1 for Rotor 2 rotated.[OE]

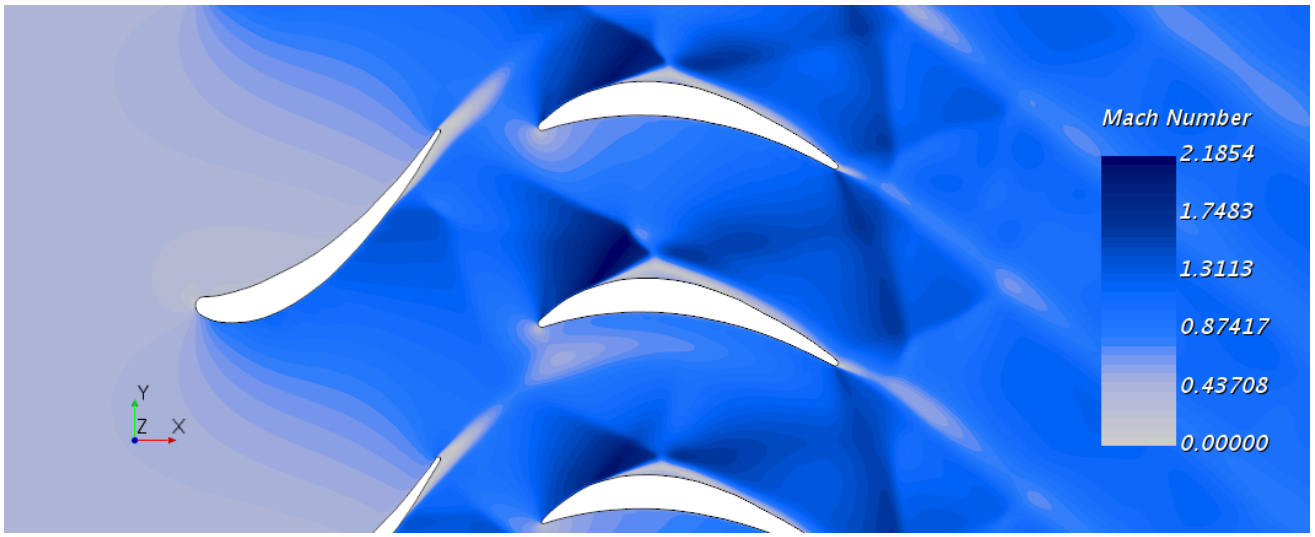

Figure A.16: Zoom of the Mach number contour of Case 1 for Rotor 2 rotated.[OE]

A.2.5 Rotated Rotor 2 curvature study of Case 3

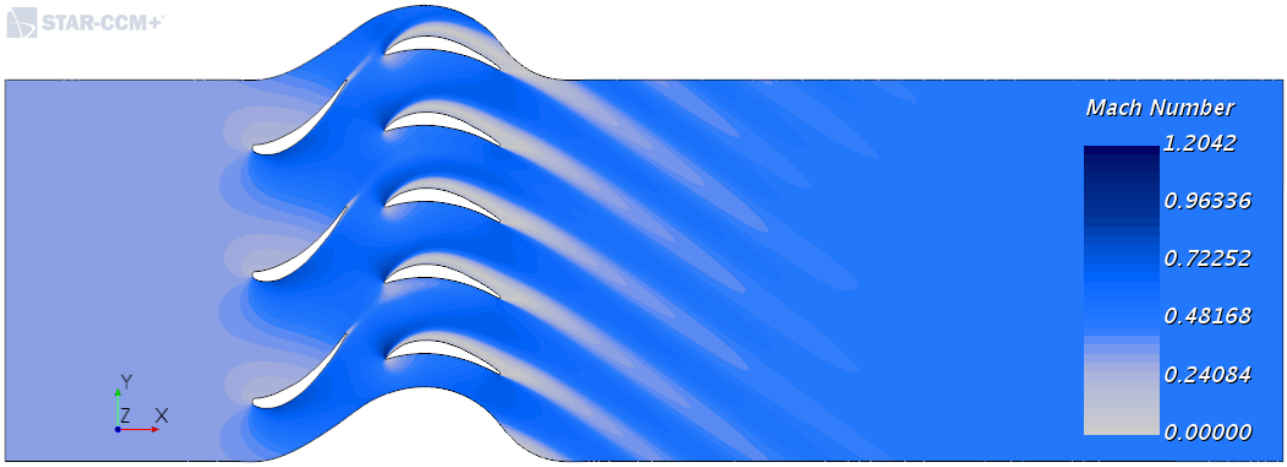

Figure A.17: Mach number contour of Case 3 for Rotor 2 rotated.[OE]

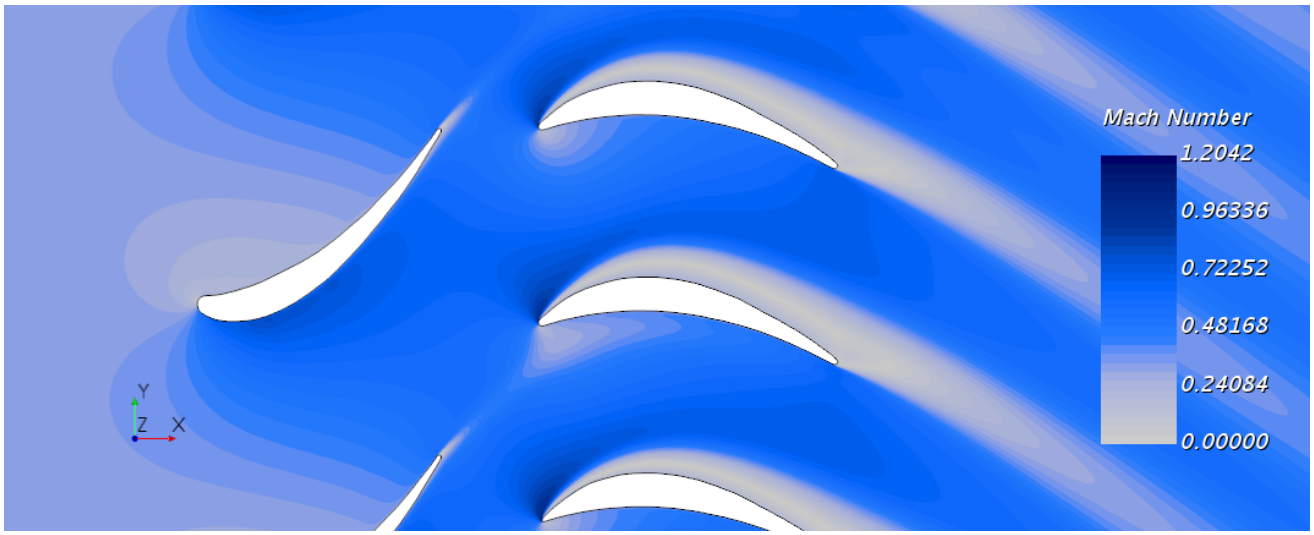

Figure A.18: Zoom of the Mach number contour of Case 3 for Rotor 2 rotated.[OE]

A.3 Rotor-Stator Number of Blades Ratio Study

A.3.1 Blade ratio study: 1.67

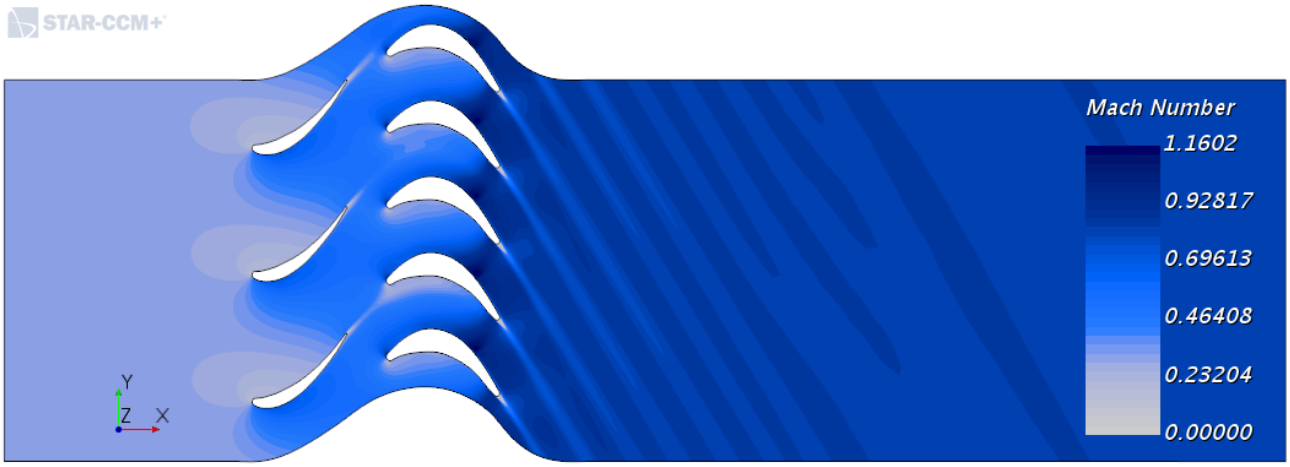

Figure A.19: Mach number contour for blade ratio of 1.67 for Rotor 1.[OE]

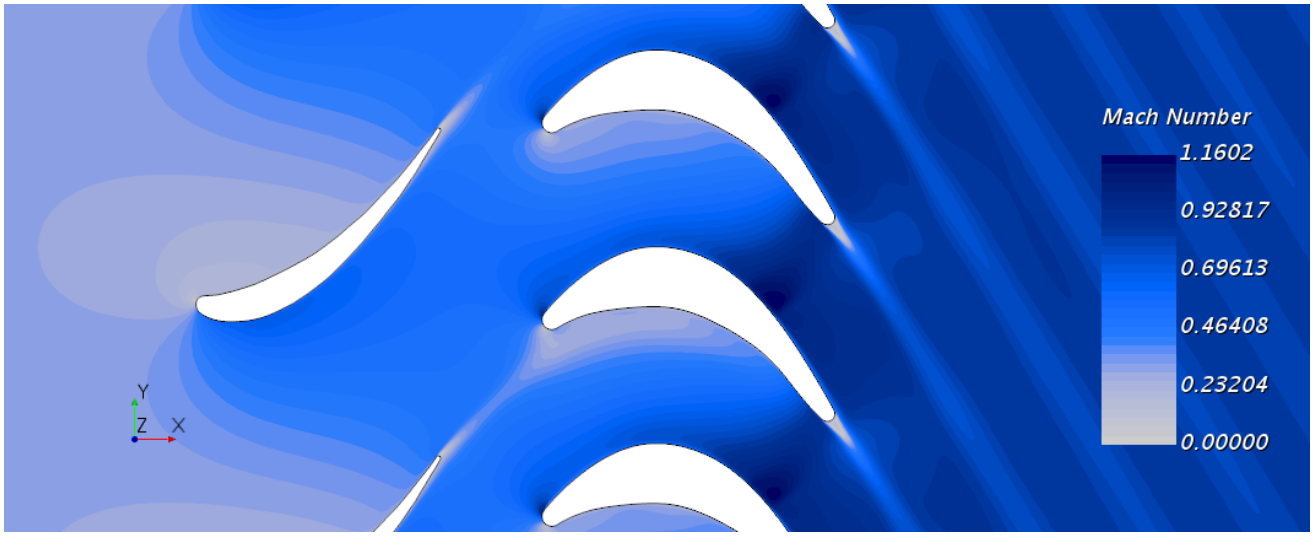

Figure A.20: Zoom of the mach number contour for blade ratio of 1.67 for Rotor 1.[OE]

A.3.2 Blade ratio study: 2.5

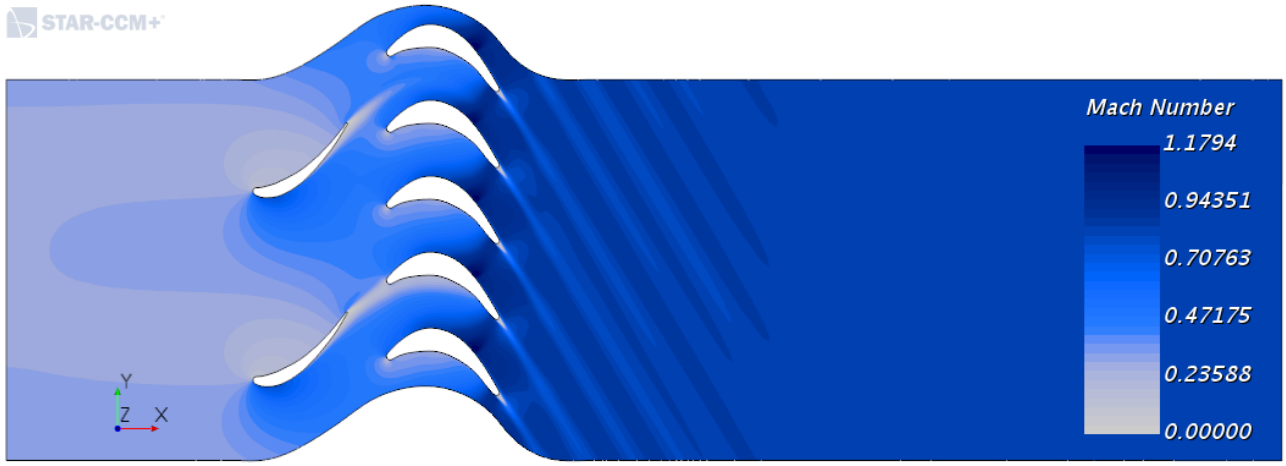

Figure A.21: Mach number contour for blade ratio of 2.5 for Rotor 1.[OE]

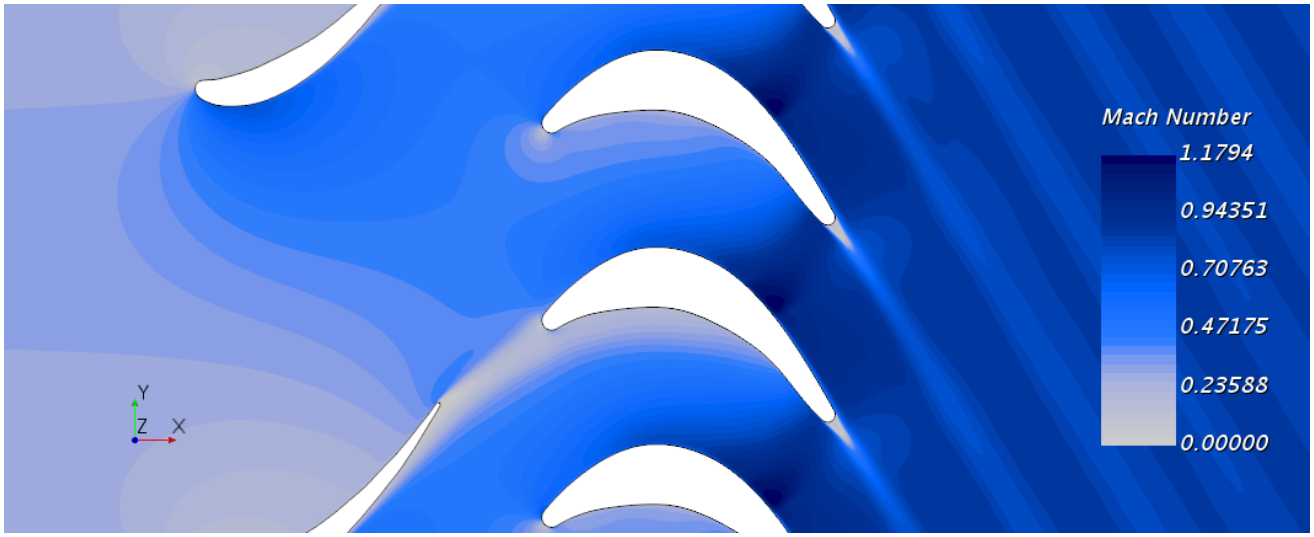

Figure A.22: Zoom of the mach number contour for blade ratio of 2.5 for Rotor 1.[OE]

A.3.3 Blade ratio study: 1

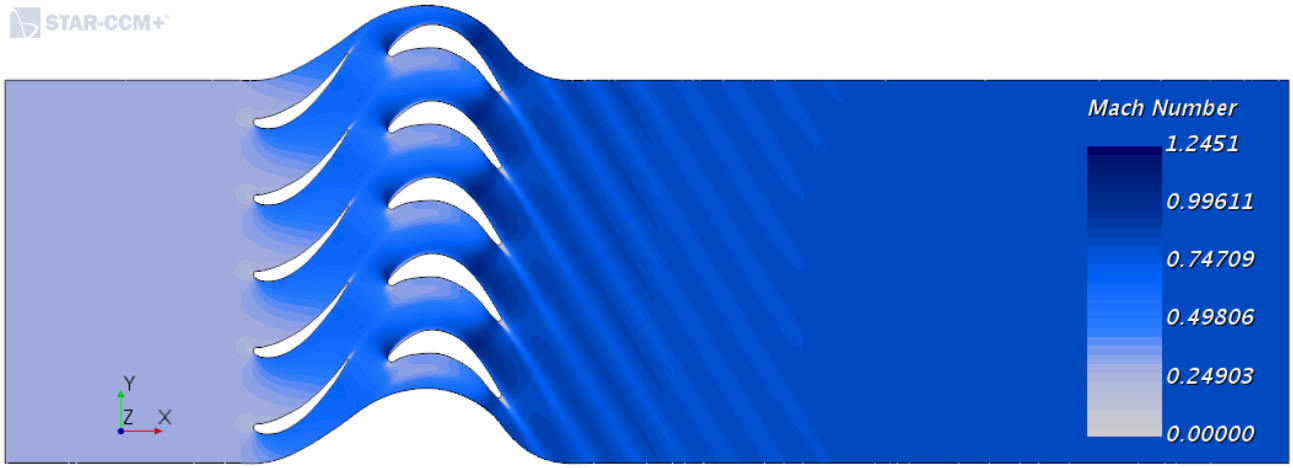

Figure A.23: Zoom of the mach number contour for blade ratio of 1 for Rotor 1.[OE]

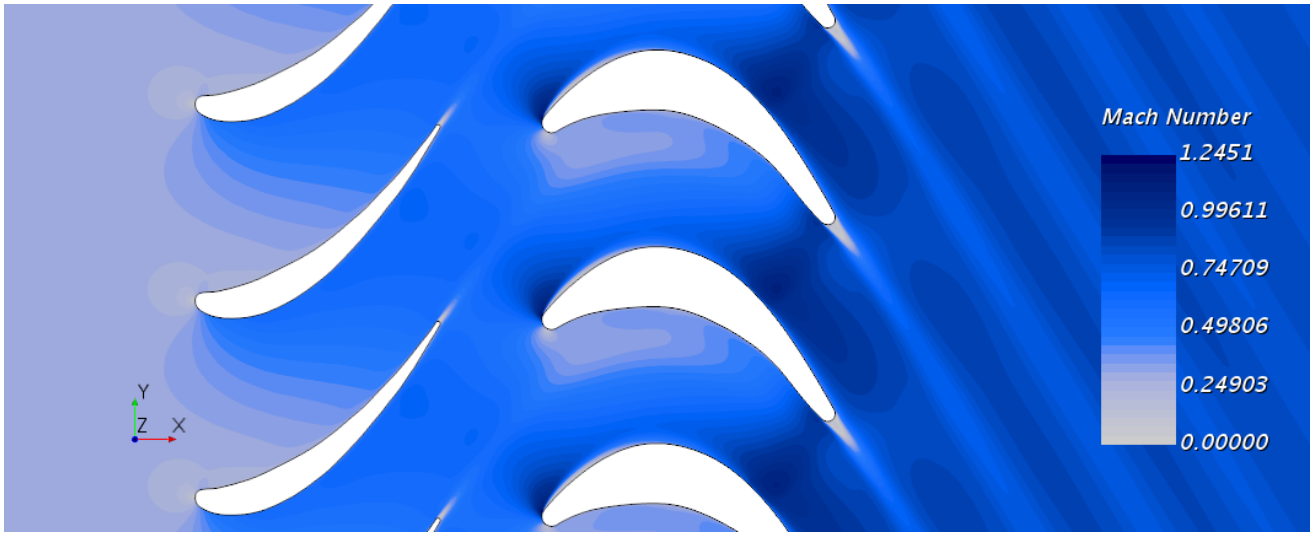

Figure A.24: Zoom of the mach number contour for blade ratio of 1 for Rotor 1.[OE]

A.4 Solidity Study

A.4.1 Solity study: 1.55

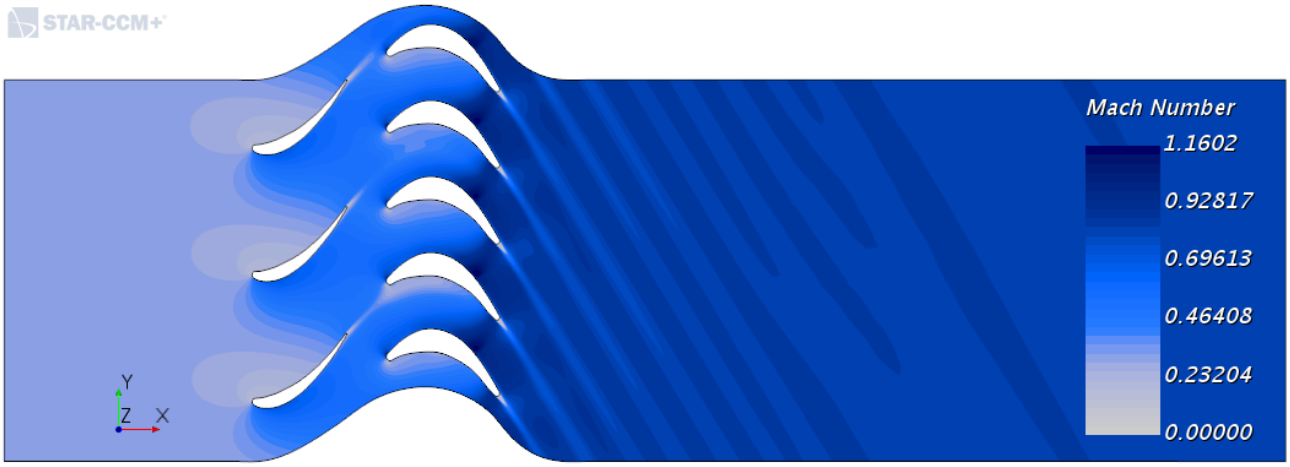

Figure A.25: Mach number contour for solidity value 1.55 for Rotor 1..[OE]

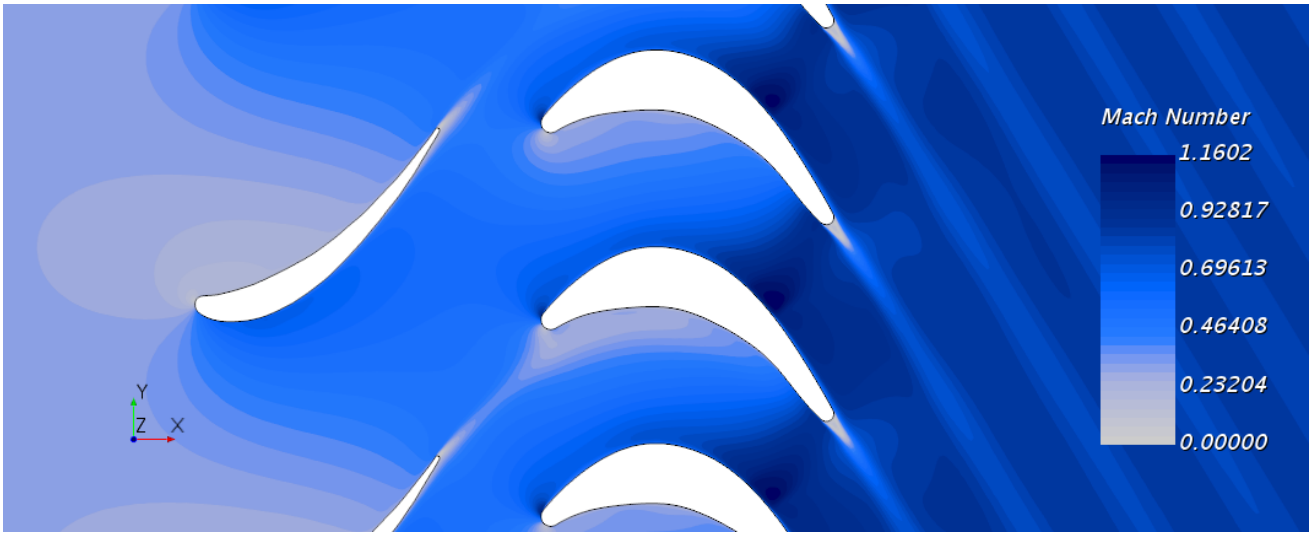

Figure A.26: Zoom of the mach number contour for solidity value 1.55 for Rotor 1.[OE]

A.4.2 Solity study: 1

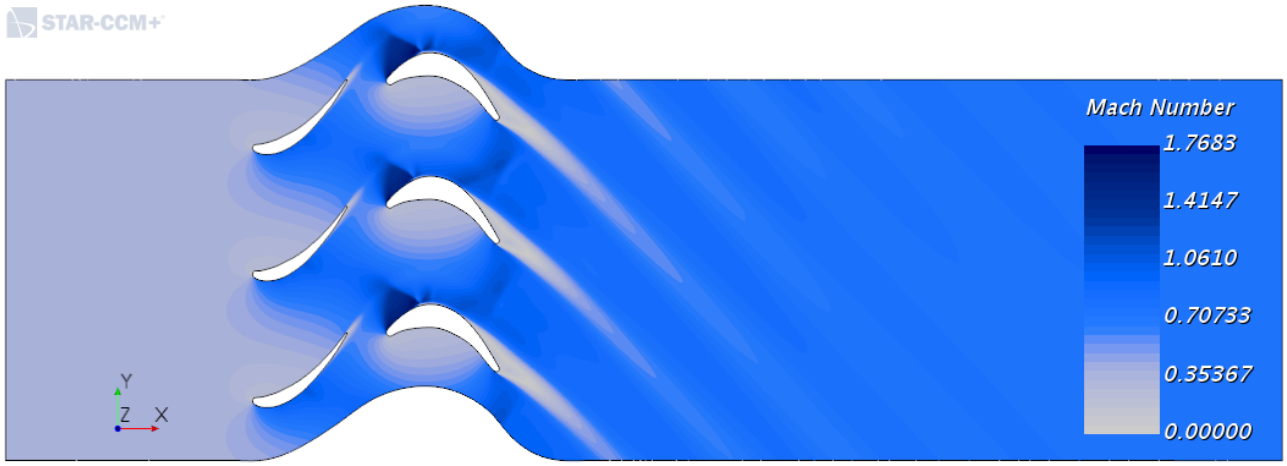

Figure A.27: Mach number contour for solidity value 1 for Rotor 1..[OE]

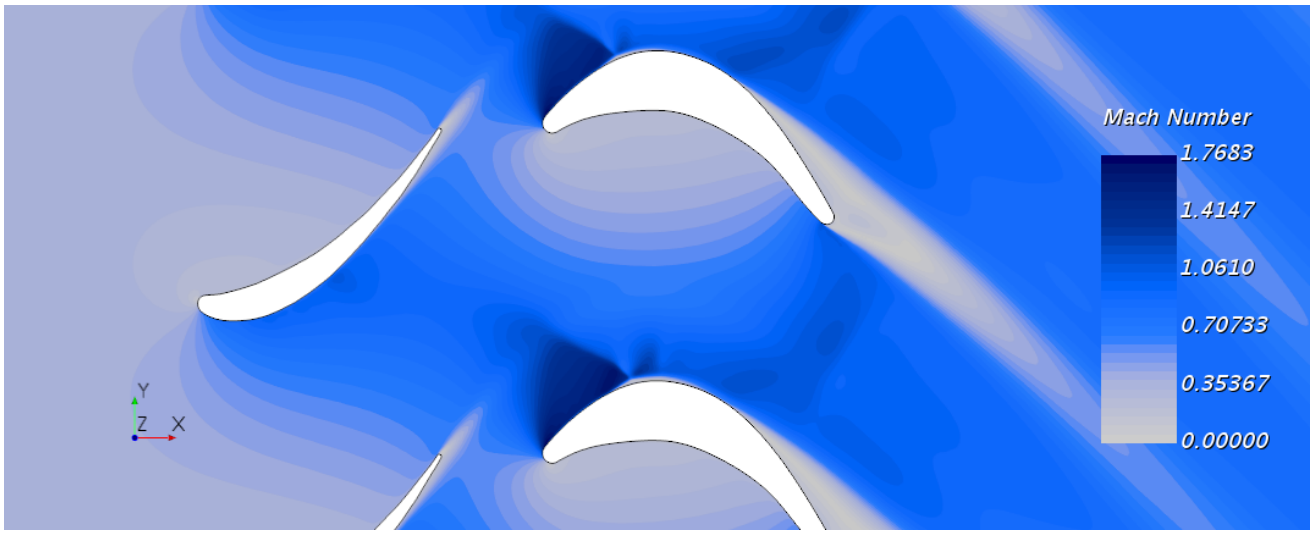

Figure A.28: Zoom of the mach number contour for solidity value 1 for Rotor 1.[OE]

Bibliography

[1] Jordi Herranz Tomás. *CFD study of the Rotor-Stator Interaction in a Francis turbine*. Universitat Politècnica de Catalunya (UPC), 2016.

[2] Zijie Zhao et al. *Experimental Study of Shock Wave Oscillation on SC(2)-0714 Airfoil*. American Institute of Aeronautics and Astronautics, 2013.

[3] Bora O. Cakir and Bayindir H. Saracoglu. *Mitigation of Turbine Vane Shock Waves Through Trailing Edge Cooling*. Karman Institute for Fluid Dynamics, 2018.

[4] R. K. Mishra et al. "Investigation of HP Turbine Blade Failure in a Military Turbofan Engine". In: *De Gruyter* (2017).

[5] Wikipedia. *History of the jet engine*. `https://en.wikipedia.org/wiki/History_of_the_jet_engine`.

[6] Wikipedia. *Ægidius Elling*. `https://en.wikipedia.org/wiki/\OT1\AEgidius_Elling`.

[7] Science Focus. *Who really invented the jet engine?* `https://www.sciencefocus.com/science/who-really-invented-the-jet-engine/`.

[8] Wikipedia. *Jet Engine*. `https://en.wikipedia.org/wiki/Jet_engine`.

[9] The Jet Engine. *A Historical Introduction*. `https://cs.stanford.edu/people/eroberts/courses/ww2/projects/jet-airplanes/planes.html`. 2004.

[10] Mete Cantekin. *Gaz türbinli motorların tarihçesi ve sınıflandırılması*. `https://www.slideshare.net/orfeomete/gaz-trbinli-motorlarn-tarihesi-ve-snflandrlmas`. 2011.

[11] Jan Mowill and Lars-Uno Axelsson. "Axial and Radial Turbines". In: *Turbomachinery International* (2012).

[12] William EmrichJr. *Principles of Nuclear Rocket Propulsion*. 2016. Chap. 3 Turbine Characteristics.

[13] Ronald D. Flack. *Fundamentals of Jet Propulsion with Applications*. Cambridge University Press, 2005. Chap. 8 Axial Flow Turbines.

[14] Ideen Sadrehaghighi. *Essentials of Turbo machinery in CFD*. CFD Open Series.

[15] Razvan Apetrei. *Transonic buffeting*. `https://www.razvanapetrei.com/rupdate-transonic-buffeting/`. 2017.

[16] Milton G.Kofskey and William J.Nasbaum. "Performance evaluation of a two-stage axial-flow turbine for two values of tip clearance." In: *NASA Technical Note (D-4388)* (1968).

[17] Warner L.Stewart. "A study of axial-flow turbine efficiency characteristic in terms of velocity diagram parameters". In: *ASME* (1962).

[18] Mohsin Obaid Muhi. "Numerical Prediction of an Axial Turbine Performance Used for Automotive Engines Turbocharger". In: *Journal of Babylon University* (2017).

[19] Nader A.Elqussas et al. "Automated axial flow turbine design with performance prediction". In: *Engineering of Science and Military Technologies* (2018).

[20] Cleverson Bringhenti et al. "One-Stage Power Turbine Preliminary Design and Analysis". In: *Journal of Aerospace Technology and Management* (2015).

[21] Tadashi Tanuma. *Advances in Steam Turbines for Modern Power Plants*. Woodhead Publishig Series in Energy, 2017.

[22] Sławomir Dykas, Włodzimierz Wróblewski, and Dawid Machalica. "Numerical Analysis of the Losses in Unsteady Flow through Turbine Stage". In: *Open Journal of Fluid Dynamics* (2013).

[23] Vladimir D. Liseikin. *Grid generation methods*. 2nd ed. Springer, 2010.

[24] STAR CCM+. *Help > User Guide > Meshing > Checking the Volume Mesh > Mesh Metrics*.

[25] Pedro Martí Gómez Aldaraví and Roberto Navarro García. *Unit 9 CFD post-processing*. 2018.

[26] Tomer Avreaham. *Turbulence Modeling Near Wall Treatment*. `https://allaboutcfd-tomersblog.com/2020/05/04/turbulence-modeling-near-wall-treatment-in-ansys-fluent/`. 2020.

[27] Henk Kaarle Versteeg and Weeratunge Malalasekera. *An introduction to computational fluid dynamics: the finite volume method*. 2nd ed. Pearson Education, 2007.

[28] Fluent incorporated. *Choosing the Solver Formulation*. 2003.

[29] Vinícius Guimarães Monteiro et al. "Numerical Simulation of Performance of an Axial Turbine First Stage". In: *Journal of Aerospace Technology and Management* (2012).

[30] Medhat M. Sorour, Mohamed A. Teamah, and Amgad M. Abbass. "Evaluation of Different Turbulence Models and Numerical Solvers for a Transonic Turbine Blade Cascade". In: *Tenth International Congress of Fluid Dynamics* (2010).

[31] D.I:Papadimitrioi, A.S. Zymaris, and K.C. Giannakoglou. "Discrete and Continuous Adjoint Formulations for Turbomachinery Applications". In: *EUROGEN* (2005).

[32] Dirección General de Empleo. "V Convenio colectivo de Airbus Defence and Space, SAU, Airbus Operations, SL, Airbus Helicopters España, SA y EADS Casa Espacio". In: *BOE* (Resolución de 22 de marzo de 2017).